

# **Estimating Human Upper-extremity Activities via Force Myography Technique during Collaborative Tasks in Human Robot Interactions**

**by  
Umme Zakia**

M.Sc., North South University, Dhaka, Bangladesh, 2007  
B.Sc., Jahangirnagar University, Dhaka, Bangladesh, 2001

Thesis Submitted in Partial Fulfillment of the  
Requirements for the Degree of  
Doctor of Philosophy

in the  
School of Engineering Science  
Faculty of Applied Sciences

© Umme Zakia 2022  
SIMON FRASER UNIVERSITY  
Summer 2022

Copyright in this work is held by the author. Please ensure that any reproduction or re-use is done in accordance with the relevant national copyright legislation.

# Declaration of Committee

**Name:** Umme Zakia  
**Degree:** Doctor of Philosophy  
**Title:** Estimating Human Upper-extremity Activities via Force Myography during Collaborative Tasks in Human Robot Interactions

**Committee:** **Chair: Michael Adachi**  
Assistant Professor, Engineering Science

**Carlo Menon**  
Supervisor  
Adjunct Professor, Engineering Science

**Kamal Gupta**  
Committee Member  
Professor, Engineering Science

**Mehrdad Moallem**  
Committee Member  
Professor, Mechatronic Systems Engineering

**Michael Hegedus**  
Examiner  
Lecturer, Engineering Science

**Rene Mayorga**  
External Examiner  
Professor, Industrial Systems Engineering  
University of Regina

## Ethics Statement

The author, whose name appears on the title page of this work, has obtained, for the research described in this work, either:

- a. human research ethics approval from the Simon Fraser University Office of Research Ethics

or

- b. advance approval of the animal care protocol from the University Animal Care Committee of Simon Fraser University

or has conducted the research

- c. as a co-investigator, collaborator, or research assistant in a research project approved in advance.

A copy of the approval letter has been filed with the Theses Office of the University Library at the time of submission of this thesis or project.

The original application for approval and letter of approval are filed with the relevant offices. Inquiries may be directed to those authorities.

Simon Fraser University Library  
Burnaby, British Columbia, Canada

Update Spring 2016

## Abstract

Force myography (FMG) is a non-invasive wearable technology that can detect underlying muscle volumetric changes when muscles contract. Common industrial physical human robot interaction (pHRI) tasks, such as object handling or transportation, mostly require hand forces to interact with machines. An FMG band made of force sensing resistors (FSRs) wrapped around an upper limb can be used to read muscle contractions during such activities. Including human feedback via FMG biosignals can be challenging yet practical in interactive pHRI environments. Therefore, the aim of this thesis was to investigate recognizing human intentions of interaction with a robot by estimating applied forces in dynamic motion using FMG technique. Initially in objective 1, real-time interactions with a 2-DoF linear robot (2D-pHRI platform) were investigated. Estimating interactive forces via intra-subject machine learning models was examined to manipulate the robot in any intended direction. In practice, a generalized (inter-subject) transfer learning model is preferable to recognize a new human worker instantly. Hence, in objective 2, domain adaptation and domain generalization were investigated using multiple source data collected over a long period (long-term data) from a 2D-pHRI platform. A few calibration (target training) data finetuned the model to quickly adapt out-of-distribution, unseen (target test) 2D-pHRI data. A study was conducted in objective 3 to interact with a 7-DoF serial robot during a challenging 3D collaborative task. Cross-domain generalization demonstrated that a transfer learning model pretrained with the 2D-pHRI long-term multiple source domains could improve force estimations in the 3D-pHRI platform. However, adequate and labeled data in practice is scarce. This was addressed in objective 4 by generating real-like synthetic FMG biosignals via domain randomization technique. By implementing a self-training technique, an unsupervised adversarial model pretrained with few labeled datasets and large amount of unlabeled synthetic data could estimate interaction forces during pHRI with a 7-DoF serial robot.

Therefore, using force myography as the only bio feedback could improve daily HRI experiences using long-term source data, calibration data, or synthetic data- labeled or unlabeled for faster adaptations. In addition, FMG-based force estimation could enhance safe collaboration by avoiding unwanted contact or impact force from the manipulator. We believe these findings will contribute to the development of a discrete wearable FMG device for practical pHRI, rehabilitation, or prosthetic control applications.

**Keywords:** Force myography technique; applied force estimation in dynamic motion; human-robot interaction; long-term multiple source FMG data; finetuning via calibration FMG data; supervised learning; domain adaptation and generalization; cross-domain generalization; unsupervised learning; generative adversarial networks; domain randomization; semi-supervised learning; self-training;

*To my beloved parents, and my dear family.*

## **Acknowledgements**

Above all, I am grateful to the almighty creator for fulfilling my dream.

First, I would like to express my deep gratitude to my senior supervisor, Dr. Carlo Menon for his continuous directives and guidance to accomplish this work. His persistence and persuasion kept me focused in continuing my research. His guidelines and keen supervision helped me accomplishing the set goal and milestones towards the thesis.

I would like to sincerely thank my supervisory committee members Dr. Kamal Gupta and Dr. Moallem Mehrdad for their valuable supports, suggestions, and timely feedbacks on my research work.

My sincere appreciation to members of the MENRVA Research Group who helped improving my work with critical knowledge sharing, raised important research questions, and encouraged improving standard writing skills in preparing the articles that are part of this thesis paper.

Lastly and most importantly, I would like to specially thank my loved ones and dear acquaintances who endlessly supported me through their inspirational companionships.

# Table of Contents

Declaration of Committee .....	ii
Ethics Statement .....	iii
Abstract .....	iv
Dedication .....	vi
Acknowledgements .....	vii
Table of Contents .....	viii
List of Tables .....	xii
List of Figures .....	xiii
Executive Summary .....	xvi
<b>Chapter 1. Introduction .....</b>	<b>1</b>
1.1. Chapter Overview .....	2
1.2. Motivation .....	2
1.3. Research Question .....	4
1.4. Research Goal and Objectives .....	5
1.5. Thesis Structure .....	7
1.6. Contribution .....	9
<b>Chapter 2. Literature Review, Materials &amp; Methods .....</b>	<b>12</b>
2.1. Chapter Overview .....	13
2.2. Human robot interactions .....	13
2.2.1. Learning human activities in HRI .....	14
2.3. Force measurements using myography techniques .....	16
2.4. Materials and Equipment .....	18
2.4.1. Upper arm and Forearm FMG Bands .....	18
2.4.2. Biaxial Stage / Linear robot (2D-pHRI) .....	20
2.4.3. Kuka robotic arm (3D-pHRI) .....	23
2.5. Participants .....	25
2.6. Methodologies .....	27
2.6.1. Regression algorithms .....	27
2.6.2. Data Driven Concepts and Approaches .....	32
A. Generalized zero-shot learning .....	32
B. Transfer Learning Techniques .....	33
2.7. Performance Matrices .....	36
2.8. Summary .....	37
<b>Chapter 3. Learning Human Intentions of Interactions in a certain direction ....</b>	<b>39</b>
3.1. Chapter overview .....	39
3.2. Introduction .....	39
3.3. Methodologies .....	40
3.3.1. Real-Time FMG-Based Integrated Control .....	40
3.3.2. Dynamic Arm Motion Patterns .....	41
3.4. Protocol .....	43



3.4.1.	Data Collection Phase.....	43
3.4.2.	Training Phase.....	44
3.4.3.	Test Phase.....	46
3.5.	Results.....	47
3.5.1.	Real-Time FMG-Based 1-DoF Interactions.....	47
3.5.2.	Real-Time FMG-Based 2-DoF Interactions.....	48
3.5.3.	Comparison of Force Estimations in Dynamic Motions.....	49
3.5.4.	Significance in Estimations.....	50
<b>Chapter 4.</b>	<b>Long-term FMG Model-based Force Estimation.....</b>	<b>53</b>
4.1.	Chapter Overview.....	53
4.2.	Introduction.....	53
4.3.	Objective 2A.....	55
Study 1:	Towards Long-term FMG Model-based Force Estimation during Human-Robot Interactions.....	55
4.3.1.	Methodology.....	56
4.3.2.	Long-Term Calibrated FMG-based (LCFMG) Model.....	57
	I. Long-term baseline dataset.....	58
	II. Calibration dataset $D_{SRT}$ .....	59
4.3.3.	Training dataset formation.....	59
	A. Scenario 1: Estimating Force in Unlearned Motion $M_U$ .....	59
	B. Scenario 2: Estimating force for Unlearned Participant $P_U$ .....	61
4.3.4.	Study Protocol.....	62
	A. Long-term training data collection period.....	62
	B. Real-time evaluation period.....	64
4.3.5.	Results.....	66
	A. Scenario 1: Unlearned Motion $M_U$ .....	67
	B. Scenario 2: Unlearned Participant $P_U$ .....	69
	C. Comparative analysis.....	71
4.4.	Objective 2B.....	75
Study 2:	Estimating interactive forces via supervised domain adaptation and generalization.....	75
4.4.1.	Materials and Methods.....	77
	A. Source and Target Domain.....	77
	B. Applied Interaction Force Estimation.....	78
	C. The proposed SFMG-DTL model.....	79
4.4.2.	Experimental Setup.....	79
4.4.3.	Protocol.....	80
	A. Training Phase.....	80
	B. Evaluation Phase.....	82
4.4.4.	Results.....	83
	A. Supervised Domain Adaptation.....	83
	B. Supervised Domain Generalization.....	84
	C. Viability of SDG.....	85
<b>Chapter 5.</b>	<b>Force Myography based Human Robot Collaboration in 3D.....</b>	<b>87</b>

5.1.	Chapter Overview.....	87
5.2.	Introduction.....	87
5.3.	Problem Statement.....	91
5.3.1.	Transfer learning for Unseen Target Domain .....	91
5.3.2.	The TL-CDG model.....	93
5.4.	Protocol.....	94
	1. Training Phase .....	94
	2. Evaluation Phase.....	96
5.5.	Results .....	97
5.5.1.	Case i: HRC in 3D (Target domain $D_{t_{3D}}$ ) .....	98
5.5.2.	Case ii: pHRI in 1D (Target domain $D_{t_{1D}}$ ) .....	98
<b>Chapter 6. Unsupervised, Semi-supervised Interactive Force Estimations via Generated Synthetic FMG Signals .....</b>		<b>103</b>
6.1.	Chapter Overview.....	103
6.2.	Introduction.....	103
6.3.	Protocol .....	105
6.4.	Unsupervised, Semi- supervised Self-trained FMG-DCGAN Algorithm.....	107
6.4.1.	Phase I: Generating synthetic FMG data.....	108
	i. The proposed FMG-DCGAN architecture .....	109
	ii. Selecting optimal $t(x)$ via $\sigma s$ and $\delta$ .....	111
6.4.2.	Phase II: Self-trained FMG-DCGAN model .....	111
	i. Pretraining Model D via Transfer Learning.....	112
	ii. Estimating Interactive Force with Self-Trained FMG-DCGAN model.....	112
6.5.	Results .....	113
A.	pHRI in 1D-X .....	114
B.	pHRI in 1D-Y .....	115
C.	pHRI in 1D-Z .....	116
6.6.	Discussion.....	117
<b>Chapter 7. Observations &amp; Concluding Remarks .....</b>		<b>119</b>
7.1.	Chapter Overview.....	120
7.2.	Observations .....	120
7.2.1.	Forearm & upper arm FMG bands .....	120
7.2.2.	Impact of 32 vs. 16-channel FMG technique .....	120
7.2.3.	Impact of band placements and winding force.....	121
7.2.4.	Muscle voluntary contractions during an intended motion .....	122
7.2.5.	Impact of intended motion .....	122
7.2.6.	Average interactive applied forces .....	123
7.2.7.	Viability of calibration .....	124
7.2.8.	Impact of long-term multiple source distributions.....	126
7.3.	Potential applications.....	126
7.4.	Limitations and Future Works .....	127
7.5.	Conclusion.....	128

**References..... 130**

**Appendix. Additional Observations ..... 139**

1. Selection of ML algorithms ..... 139

2. Real-time interactive force estimations ..... 141

3. Redundant degree-of-freedom of human arm..... 141

4. Instantaneous force recognition without fine-tuning (no calibration)..... 142

## List of Tables

Table 2-2-I. Demographics of the participants .....	27
Table 2-2-II. Regression models parameters .....	29
Table 2-2-III. Transfer Learning .....	36
Table 3-I. Five interactive arm motion patterns.....	42
Table 3-II. Algorithm I: Logic flow of RT FMG-based integrated control.....	45
Table 3-III. Training data and test data (estimated forces collected during real-time interactions). .....	47
Table 3-IV. Real-time performance evaluation: $R^2$ and NRMSE. ....	49
Table 3-V. Mean absolute errors (MAE) of regression models in different arm motions. ....	50
Table 3-VI. Two-way repeated measures ANOVA.....	51
Table 4-I. Training datasets used in scenario 1 and 2 (intended motion: $M_1$ ).....	63
Table 4-II. Summary of training datasets in Long-Term Calibrated FMG-based Model..	70
Table 4-III. Acronyms used.....	78
Table 4-IV. Source and target domains. ....	82
Table 5-I. HRI/HRC Experimental Setup .....	90
Table 5-II. Performances of TL-CDG Models .....	97
Table 5-III. pHRI with Kuka: Intra-Session Evaluation with Baseline FMG-DCNN! .....	101
Table 6-I. Model Performance in Force Estimations during pHRI in 1D-X.....	114
Table 6-II. Model Performance in Force Estimations during pHRI in 1D-Y.....	115
Table 6-III. Model Performance in Force Estimations during pHRI in 1D-Z.....	116

## List of Figures

Figure 1.1. Human worker applies force during a collaborative task with a Kuka robot.....	3
Figure 2.1. Human robot collaborations [21, 22], [52]-[54]. .....	14
Figure 2.2. sEMG signals to understand human activities during collaborative task [55]. .....	15
Figure 2.3. (a) A wearable FMG band, (b) data communication to a computer using DAQ, and (c) bands placements in upper and lower limb [16],[17]. .....	17
Figure 2.4. Some applications of FMG signals [32, 38, 40, 33]. .....	18
Figure 2.5. Custom-made Force myography bands [56]. .....	19
Figure 2.6. A 2-DoF linear robot/ biaxial stage.....	20
Figure 2.7. Top view of a human participant wearing FMG bands on upper extremity (UE) interacts with the biaxial stage by grasping the gripper/ knob.....	21
Figure 2.8. Labview interface of the RT FMG-based integrated controller: (a) control pane of FMG-based force estimation, (b) display pane of a target motion pattern to follow and maintain muscle volumetric contraction (MVC) [56]. .....	22
Figure 2.9. Experimental setup of pHRI & HRC with the Kuka robot [59]:.....	23
Figure 2.10. Force control implementing compliant collaboration with the Kuka robot via external interactive applied force. ....	25
Figure 2.11. Proposed FMG-CNN architecture (Model X, Y) [58]. .....	29
Figure 2.12. FMG-based transfer learning: (a) estimating applied interactive forces via SDA and SDG and (b) fine-tuning process of the pretrained SFMG-DTL model. ....	35
Figure 3.1. FMG-based real-time (RT) force control of a biaxial stage: the data collection and training phase are shown in green color, and the RT test phase is shown in magenta color [56]. .....	41
Figure 3.2. A participant wearing FMG bands interacts with the biaxial stage using an RT FMG-based integrated controller [56]. .....	44
Figure 3.3. RT test phase, where a participant interacted with the biaxial stage by FMG- based estimated hand forces in intended X and Y arm motions with FMG signals [56]. .....	46
Figure 3.4. Performances of regressors estimating FMG-based hand forces during intended one-degree-of freedom (1-DoF) arm motions: (a) x-direction only; and (b) y-direction only. ....	47
Figure 3.5. Performances of regressors estimating FMG-based hand forces during intended two-degree-of-freedom (2-DoF) arm motions: (a) diagonal; (b) square; and (c) diamond [56]. .....	48
Figure 3.6. Performances (average $R^2$ ) of the SVR and the KRR in estimating exerted forces with FMG signals during different arm motions [56]. .....	50
Figure 4.1. Implementing modified generalized zero-shot learning with multiple source domain adaptation in FMG-based HRI reproduced from [57] © [2021] IEEE with permission. ....	56

Figure 4.2. Proposed framework for Long-term calibrated FMG model reproduced from [57] © [2021] IEEE with permission. ....	57
Figure 4.3. Schematic of scenario 1: long-term calibrated FMG-based model generation to recognize a new unlearned motion ( $M_1$ ) reproduced from [57] © [2021] IEEE with permission. ....	60
Figure 4.4. Schematic of scenario 2: long-term calibrated FMG-based model generation to recognize unlearned participant applying force in motion ( $M_1$ ) reproduced from [57] © [2021] IEEE with permission.....	62
Figure 4.5. Applied forces and displacements during interaction between a contributing participant ( $P_6$ ) and the linear stage in real-time evaluation. Reproduced from [57] © [2021] IEEE with permission. ....	65
Figure 4.6. Real-time test phase evaluating a long-term calibrated FMG model in recognizing unlearned motion or unlearned participant reproduced from [57] © [2021] IEEE with permission. ....	66
Figure 4.7. 5-fold cross validation accuracies on training dataset for: (a) Inter-Participant-2 in Scenario 1, and (b) Inter-Motion-2 in Scenario 2 reproduced from [57] © [2021] IEEE with permission. ....	67
Figure 4.8. Real-time evaluation of scenario 1: Normalized root-mean-square error (NRMSE) values are reported for each trained model. ....	68
Figure 4.9. Real-time evaluation of scenario 2: Co-efficient of determination ( $R^2$ ) values are reported for each trained model. ....	68
Figure 4.10. Real-time evaluation of scenario 2: Normalized root-mean-square error (NRMSE) values are reported for each trained model. ....	68
Figure 4.11. Real-time evaluation of scenario 1: Co-efficient of determination ( $R^2$ ) values are reported for each trained model. ....	68
Figure 4.12. Comparison of performance of different models in estimating user-applied forces during different movement patterns. Reproduced from [57] © [2021] IEEE with permission. ....	71
Figure 4.13. Effects of calibration dataset in estimating force in 'Diagonal' motion in Scenario 1 and 2 (reported for best models only) reproduced from [57] © [2021] IEEE with permission.....	72
Figure 4.14. The proposed SFMG-DTL transfer learning model for estimating applied force during pHRI on a planar workspace with a linear robot [58]. ....	77
Figure 4.16. Setup used for data collection and evaluation of SFMG-DTL [58]:.....	80
Figure 4.17. SFMG-DTL: unified transfer learning framework for SDA and SDG [58]. ...	81
Figure 4.18. Target dataset 1 used in SDA:.....	83
Figure 4.19. Performances of ML and DL models in case i: on target dataset 1 (supervised domain adaptation) [58]: .....	84
Figure 4.20. Performances of ML and DL models in case ii: on target dataset 2 (supervised domain generalization) [58]: .....	84
Figure 4.21. Comparing SFMG-DTL model with intra-session evaluation on case ii: target dataset 2 model in estimating forces in X and Y dimensions in domain generalization [58]. ....	85

Figure 5.1. Cross-domain generalization via FMg-based SDG-TL-1 transfer learner in evaluating target HRC domain, $Dt_{3D}$ (moving a wooden rod with Kuka robot in 3D). Reproduced from [59] © [2022] IEEE with permission. ....	89
Figure 5.2. Transfer learning steps with TL-CDG-1 model for target domain, $Dt_{1D-Y}$ : HRI in 1D-Y (traversing arm while grasping cylindrical EEF in right and left directions). Reproduced from [59] © [2022] IEEE with permission.....	95
Figure 5.3. Few samples of target FMG distributions (a, c, e) and performances of the SDG-TL models (b, d: bar plot result for Model X and Y in 1D, and f, g, h: boxplot results for Model X, Y, Z in 3D). Reproduced from [59] © [2022] IEEE with permission. ....	99
Figure 6.1. Experimental setup of the study: .....	106
Figure 6.2. The proposed dual-phased unsupervised, self-trained FMG-DCGAN algorithm. Reproduced from [60] © [2022] IEEE with permission. ....	107
Figure 6.3. Domain randomization: a variety of transformation functions investigated. Reproduced from [60] © [2022] IEEE with permission.....	108
Figure 6.4. Performance evaluation of unsupervised, self-trained FMG-DCGAN model with different transformation functions compared to the supervised baseline model:.....	118
Figure 7.1. Winding forces of the FMG bands at the beginning of an interaction within participants [56].....	121
Figure 7.2. (a) FMG signals of arm motions in the x- and y-directions; (b) K-means clustering of FMG signals [56]......	122
Figure 7.3. Averaged estimated hand forces and standard deviations (SDs) (within participants) in intended arm motions [X, Y, diagonal (DG), square (SQ), and diamond (DM) patterns] [56]......	123
Figure Appendix.1. Five-fold cross-validation results for 2-DoF interactions in diamond arm motion. Reproduced from [56] with permission.....	140

## Executive Summary

In common industrial collaborative tasks such as moving objects, human workers commonly use hand forces to interact with machines. In the literature, there are only a few studies where applied force is estimated using biosignals such as the surface electromyography (sEMG) technique. Practical challenges associated with using biosignal-based control designs include redundant degrees of freedom of the human arm in the workspace, the tools involved, and individual-specific muscle contractions during certain human robot interaction (HRI) tasks. As a contemporary technology like the conventional sEMG technology, force myography (FMG) is a non-invasive, wearable technique that often utilizes force sensing resistors (FSRs). The off-the-shelf FSRs can detect resistance changes when pressure is applied on their surfaces. An FMG band wrapped around an upper or lower limb can be used to detect underlying muscle volumetric changes when the muscle contracts. For gesture recognition, prosthetic control, finger movements regression, rehabilitations, activities in daily life (ADL), grasping forces and human-machine interactions (HMI), FMG bio-signals are comparable to traditional sEMG biosignals. However, there is a gap in the literature when estimating human exerted forces during physical HRI (pHRI) tasks using the FMG technique. Hence, in this thesis, we have investigated human robot interactions and collaborations via force myography biosignals in recognizing interactive applied forces in dynamic motions using data-driven models. We considered physical interactions with a robot using human applied hand force, so reading FMG signals from upper limb of a participant was the obvious choice.

In this thesis, the research goal was achieved via four objectives. In the first objective, a preliminary study on interactive force estimation to manipulate a linear robot (a biaxial stage) using force myography signals derived from 32 channels was investigated. In this 2D interactive planar workspace, interactions occurred in five different dynamic motions (1D-X, 1D-Y, 2D-diagonal/DG, 2D-square/SQ and 2D-diamond/DM). These motions were examined to understand human intentions of manipulating the robot in any intended direction. These motions were selected to enable the gradual addition of more complex muscle activities and arm movements with more shoulder and arm abduction, adduction, flexion, and extension, which also covered the whole 2D surface. Intra-session (training and testing in same session) supervised machine learning methods



(support vector regressor and kernel ridge regressor) were found effective in real-time force estimations ( $R^2$ : 90%- 94% in 1D and 82% - 91% in 2D motions). However, a separate trained model was required for each participant to manipulate the robot in a certain direction, i.e., an individual model for each participant for each motion.

The potential application of a wearable FMG band for human workers in industrial pHRI workspaces requires general applicability to all workers for control and safety aspects of their work. A trained model that can estimate dynamic hand force via FMG signals is preferable for any individual in any intended motion during pHRI. Hence, the second objective was to investigate a generalized model to recognize applied forces for out-of-distribution (OOD) target data via domain adaptation and domain generalization. Two separate 2D-pHRI studies were conducted where a large volume of multiple source domains collected over a long period of time was utilized. These population data were collected over long period of time in multiple sessions during real-time interactions between several participants and the linear robot in selected motions (1D-X, 2D-diagonal/DG, 2D-square/SQ and 2D-square of different sizes/SQ-diffSize). A generalized model trained with the long-term FMG distributions predicted unseen target data in repetitive usage or during interactions with a new participant (*Study 1: unseen, unlearned target test data #  $R^2$ : 90%- 94% [1D-X], 80%-85% [2D-DG]* and *Study 2: unseen, similar target test data #  $R^2$ : 88% [2D-SQ], 89% [2D-SQ-diffSize]*).

Objectives 1 and 2 were conducted in an interactive 2D-pHRI environment with 32 FMG channels on the forearm and upper arm positions. However, conducting human robot collaborative tasks in 3D using FMG biosignal proved to be challenging. The procedure required human participants to handle objects or tools by applying adjustable forces with redundant degrees-of-freedom in arm trajectories, which needed investigation. Hence, in objective 3, the focus was on investigating an HRC task of moving a wooden rod in collaboration with a Kuka LBR IIWA 14 robot. Initially, pHRI with the 7-DoF Kuka robot was investigated by estimating grasping forces in dynamic motion interactions in certain directions of the 1D, 2D and 3D workspace. A 16-channel FMG forearm band was used to capture the muscle readings during the task. An intra-session trained deep learning model moderately estimated the forces, which required further improvement. Having more participants or collecting more inter-session data during the HRC task with the Kuka robot was not practical or possible due to time constraints. On the other hand, a large volume of source data (long-term data) collected over a long period of time from other pHRI

platforms can be useful providing adequate training data. A cross-domain generalization (CDG) technique was useful when using unrelated source and target data that allows a pretrained model to transfer knowledge between different platforms/systems. Furthermore, it generalized the trained model beyond source distributions. However, it was not studied in bio-signal-based HRI tasks. Therefore, in this objective 3, we conducted an FMG-based HRC task of moving the wooden rod using the supervised CDG technique. Multiple long-term source data collected over a long period of time from the 2D-pHRI platform were used in pretraining a transfer learning model with CDG and was evaluated on the target 3D-HRC task for the first time. The pretrained model performed better in simple 1D grasping interactions ( $R^2$ : 79-87%) while its performance slightly improved during collaborative task of moving the rod in 3D ( $R^2$ :  $\approx$ 60-63%).

The studies conducted in objective 1, 2, and 3 utilized labeled training data via supervised, traditional, or deep learning algorithms. However, in real-world pHRI applications, obtaining enough training data, having more participants, or labeling all data are not always possible. In the case of unlabeled data, unsupervised learning can be an option which does not need labeled data. It learns latent feature distributions and may generate labels based on the learning process. In recent pHRI studies, there is a growing interest in using limited amounts of labeled data with large quantities of unlabeled data for realistic predictions. Semi-supervised or weakly supervised learning can be useful and needs only a few labeled training datasets and may perform similar/close to the supervised learning. For scenarios where training data is hard to collect or there is no previous data available from other related sources, synthetic data could be a favorable alternative. Therefore, in the final objective, unsupervised adversarial learning was used for generating synthetic data via domain randomization. Knowledge from the latent feature distributions was transferred via semi-supervised learning during intra-session test data evaluation. For this investigation, pHRI with the Kuka robot in 1D (X, Y and Z directions) was investigated using 16-channel forearm FMG signals. The proposed model performed ( $R^2$ : 77%-84%) like the supervised model ( $R^2$ : 78%-88%) even with fewer labeled training datasets (labeled vs unlabeled = 1:4) and a large volume of unlabeled, generated synthetic FMG data (real vs syn. = 1: 2.5).

Recognizing interactive forces in any intended dynamic arm motion via FMG signals would be beneficial in practical HRI scenarios. Because it would help understanding human intentions of interactions during collaborative tasks. Long-term

FMG-based force estimation via domain adaptation and generalization approaches are particularly effective in daily application where finetuning with a few calibration dataset can recognize unseen HRI target data. Furthermore, cross-domain generalization using one arm band can be useful where source and target HRI platforms are totally different from each other. Scarcity of labeled data in real-world applications can be dealt with by careful synthetic data generation using adversarial learning and self-training approaches. Therefore, the use of the wearable FMG band for recognition of human activities can enhance pHRI quality in safe collaborations, rehabilitation applications, or prostheses control to interact with machines on a daily basis.

This papers-based thesis is organized into 7 chapters. The introductory chapter 1 describes motivations, research goal and objectives, and expected contributions. Chapter 2 describes a literature review of HRI and force myography signal, experimental setups and methodologies involved during the studies. Chapter 3-6 describe the detailed studies conducted in objectives 1-4 in a consecutive manner, which were published in peer-reviewed journals. The thesis concludes in chapter 7 with discussion of observations made, limitations and future work with concluding remarks.

# Chapter 1.

## Introduction

This thesis is a papers-based manuscript with published articles in peer-reviewed journals. Specifically, chapters 3, 4, 5 and 6 are excerpts from the published papers. Chapters 1 and 2 introduce the subject and provide background information to facilitate the understanding of the subsequent chapters 3-6.

The material presented in this chapter is extracted, reproduced, and modified with permission from the following papers:

[56] U. Zakia and C. Menon, "Estimating Exerted Hand Force via Force Myography to Interact with a Biaxial Stage in Real-Time by Learning Human Intentions: A Preliminary Investigation", *Sensors*, vol. 20, no. 7, (22pp), Apr. 2020.

[57] © [2021] IEEE with permission. U. Zakia and C. Menon, "Toward Long-Term FMG Model-Based Estimation of Applied Hand Force in Dynamic Motion During Human–Robot Interactions," in *IEEE Transactions on Human-Machine Systems*, vol. 51, no. 4, pp. 310-323, Aug. 2021, doi: 10.1109/THMS.2021.3087902.

[58] U. Zakia and C. Menon, "Force Myography-Based Human Robot Interactions via Deep Domain Adaptation and Generalization," *Sensors*. 2022; 22(1):211. <https://doi.org/10.3390/s22010211>.

[59] © [2022] IEEE with permission. U. Zakia and C. Menon, "Human Robot Collaboration in 3D via Force Myography based Interactive Force Estimations using Cross-Domain Generalization," *IEEE Access*, Mar. 2022, doi: 10.1109/ACCESS.2022.3164103.

[60] © [U. Zakia, A. Barua, X. Jiang, and C. Menon, "Unsupervised, Semi-Supervised Interactive Force Estimations During pHRI via Generated Synthetic Force Myography Signals," *IEEE Access*, June 2022, doi: 10.1109/ACCESS.2022.3187115.61.

Sections of this chapter are reprinted or adapted from the above articles for clarification and to fit the formatting and scope of this document.

## 1.1. Chapter Overview

In this chapter, the motivation behind the research work is outlined, and research questions and objectives are defined. Finally, the structure of this thesis is explained.

## 1.2. Motivation

The use of human robot interaction (HRI) in manufacturing environments has allowed increased productivity of industries utilizing assembly lines [1-3]. A variety of measures, such as vision system (cameras, image/depth sensors, tracking systems), ultrasonic or wideband/RF transceivers, proximity detections (capacitive, inductive, infrared, or magnetic sensors) are implemented for surveillance, monitoring, and sharing the workplace with robots [4-7]. These tools can be either attached to the robot or installed in the workspace. However, proper supervision can be impeded due to the obstructions of signals, limited signal ranges, and difficulties with installations of monitoring devices within the workspace. Besides, the dynamic, and unpredictable environment during HRI collaborations introduces uncertainties that increase the risks of injuries to the workers [8-10]. To enhance human-machine interactions, an input signal from the human worker directly to the robot would help implementing better collaboration and enhance a safe working environment for the worker.

In physical human robot collaboration (HRC), human workers commonly use hand forces during activities such as object handling or transportation tasks to interact with machines. These interactions require dynamic arm movements where the force interactions occur through hand movements [Figure 1.1]. Predicting human intentions through body movements such as human hand force and arm motions have been studied extensively to facilitate such collaborative tasks with robots [11-14]. Commercially available force/torque sensors can accurately measure applied forces during collaborative tasks. These sensors can be attached directly to the robot body allowing full tactile sensation. However, they are expensive, bulky, and restricts the free movements of a human worker in the workspace. Hence, indirect force measurements are preferred for recognizing applied hand forces during interactions. Utilizing wearable sensing devices based on biosignals provides the worker more flexibility in movements and insight about their intentions. So, the current research focuses on including biosignals for understanding human activities during interactions with machines [15, 16]. Among such biosignals, the

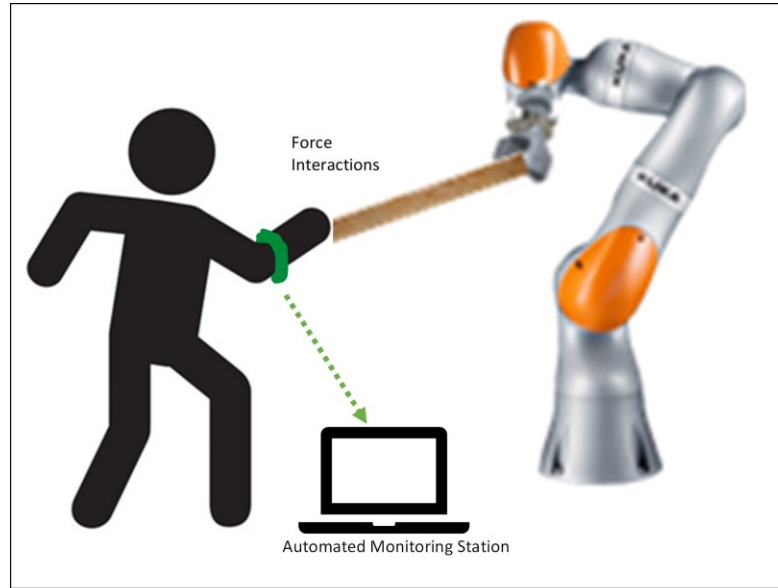


Figure 1.1. Human worker applies force during a collaborative task with a serial robot.

traditional surface electromyography (sEMG) has been studied over the last few decades. It is a non-invasive technique that can interpret electrical activities associated with muscle contraction variations under the skin. This technique has been studied for gesture recognition, hand force recognition, prosthetic limb controls, rehabilitation applications and human-robot interactions [17-28].

Recently, an innovative wearable sensing system integrating the force myography (FMG) technique has gained interest. Force myography (FMG) is a non-invasive technology that often utilizes force sensing resistors (FSRs) to detect resistance changes when pressure is applied [29]. FSRs are small, easy to use, inexpensive and durable, which is essential for any wearable device. An FMG band wrapped around upper or lower limbs can detect muscle volumetric changes during certain activities. As a contemporary technique to sEMG, FMG signals have proven their use in similar research of finger and gesture recognition, isometric grasp/hand force recognition, prosthetic upper limb control, rehabilitation applications, and assistive solutions for elders in their activities in daily life (ADL) [30-42]. This technique was found comparable and sometimes better than sEMG in similar applications. Recent research has shown the FMG technique has advantages compared to sEMG in terms of lower cost, simple signal processing, easy incorporating in a wearable device and a better choice for human machine interfacing compared to sEMG [43-45].

In the literature, a few studies were conducted to estimate hand force or position for improving human-robot interactions via biosignals such as sEMG [22,23]. However, there is a lack of studies in the literature on conducting human robot collaborative tasks in 3D via FMG-based force estimations. Recognizing interactive forces in dynamic motions with biosignals is challenging due to the dynamic nature of the task, tools involved and the redundant degree-of-freedom of the human arm in 3D. Studying the use of FMG in the recognition of certain human intention in the manipulation of robots in any intended direction would be useful. In practical pHRI applications, obtaining enough training data, having more participants, or labeling all data are not practical or always possible. Therefore, using existing source data in training a generalized model to recognize out-of-distribution, out-of-domain, the same or cross platform HRI applications could be helpful in the recognition of human activities in unseen scenarios. Also, generating real-like synthetic FMG data in realizing forces in dynamic motion via unsupervised learning could provide a viable solution in industrial HRC activities. Since force myography can be a potential technique for pHRI applications and there is a gap in research to address these practical challenges, FMG-based force control requires investigation. Therefore, the focus of this thesis was to investigate human robot collaboration by recognizing interactive forces in dynamic motion via force myography signals. Using FMG biosignals as the only input in learning human activities appears promising for safe interactions.

### **1.3. Research Question**

*Can force myography estimate human upper-extremity activities to interact with robots?*

By estimating human upper-extremity activities, we mean:

- estimating applied hand force in dynamic motion,
- recognizing arm motion during interactions with machine.

Including FMG biosignals in physical human robot interactions will:

- facilitate collaborative activities,
- avoid complexity of dynamic hand modelling.

## 1.4. Research Goal and Objectives

The research goal of this thesis was to develop force myography based pHRI system by recognizing interactive force in dynamic motions. During interactions with a robot via compliant collaboration, a human participant exerted forces to its end-effector and the robot moved in the same trajectory, which required impedance control. Learning human intentions during the interactions can be achieved using the FMG technique, however, it had certain challenges. Hence, this thesis is described as objectives and methods to achieve the research goal while proposing solutions to overcome inherent challenges of the dynamic environment. The overall goal of this thesis is divided into four objectives that answer four research questions as follows:

### Research question 1:

- Can we estimate applied hand force in an intended direction in 2D via force myography signals?

### **Objective 1: *Estimating applied hand force in certain motion via FMG signals during interactions with a linear robot***

To understand human activities by estimating exerted hand force via FMG signals, a preliminary study was conducted where human participant manipulated a biaxial stage that resembled a simple 2-dof planar robotic arm or a linear robot. Two FMG bands (32-channel) wrapped around forearm and upper arm muscles were used for intra-session force estimations. Interactive forces during five different arm motions were considered. These motions were examined for understanding human intentions of manipulating the linear robot in any direction. Supervised machine learning techniques via a simple interactive setup with constrained protocol allowed dynamic force estimations in real time.

### Research question 2:

- Can an FMG-based regression model estimate interactive hand force in unseen 2D scenarios?

### **Objective 2: *Training a long-term FMG-based generalized model to estimate applied hand force in unseen scenarios***



To investigate if an FMG-based regression model could predict new, unlearned target sample data that would be out-of-distribution (OOD) of the population data, we conducted two separate studies. In the **1<sup>st</sup> study (objective 2A)**, a dataset was collected in multiple sessions over a long period of time where several participants interacted with the linear robot and applied forces in five different intended motions. A generalized model trained with the long-term multiple source domains was then evaluated for predicting OOD, unseen target data. In this study, two target scenarios were evaluated where: 1) a participant applied forces in a new, unseen arm motion, and 2) an unknown, new participant applied forces in a learnt motion. In the **2<sup>nd</sup> study (objective 2B)**, multiple session force data from interactions between a participant and the linear robot in a certain complex arm motion were used in pretraining a deep learning model. This model was evaluated in estimating forces via 1) domain adaptation for repeated interactions between the same participant and the robot, and 2) domain generalization where unseen (OOD) participants interacted with the robot in a similar way. Supervised machine learning and deep learning techniques were implemented in these studies.

In this objective, a 32-channel FMG-based regression model trained with a long-term dataset was used in estimating forces for unseen/unlearned sample data using the forearm and upper arm FMG bands. This technique generalized the trained model, reduced training, and fine-tuned the model with a small amount of instantaneous, calibration data.

### **Research question 3:**

- Can FMG signals estimate applied hand force in 3D dynamic motion during a collaborative task with a serial robot?

### **Objective 3: *Performing a collaborative task with a robotic arm in 3D via FMG-based force estimation***

To validate force estimations in dynamic motion, a practical collaborative task such as transporting a wooden rod in 3D with a 7-DoF Kuka robot was conducted. For the challenging task of force estimation in dynamic 3D motion with 16-channel FMG signals, a supervised cross-domain generalization (CDG) method with deep transfer learning was investigated. In this study, multiple long-term source data from the 2D-pHRI platform (objective 1) was used in pretraining a transfer learning model with CDG. The proposed

model was evaluated on the target 3D-HRC task for the first time using fine-tuned calibration data. FMG-based pHRI with the Kuka robot was also investigated in estimating grasping forces in certain directions of the 1D, 2D and 3D workspace. Using fewer FMG channels and learning interactive forces in motions from forearm muscle belly was considered appropriate for practical industrial approaches.

#### **Research question 4:**

- Can an FMG-based transfer learning model trained using a few, unlabeled source data estimate interactive forces in dynamic motion?

#### **Objective 4: Estimating interactive forces via *FMG signal using unsupervised adversarial learning with domain randomization and self-training***

To estimate interactive forces, unsupervised transfer learning was investigated in situations when obtaining enough training data, having more participants, or labelling all data was not possible. This critical approach enabled training a deep convolutional neural network quickly with a relatively smaller amount of data instead of training the model from scratch. In this study, an adversarial machine learning technique was used to mislead a model with malicious input and real-like synthetic data was generated via an unsupervised, generative adversarial network (GAN) to build adequate a training dataset. Domain randomization was implemented to minimize the reality gap between the real-like synthetic data and the real data via a few unique transformation techniques. Domain adaptation was implemented for transferring knowledge using the GAN discriminator model where the source and target domains had the same feature space but different distributions. A semi-supervised self-training approach with a few labeled real data and pseudo-labeled synthetic data helped pretraining of a transfer learning model to evaluate target data. For this study, interactions with the Kuka robot in 1D was evaluated using forearm FMG signals. This study showed unsupervised, adversarial learning via domain adaptation could be a viable solution where supervised learning would not be applicable to interact with industrial robots.

## **1.5. Thesis Structure**

This thesis contents are structured in consequent chapters as described below:

- Chapter 2 provides background study on human robot interactions and the force myography technology explored in force estimations in the literature. The machine learning approaches and techniques adopted in this thesis are described. The FMG bands, robots and force control mechanism developed using the data-driven model are discussed also.
- Chapter 3 describes the study conducted in accomplishing Objective 1. The methodology, the hardware and the software developed for real-time interactions with a linear robot in this study are discussed. Data analysis methods used, and the results obtained are discussed at the end of the chapter.
- Chapter 4 outlines the two separate studies conducted to answer the research question of Objective 2. In Objective 2A, the first study on transfer learning using long-term multiple source domains (from interactions between a linear robot and several participants) in predicting unseen target data (unseen participants or unseen motion interactions) is presented. The second study on deep domain adaptation and domain generalization via multiple session data (from interaction with a linear robot and one participant) in estimating unseen target data (unseen session or unseen participants) is discussed in Objective 2B. Each study is described in terms of the materials, methods and experimental setups with the protocols followed. Observations and results are reported and discussed in subsequent studies.
- Chapter 5 describes the study conducted to fulfill Objective 3. Materials and experimental setup for performing a collaborative task with a Kuka robot via cross-domain generalization method are explained in this chapter. Results of the study are reported and discussed towards the end of the chapter.
- Chapter 6 outlines the study approach adopted to accomplish Objective 4. The unsupervised learning approach used in real-like synthetic FMG bio data generation are explained in detail. The transfer learning method in pretraining a model via self-training is discussed followed by evaluation of the target data (interactions with a Kuka robot in 1D) with a data analysis method. Results obtained are discussed at the end of the chapter.
- Chapter 7 discusses observations and conclusions drawn based on results of the four studies explained in Chapters 3 to 6. It explains how the objectives are fulfilled and

points out limitations and future works that can be done based on the findings of this thesis.

## 1.6. Contribution

This thesis investigated applied forces in collaborative tasks between a human worker and a robot using FMG biosignals. Force sensing resistors (FSRs) in a wearable band (FMG band) were used to capture FMG biosignals because they are cheap, durable, reliable, and off-the-shelf. The non-invasive, easy to wear FMG bands provided flexibility and comfort during human movements within the workspace. With careful method selections and control designs as discussed in this thesis, the ability to interpret human intended directions of interactions using FMG biosignals became viable in platform independent HRC applications.

Contributions of this thesis were:

- estimating interactive hand forces using data-driven approaches instead of developing complex hand modeling,
- addressing the real-world problem of inadequate training data by utilizing existing data collected over a long period of time,
- quickly calibrating the ready-to-use FMG band with a small amount of instantaneous data using a transfer learning technique,
- providing a way to bridge between different HRI platforms via domain adaptation, domain generalization and cross-domain generalization methods to estimate interactive forces either from forearm or upper arm muscle readings for a first-time or repeated user,
- generating real-like synthetic FMG biosignals to supplement the severe data scarcity problem using the domain randomization method,
- estimating forces from unlabeled data using unsupervised and semi-supervised adversarial learning techniques,

- implementing compliant collaboration to enable the robot to follow trajectories of human intended interactions and prevent the human participant from getting injured or trapped by the robot.

This thesis work generated the following publications:

[56] U. Zakia and C. Menon, "Estimating Exerted Hand Force via Force Myography to Interact with a Biaxial Stage in Real-Time by Learning Human Intentions: A Preliminary Investigation", *Sensors*, vol. 20, no. 7, (22pp), Apr. 2020.

[57] © [2021] IEEE with permission. U. Zakia and C. Menon, "Toward Long-Term FMG Model-Based Estimation of Applied Hand Force in Dynamic Motion During Human–Robot Interactions," in *IEEE Transactions on Human-Machine Systems*, vol. 51, no. 4, pp. 310-323, Aug. 2021, doi: 10.1109/THMS.2021.3087902.

[58] U. Zakia and C. Menon, "Force Myography-Based Human Robot Interactions via Deep Domain Adaptation and Generalization," *Sensors*. 2022; 22(1):211. <https://doi.org/10.3390/s22010211>.

[59] © [2022] IEEE with permission. U. Zakia and C. Menon, "Human Robot Collaboration in 3D via Force Myography based Interactive Force Estimations using Cross-Domain Generalization," *IEEE Access*, Mar. 2022, doi: 10.1109/ACCESS.2022.3164103.

[60] © [2022] IEEE with permission. U. Zakia, A. Barua, X. Jiang, and C. Menon, "Unsupervised, Semi-Supervised Interactive Force Estimations During pHRI via Generated Synthetic Force Myography Signals," submitted in *IEEE Access*, June 2022, doi: 10.1109/ACCESS.2022.3187115.

[61] U. Zakia and C. Menon, ""Dataset on Force Myography for Human Robot Interactions", MDPI Data (submitted June 2022).

Including human bio feedback in a robotic control scheme can be used to improve safe collaboration with the robot by using FMG signals. If a safety issue arises such as to avoid unwanted contact or impact force from the manipulator, the participant can push the robot to move it away further in a certain direction.

Likewise, we believe the supervised domain adaptation and generalization methods using a few instantaneous calibration data or the unsupervised adversarial transformation techniques in generating real-like synthetic data can be useful for other types of biosignals for overcoming similar design constraints. Such concepts and methods are mainly used in image processing or in natural language processing (NLP) applications. However, to implement FMG biosignal-based HRI, modified versions of these methods were adapted in this thesis. A version of modified generalized zero shot learning (GZSL) was used here where a few target training datasets were included in the training/finetuning process. Transfer learning methods were modified for pHRI implementation, such as: for domain adaptation, a model trained with 1D-X interactions of 5 participants with the biaxial stage was tested on a new participant interacting in 1D-X. For domain generalization, the model trained with 5 participants interacting in 1D-Y, 2D-diagonal, 2D-square and 2D-diamond with the biaxial stage was tested on a new participant interacting with the biaxial stage in 1D-X. And for cross-domain generalization, the model trained with 1D-X, Y, 2D-diagonal, 2D-square and 2D-diamond interactions of 5 participants with biaxial stage was tested on a new participant interacting with Kuka robot in 1D-X.

So, using force myography biosignals as the only input in learning human activities appears promising in pHRI, developing safe collaborations, rehabilitation applications, or prostheses control to interact with machines on daily basis.

## Chapter 2.

### Literature Review, Materials & Methods

The material presented in this chapter is excerpted, reproduced, and modified with permission from the following papers:

[56] U. Zakia and C. Menon, "Estimating Exerted Hand Force via Force Myography to Interact with a Biaxial Stage in Real-Time by Learning Human Intentions: A Preliminary Investigation", *Sensors*, vol. 20, no. 7, (22pp), Apr. 2020.

[57] © [2021] IEEE with permission. U. Zakia and C. Menon, "Toward Long-Term FMG Model-Based Estimation of Applied Hand Force in Dynamic Motion During Human–Robot Interactions," in *IEEE Transactions on Human-Machine Systems*, vol. 51, no. 4, pp. 310-323, Aug. 2021, doi: 10.1109/THMS.2021.3087902.

[58] U. Zakia and C. Menon, "Force Myography-Based Human Robot Interactions via Deep Domain Adaptation and Generalization," *Sensors*. 2022; 22(1):211. <https://doi.org/10.3390/s22010211>.

[59] © [2022] IEEE with permission. U. Zakia and C. Menon, "Human Robot Collaboration in 3D via Force Myography based Interactive Force Estimations using Cross-Domain Generalization," *IEEE Access*, Mar. 2022, doi: 10.1109/ACCESS.2022.3164103.

[60] © [2022] IEEE with permission. U. Zakia, A. Barua, X. Jiang, and C. Menon, "Unsupervised, Semi-Supervised Interactive Force Estimations During pHRI via Generated Synthetic Force Myography Signals," *IEEE Access*, June 2022, doi: 10.1109/ACCESS.2022.3187115.

Sections of this chapter are reprinted or adapted from the above articles for clarification and to fit the formatting and scope of this chapter.

## 2.1. Chapter Overview

In this chapter, background study and literature review on related research work briefly outlined. The materials, experimental setups and methods followed to address the research questions in this thesis are summarized too.

## 2.2. Human robot interactions

In the last 60 years, robots are being employed in the automotive industries. The assembly lines of car manufacturer companies rely on the industrial robots to increase quality and capacity while reducing production time and costs. Engaging robots in the heavy, difficult, and dangerous works have relieved human workers and offer better safety. Also, health hazards such as musculoskeletal disorders resulting from lifting, twisting and repetitive motions can be prevented with the aid of robots performing those tasks. In the last few decades, human robot interaction (HRI) has been observed as a growing interest in the manufacturing environments. Since industrial robots are heavy machineries, despite the safety measurements, there are possible threat of injuries for human workers. Statistics reveal that the common injuries for human workers occur in the wrists or hands (38%) as exposures to immense mechanical forces by the robots [9, 10].

HRI emphasizes the needs of safety precautions as a ground rule. Various safety measures are implemented in the industrial workplaces where human workers are present with robots. To prevent collisions between humans and uncaged robots, a vision system is used to detect humans around the workspace of a robot [4]. While cameras can be used for this purpose, they are still bulky and require high computational resources. An alternative technique is to use ultrasonic transceivers that are usually directional and should be arranged into an array to obtain a reliable image of the surroundings [5-6]. Even though humans are relatively large targets, the amount of ultrasound reflections from them is quite small because humans absorb most of the ultrasonic energy. Another family of proximity detector are capacitive sensors, which can be employed to detect the presence of a wide variety of materials [7]. A challenge of using capacitive sensors is their relatively short range which is typically between 10 $\mu$ m to few tens of centimeters. Magnetic sensors may also be used for proximity detection. However, the main limitation of typical magnetic sensors is that they only detect conducting materials over short ranges [7].



## 2.2.1. Learning human activities in HRI

To understand human activities, recent research focus on including human biosignals during collaborative tasks. Wearable safety devices for workers monitoring biosignals can help adopting safety designs in the industrial environment. AB Research report suggests that enterprise wearable devices will be dominating in workplaces and by 2021, wearable devices would be around 154 million [46]. Popular wearable devices are targeted for industrial and consumer markets such as body sensors, smart glasses, smart watches, fitness trackers, smart clothing, wearable cameras etc. Among these wearable sensing systems, many techniques mainly aim at detecting collisions of the hand with moving objects. Therefore, both position and applied force of the hand should be monitored. A data-glove, such as the Cyber glove [47] which incorporates both inertial measurement units (IMUs) and flexible bend sensors, could be used to measure the position. However, data-gloves limit the tactile sensation of the user's fingers.

Human robot interactions are carried out for performing collaborative tasks where human interacts with a robot mainly through object handling/takeover, reaching for

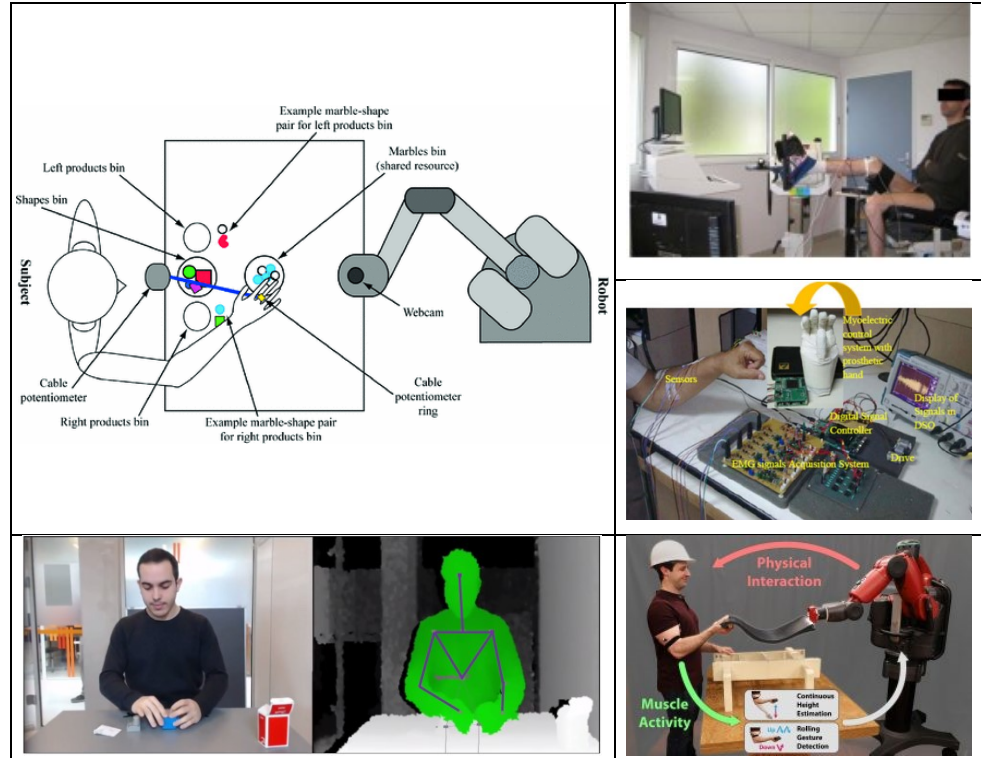


Figure 2.1. Human robot collaborations. Reproduced from [22, 25, 52, 53, 54] with permissions.

different objects on a workbench, reaching predetermined targets, object transporting, as shown in Figure 2.1. To understand human intentions, arm motions are learned through vision systems such as 3D depth sensor, 3D camera, motion tracking sensors, biomarkers, tactile sensors, IMU sensors, force sensors [48-54]. These sensors can be attached to the robot's body (end-effector, joints, or surface) or around the environment within the workspace. In research, some of these sensors are attached to human body to include biosignals to understand human activities during interactions. Biosignals can be measured, monitored continuously, and offers better user mobility while providing bio feedback.

Learning human intentions during collaborative tasks with robots is vital in a dynamic and uncertain environment. Much research is carried out to understand human physiological activities by continuously measuring and monitoring biosignals. A variety of biosignals such as, electroencephalogram (EEG), electrocardiogram (ECG), electromyogram (EMG), electrooculogram (EOG) are well known examples of biosignals. Among these, the sEMG signals have been studied in learning human intentions to enhance collaborative interactions during physical HRI (pHRI) [22-28], as shown in Figure 2.2. Machine learning techniques (such as artificial neural network (ANN), 3D convolutional neural network (CNN), support vector regression (SVR), linear discriminant analysis (LDA), K-nearest neighbor (KNN)) are implemented for estimating motion intention is integrated into adaptive impedance control.



*Figure 2.2. sEMG signals to understand human activities during collaborative task. Reproduced from [55] with permission.*

Human robot collaboration requires sharing the workspace while complementing each other. The robot can perform a regular task efficiently and effectively while the human partner can provide reasoning to understand environments and uncertainties involved. Understanding human intention of motion is critical in control design during physical collaboration. Human activity can be defined as intentional, purposive, conscious, and subjectively meaningful sequences of actions. In this regard, to make the robot track a prescribed trajectory is not applicable. Utilizing impedance control scheme [64], the robot can be in compliant collaboration by changing its motion according to the applied hand force of the human partner during interactions. Intentions of changing motion will act as a load, so applied hand force in intended motion needs to be estimated and integrated into the robot control.

### **2.3. Force measurements using myography techniques**

Over the past several decades, many studies have been carried out to characterize dynamic and kinematic aspects of human movements. In particular, force measurements of human body have become an important aspect in various fields, including human-robot interaction (HRI), rehabilitation, and neuromuscular diagnostics. Using commercially available force/torque sensors to monitor direct force measurements of human body is advantageous. Even though this method frees the hand and allows full tactile sensation, attaching these transducers to the robot's body can limit human movements within the workspace. In addition, they are bulky, expensive, and requires special signal processing equipment. So, these sensors are hard to be wearable on human body to detect hand force. Thus, indirect force measurement is appropriate for free human movements.

Wearable sensing systems incorporating myography sensors are considered as a good alternative of the direct force measurement methods. Examples of these wearable systems include surface electromyography (sEMG) and force myography (FMG) signals. sEMG is a good source of information about muscle activity by registering electrical activity due to muscle contraction. This is a non-invasive technique that can interpret electrical activities associated with muscle contraction variations under the skin. This typical technique has been studied for gesture recognition, hand force recognition, prosthetic limb controls, rehabilitation applications, and in pHRI [17-28]. But the electrical signals that the sEMG electrodes are measuring is weak and requires extensive signal processing. These electrodes require an accurate placement and excellent contact to the skin. In addition,

complex signal processing is required to make use of the signals.

The contemporary FMG signal has gained momentum in innovative and novel device design over the typically dominated sEMG. Figure 2.3. shows an FMG band using off-the-shelf 8 force sensing resistors (FSRs) of approximately 30 cm long. Voluntary muscle changes are read from the FSRs with voltage divider circuit through a DAQ (b) and are passed to a computer for further processing [29]. Engaging force myography signals using machine learning techniques for a variety of applications such as gesture recognition, prosthesis control, grasp force, isometric hand force, rehabilitations are found very promising [30-42], as shown in Figure 2.4.

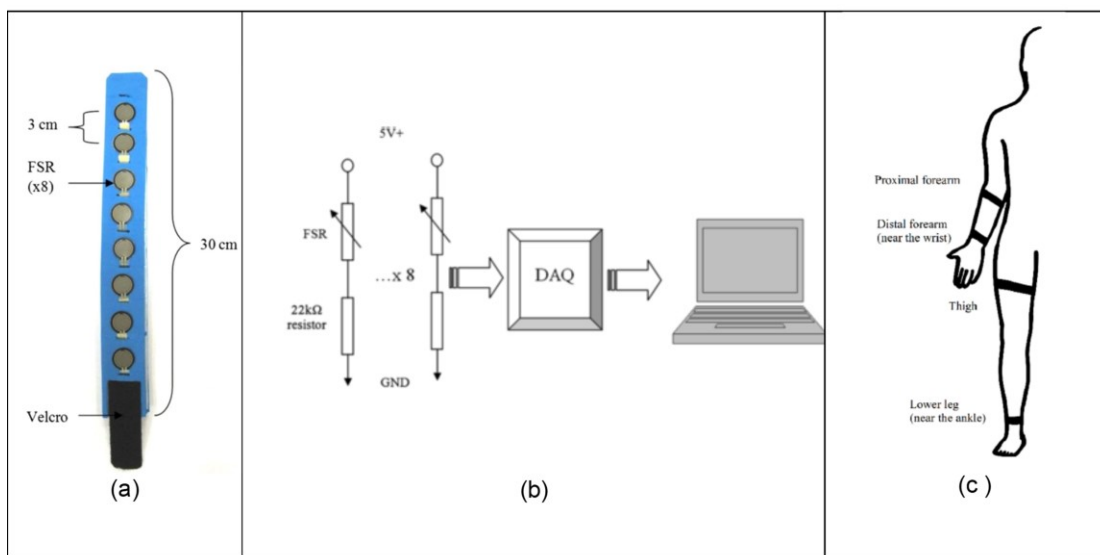


Figure 2.3. (a) A wearable FMG band, (b) data communication to a computer using DAQ, and (c) bands placements in upper and lower limb. Reproduced from [29],[30] with permissions.

Research shows that FMG is low cost, easy to implement, simple signal processing, and a better choice for human machine interfacing (HCI) [43]-[45]. This technique has several advantages such as: (1) robust to external electrical interference and sweating, (2) does not require for sensors to be placed at specific anatomical points on the body or extensive skin preparation, (3) does not require complex signal processing like sEMG, (4) cost effective method of tactile sensing, with off-the-shelf discrete force-sensing resistors, and (5) provides repeatability and less variable in time. Thus, FMG technique can be a viable alternative to the traditional sEMG technique. Although sEMG signals are studied in human robot collaboration over the last few decades, there is a research gap in FMG based pHRI by learning human intentions. Therefore, in this

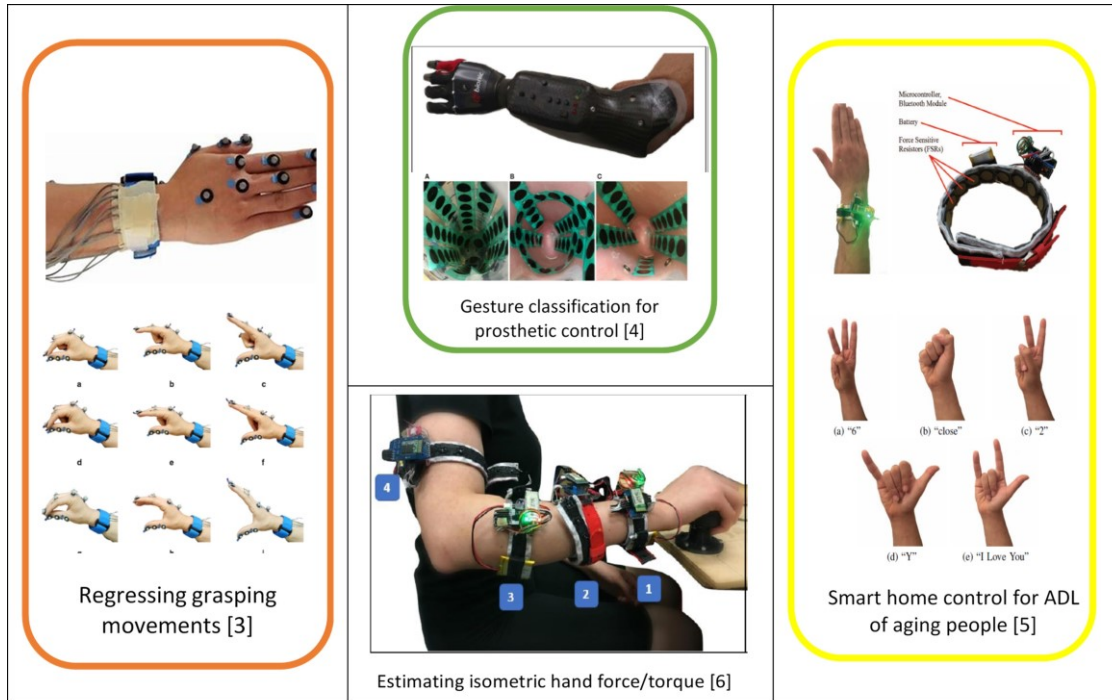


Figure 2.4. Some applications of FMG signals. Reproduced from [32, 33, 38, 40] with permissions.

research, human activities were estimated via FMG technique.

## 2.4. Materials and Equipment

This section discusses the materials, equipment and experimental setups used in this thesis. The rationalities behind each setup are also explained. Using higher or lesser no. of FMG channels and their positions on upper extremities were investigated for suitable practical situations. Interactions in 1D and 2D planes with a simple linear robot that had 2-DoF were investigated for recognizing human actions. Interactions with a 7-DoF Kuka robot in 1D, 2D and 3D planes were further investigated to understand FMG-based force estimations and associated challenges in industrial applications.

### 2.4.1. Upper arm and Forearm FMG Bands

Two custom-made wearable FMG bands, as shown in Figure 2.5 were specifically developed by the author for the studies conducted in this thesis to read muscle contractions from forearm and upper arm positions during interactions. These positions were selected based on the previous studies in the literature [40] that could provide useful

information of the exerted human grasping forces in dynamic motions. Two FMG bands on the forearm and upper arm positions were used to maximize muscle volumetric readings during interactions with a biaxial stage (linear robot). These data were used in objective 1, and 2 and 3. One forearm FMG band was used during interactions with a Kuka robot and was used in objective 3 and 4. The use of one band was reasonably chosen considering a human worker's comfort and ease of wearability while reading enough interactive force data with lesser channels, appropriate in a practical industrial scenario.



*Figure 2.5. Custom-made Force myography bands. Reproduced from [56] with permission.*

The FMG band was made of FSRs whose resistances changed as the muscles contracted. The FSRs exhibited high resistances ( $\sim 10 \text{ M}\Omega$ ) at no pressure, and their resistances decreased as the pressure increased (during interactions). These sensors had an active area of 14.7 mm, actuation forces less than 15 g, and a pressure sensitivity range of 100–200 psi (pound of forces per square inch). Figure 2.6 shows the biaxial stage with a gripper securely placed on the planar horizontal surface of a table (6 inches) and could easily sense muscle contractions in the underlying skin. Each band had 16 FSRs (TPE 502C, Tangio Printed Electronics, Vancouver, Canada) [62], approximately 30 cm long, and were wrapped around forearm and upper arm muscles. Using voltage dividers to extract signals from these sensors, two data acquisition (DAQ) devices with a 16-channel analog input (NI USB 6259 and 6341, National Instruments, Austin, TX, US) were used for FMG data acquisition from these bands at 50 Hz.

## 2.4.2. Biaxial Stage / Linear robot (2D-pHRI)

Data collected during interactions with a custom-setup of a linear robot/ biaxial stage was used in studies conducted for research objective 1, 2 and 3. This simple setup was used for applied force interactions in 1D and 2D planes. Understanding human intentions to manipulate the linear robot in any directions of 1D was carried out at first and then were followed by complex interactions in dynamic motions in the 2D plane.

The linear robot had two perpendicular linear stages (X-LSQ450B, Zaber Technologies, Vancouver, BC, Canada) in X and Y directions on a planar surface. Both linear stages had built-in motor controllers for desired translational movements [63]. The biaxial setup used in this thesis resembled a 2-DoF robotic arm (XY-plane). It was a type of gantry-positioning stage sometimes known as a linear or cartesian robot. The stages had 450 mm travel distance, support up to 1 m/s speed and 100 N thrust; these were chosen because of high stiffness and back drivability. Binary communication protocol is used to exchange commands between the biaxial stage and the FMG-based real-time integrated controller at 9.6 kbps. A customized 3D printed knob was designed and created using ABS material and was used as a gripper mounted on top of the biaxial stage; this allowed participants to grab the gripper/knob and applied forces to slide it on the planar surface during real-time interactions. External forces acting upon the biaxial stage were measured using a 6-axis force torque sensor (mini45, ATI industrial automation, Apex, NC, USA) [64]. It is placed inside the gripper/knob to measure true label data of exerted hand forces during interactions. Figure 2.6 shows the biaxial stage with a gripper securely placed on the planar horizontal surface of a table. We did not conduct the study using

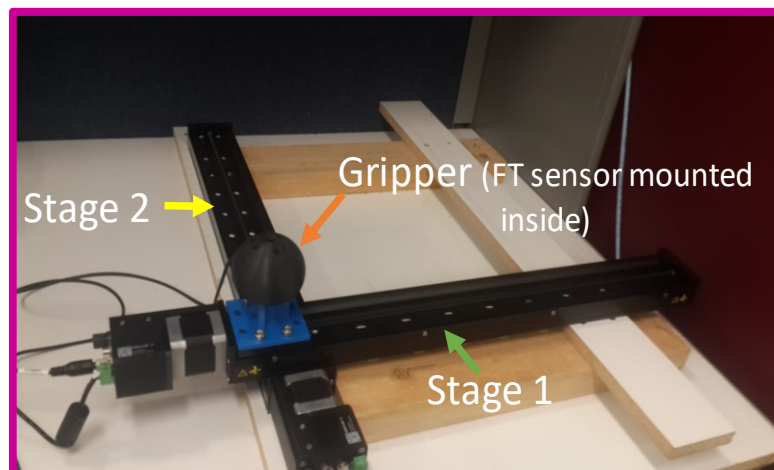


Figure 2.6. A 2-DoF linear robot/ biaxial stage. Reproduced from [56] with permission.

vertical placement of the biaxial stage because the pHRI study was also conducted with an industrial Kuka robot in a variety of 1D, 2D and 3D planes covering all. So, conducting interactions with the biaxial stage on a vertical surface was not necessary and would have been time-consuming.

For the real-time control design, a traditional admittance control scheme was implemented [65]. Therefore, external forces applied to a gripper/knob were translated into torques at each joint, and the stage moved to a new position based on the calculated displacement. The kinematics of the considered biaxial stage was shown as:

$$\begin{pmatrix} x \\ y \end{pmatrix} = \begin{pmatrix} 1 & 0 \\ 0 & 1 \end{pmatrix} \begin{pmatrix} d_x \\ d_y \end{pmatrix} \quad (2.1)$$

where  $x$  and  $y$  were the end positions of the gripper, and  $d_x$  and  $d_y$  were the displacements of the biaxial stage in the  $x$ - and  $y$ -directions, respectively. Actual and estimated hand forces ( $N$ ) were first converted to velocities ( $mm/s$ ) for the motor controllers of the stage and then as micro steps (*displacements*) per seconds according to Equation (2.2) as in the documents from Zaber technologies, which was written as [63]:

$$\mathbf{Displacement}_{x,y} = \mathbf{Velocity}_{x,y} / (\mathbf{Microstepsize}_{x,y} / 1000 / 1.638) \quad (2.2)$$

Interaction between a participant and the biaxial stage in real time is shown schematically in Figure 2.7. The participant could freely slide the gripper on the entire

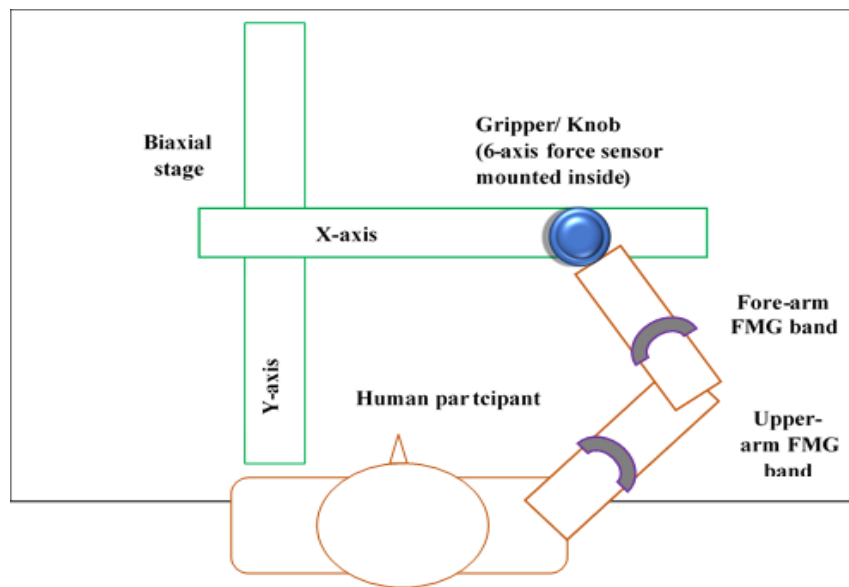
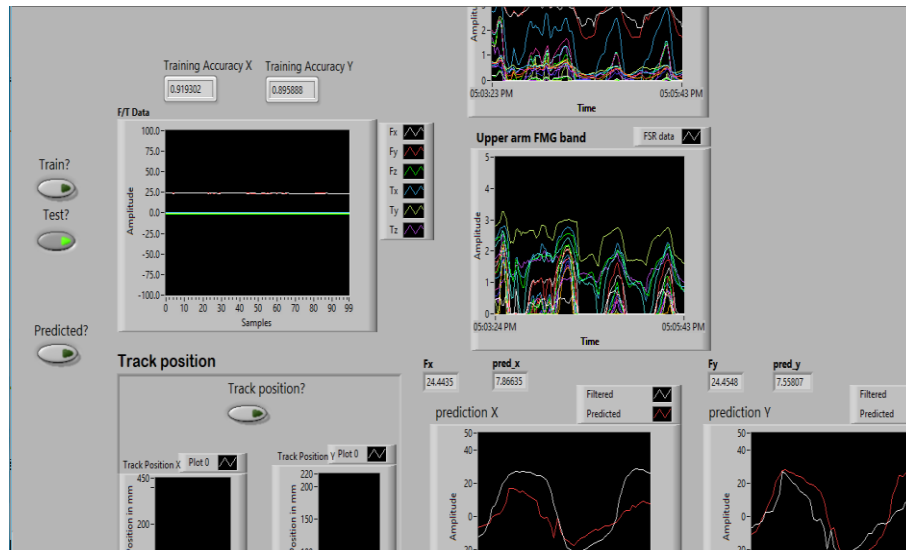


Figure 2.7. Top view of a human participant wearing FMG bands on upper extremity (UE) interacts with the biaxial stage by grasping the gripper/ knob. Reproduced from [56] with permission.

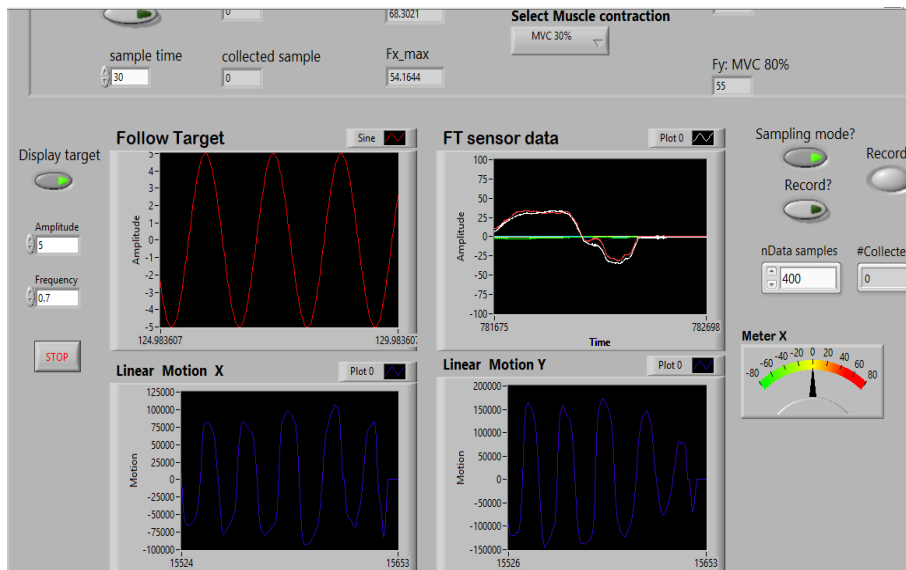


workspace by an exerted hand force. All mechanical devices were synchronized properly for real-time operation, and fine tunings were implemented to reduce the stiffness and smooth control of the manipulator. These measurements helped reducing muscles fatigue by smooth interaction with the biaxial stage while avoiding damages to the hardware.

The real-time FMG-based integrated controller was implemented as a LabVIEW interface (LabVIEW 2014, National Instrument, Austin, Texas, USA) that controlled the mechanical system components. It used MATLAB scripts (MATLAB, MathWorks, Natick,



(a)



(b)

Figure 2.8. Labview interface of the RT FMG-based integrated controller: (a) control pane of FMG-based force estimation, (b) display pane of a target motion pattern to follow and maintain muscle volumetric contraction (MVC). Reproduced from [56] with permission.

MA, USA) to implement regression models for force estimation with FMG signals, as shown in Figure 2.8.

Controlling the biaxial stage in real time with dynamic forces exerted by human hands involved careful system design considerations. The allowed external forces applied to stage were between 3 and 90 N, and certain ranges of MVC (30% and 80%) were maintained to keep the limits of the maximum thrust for proper operations of the linear stages. The smooth sliding of the gripper was ensured for the participant's comfort and ease of control. An HP Zbook laptop (HP, Palo Alto, California, USA) with Intel Core i7 was used for implementing the real-time FMG-based integrated controller. The higher data acquisition rate (50 Hz), high-speed computations, and data transmission to the biaxial stage (9.8 kbps) with a minimal time delay (within 8ms) made the real-time control achievable.

### 2.4.3. Kuka robotic arm (3D-pHRI)

Studies conducted in objective 3 and 4 used the 7-DoF Kuka robotic arm for implementing FMG-based human-robot interactions in 1D, 2D, and 3D planes. This setup

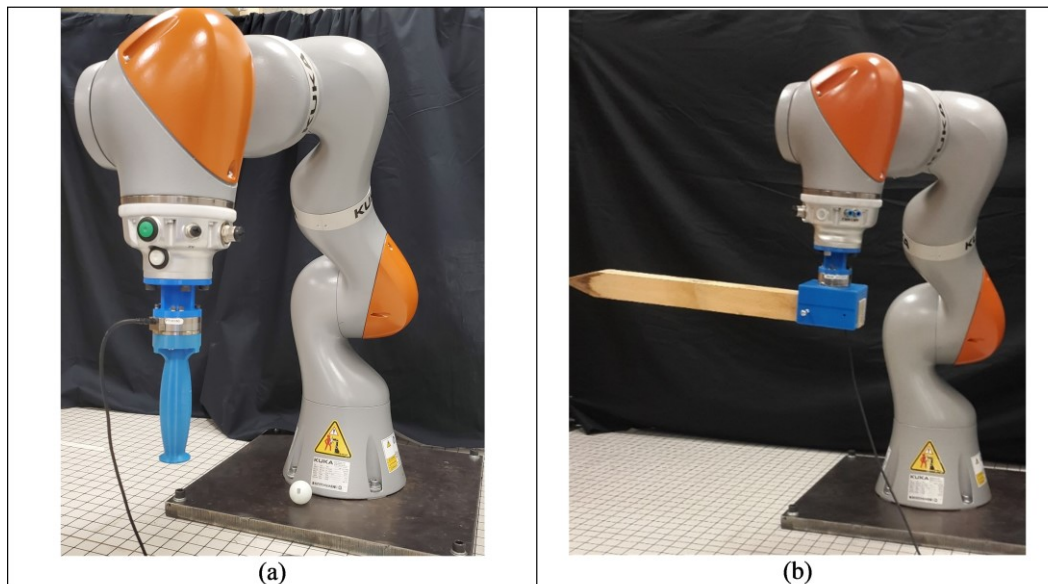


Figure 2.9. Experimental setup of pHRI & HRC with the Kuka robot, reproduced from [59] ©[2022] IEEE with permissions.

(a) by grasping a cylindrical gripper attached as the EEF, (b) collaboratively moving a wooden rod from point A to point B attached at the EEF of the robot.

represented real-world situations where interactions could occur in any directions as both human arm and the robotic arm could have redundant degree of freedom (DoF) of trajectories in the 3D space.

The advanced KUKA LBR IIWA 14 R820 collaborative robot featured a 14 kg payload, with 820 mm reach and Protection Class IP54 rating [66]. It had built-in torque sensors in all joints and had its own controller known as 'Kuka Sunrise Cabinet'. The Kuka robot was securely mounted on a table and its surroundings were caged for safety measures. For pHRI activities, a custom-made cylindrical gripper was attached as the end-effector of the robot via a customized adapter developed by the author (Figure 2.9 (a)). A 6-axis FT sensor (NI DAQ 6259, National Instruments, Austin, TX, US) was placed between the gripper and the adapter for true label generation. The orientation of the gripper was always at  $\{0, \pi, 0\}$ , thus the gripper-handle pointed downwards for easy human grasps.

For HRC activities, a wooden rod was attached to the robot for bearing the load during a collaborative HRC task in 3D space (Figure 2.9(b)). The 45 cm rectangular wooden rod was attached to the flange of the robot. The rod was firmly connected at one end [oriented at fixed angle  $\{0, \pi, 0\}$ ] via a custom-made adapter developed by the author while the other end was parallel with the horizontal X dimension in the 3D plane, free to grasp and apply force. The rod weighed approximately 5 lb including the adapter. The 6-axis FT sensor via NI DAQ 6259 was placed in between the adapter and the end-effector for true force readings. Interaction forces were applied at the tip of the cantilever rod.

Compliant collaboration using torque control was implemented where the robot moved in space proportional to the applied human forces and directions. MATLAB scripts were written (MATLAB, MathWorks, Natick, MA, USA) using Kuka Sunrise Toolbox to run externally on a desktop PC (Intel Core i7 processor and Nvidia GTX-1080 GPU) with V-REP robot simulator and to communicate with Kuka Sunrise Controller. It allowed a participant to move the wooden rod from point A to point B in a half-circular 3D path where displacements and trajectories were governed by the applied forces and directions.

For safe interactions, the Kuka robot would react to minimum of 2N of external forces while the maximum forces in X, Y, Z was within 15N to 25N. The 7-axis joint speed limits were set to  $\{50, 50, 70, 75, 70, 75, 75\}$  degree/s while maximum speed of forced



Figure 2.10. Force control implementing compliant collaboration with the Kuka robot via external interactive applied force.

move was kept at 70 cm/s. For force control, desired joint angles were read from the V-Rep simulator from Coppelia Robotics using inverse kinematics and sent to the Kuka Sunrise Controller, current position and orientations of the EEF was collected from the Kuka Sunrise Controller, and the desired EEF position was generated based on the EEF force and position, as shown schematically in Figure 2.10. In 3D, the displacements were calculated such as:

$$Displacement_{x,y,z} = (speed\_forced\_move * EEF\_force\_current/abs\_force) * s\_interval \quad (2.3)$$

where speed\_forced\_move was set at 70 cm/s, EEF\_force\_current was the external force readings, abs\_force was the magnitude of the current force exerted on the flange, and sampling interval (s\_interval) was 0.025s.

The displacements range of the Kuka robot was kept within certain boundaries during interactions in 1D (X, Y, Z directions), 2D (XY, YZ, XZ planes) and 3D (XYZ plane), as shown in Table 2-1. These values were the selected boundaries in X, Y and Z directions for each type of HRI interactions with the Kuka robot. Even when the interaction was in 1D-X, the set boundaries in X, Y and Z allowed human participant and the Kuka robot to interact comfortably within a narrow, 6-axis rectangular area instead of strictly following one path trajectory in a certain direction.

## 2.5. Participants

In objective 1, 10 right-handed healthy participants (9 males and 1 female) with the mean age of 33 voluntarily took part. In objective 2, 15 healthy participants (12 males and

Table 2-I: Trajectory boundaries set for safe interactions with Kuka robot

<i>In 1D:</i>	<i>In 2D:</i>	<i>In 3D:</i>
<b>For 1D-X</b>  In X direction: from 0.4 to 0.7 m, In Y direction: from -0.3 to 0.2m, In Z direction: from 0.4 to 0.42m	<b>For XY</b>  In X direction: from 0.45 to 0.65 m, In Y direction: from -0.3 to 0.2m, In Z direction: from 0.4 to 0.42m	X Dimension: 0.2: 0.6 m  Y Dimension: -0.5:0.5 m  Z Dimension: 0.2:0.7m
<b>For Y#</b>  In X direction: from 0.6 to 0.6 m, In Y direction: from -0.35 to 0.2m, In Z direction: from 0.4 to 0.4m	<b>For YZ #</b>  In X direction: from 0.6 to 0.62 m, In Y direction: from -0.3 to 0.2m, In Z direction: from 0.3 to 0.45m	
<b>For Z</b>  In X direction: from 0.6 to 0.7 m, In Y direction: from -0.3 to 0.2m, In Z direction: from 0.25 to 0.7m	<b>For XZ</b>  In X direction: from 0.45 to 0.65 m, In Y direction: from -0.1 to 0.25m, In Z direction: from 0.3 to 0.5m	
<b>In summary:</b>  X: 100-300mm  Y: 400-500mm  Z: 200-700mm	<b>In summary:</b>  X: 450-650mm  Y: 100-500mm  Z: 300-500mm	<b>In summary:</b>  X: 200-600mm  Y: 50- 500mm  Z: 200-700mm

3 females) voluntarily participated for the 1<sup>st</sup> study. In the 2<sup>nd</sup> study, a total of 6 participants (all males) volunteered in this study. In objective 3, 6 participants (all males) volunteered as end-users. Finally, in objective 4, one healthy adult (male) participated. In some cases, time was limited, and it was hard to find volunteers. In objective 1, 2A, 2B, 3, and 4, a total of 10, 15, 6, 6 and 1 participants, respectively, voluntarily contributed to the studies. There was statistical significance for the sample sizes in objective 1-3. In objective 4, we did a pilot study with 1 participant only and did not run significance testing on the sample size.

All participants were healthy, right-handed and their average age was 33±8 years. Demographics of the participants are given in Table 2-II. Generally, participants had no prior knowledge about the FMG technique. All participants acknowledged the study protocol and gave their written consent as approved by the Office of Research Ethics at Simon Fraser University, Canada.

Participants ranging from 22 years to 47 years of age, of diverse ethnicities and

different demographics were involved. Results indicated that the machine learning models generated in these studies were capable of recognizing applied forces in certain directions of arm motions despite their demographic variations.

*Table 2-II. Demographics of the participants. Reproduced from [56] with permission.*

Feature	Age (year)	Height (cm)	Arm length (cm)	Upper arm (cm)	Forearm (cm)
Mean	33	175	74	29	27
Standard deviation	8	5	4	3	3
Mode	35	178	78	29	27

## 2.6. Methodologies

The data driven approaches and machine learning algorithms used in this thesis are discussed in this section. For regression analysis, initially we implemented traditional machine learning algorithms via supervised learning and then gradually moved towards deep learning algorithm via supervised transfer learning approaches. In the final stage of the thesis, adversarial algorithm via semi-supervised (few labelled training data) and unsupervised learning (unlabelled training data) was implemented. Therefore, we started with simple approaches and progressively focused on complex methods to estimate interactive forces via force myography signals.

To solve real-world data scarcity scenario, few concepts and methods were investigated. For generalization of a trained model, generalized zero-shot learning and transfer learning were found effective via quick calibration (retraining a pretrained model with a few target training data). Three different transfer learning approaches such as domain adaptation, domain generalization and cross-domain generalization were investigated for FMG-based pHRI. These approaches focused on solving situations that became gradually difficult.

### 2.6.1. Regression algorithms

In this thesis, we progressively investigated supervised, semi-supervised and unsupervised machine learning algorithms from objective 1 towards objective 4. The traditional machine learning algorithms were studied and found effective for intra-subject analysis. While for transfer learning approaches (model generalization), deep learning

algorithms were found appropriate for fine-tuning with calibration data. Transfer learning allowed using a pretrained model during evaluation; this saved time in collecting a few target training data only and facilitated faster finetuning of the model within few seconds for recognition of the target test data. Unsupervised generative adversarial network and semi-supervised self-training algorithms in the final stage of the thesis proved as realistic and reliable approaches in industrial pHRI environments.

## A. Supervised learning

In objective 1, two supervised regression models, the support vector regressor (SVR) and the kernel ridge regressor (KRR) were used [67]. The popular, traditional SVR algorithm was also used in the 1<sup>st</sup> study of objective 2. In the 2<sup>nd</sup> study of objective 2 and objective 3, the convolutional neural network (CNN) algorithm was implemented. Hence, studies conducted in objective 1 to 3 used supervised learning technique. All these algorithms were implemented from scratch using MATLAB running in external laptop or desktop in Windows platform.

### *i) Traditional Machine Learning Algorithms*

For force estimation during interactions with the biaxial stage, the SVR and the KRR were chosen among several other machine learning techniques (such as the multidimensional SVR (MSVR) and the general regression neural network (GRNN)). The SVR is a well-known regressor useful for the regression of real-time signals, while the KRR is reported to perform better with small datasets [68]. The selected features and hyperparameters were chosen carefully to create relevant separation among hyperplanes such as  $L_2$  regularizers, and penalty functions (Cost and Lambda), as shown in Table 2.III. Data preprocessing, i.e., scaling both training and test datasets (between 0 and 1), was required. The enhanced performances of the selected radial basis function (RBF) kernel features (also known as Gaussian kernel) of both algorithms were observed. The regressors differed in the loss functions, as the SVR used an epsilon-insensitive function and the KRR used a least squared error function. The best values for Cost (C) and Gamma (G) of the SVR model were obtained by grid searches. The regularization penalty (lambda) and the kernel width parameter of the KRR were selected through trial and error. These algorithms were preferred because of lower computational time, special features of the SVR and the KRR (such as a higher number of support vectors and kernel trick), and ability to handle real instantaneous data. Therefore, real-time training and testing of force

Table 2-III. Regression models parameters. Reproduced from [56] with permission.

Model	Hyperparameters ranges	Parameter selection	MATLAB toolbox
Support vector regressor (SVR)	Cost = 20, Gamma = 1	Grid search	livsvm
Kernel ridge regressor (KRR)	Lambda = 1, Kernel width parameter = 0.9	Trial & Error	Kernel methods toolbox

estimations in motions were possible with their appropriate features and provided reasonably higher performances.

### ii) Deep Learning Algorithm

The popular deep learning algorithm, convolutional neural network [69] implemented in objective 2B and 3 had different network architectures for learning the discriminative feature distributions collected from the 2D-pHRI and 3D-pHRI platforms. The CNN models with different architecture were generated from scratch using MATLAB and Python in Windows platform. Detailed discussions are presented in relevant chapters.

Figure 2.11 shows the proposed FMG-CNN architecture used in Objective 2B. Raw FMG signals were used for training and evaluating trained model for supervised domain adaptation (SDA) and supervised domain generalization (SDG). For 2D-pHRI, two separate models such as Model X and Model Y were constructed from scratch using MATLAB code to estimate forces in X and Y direction. In both model's architecture, an

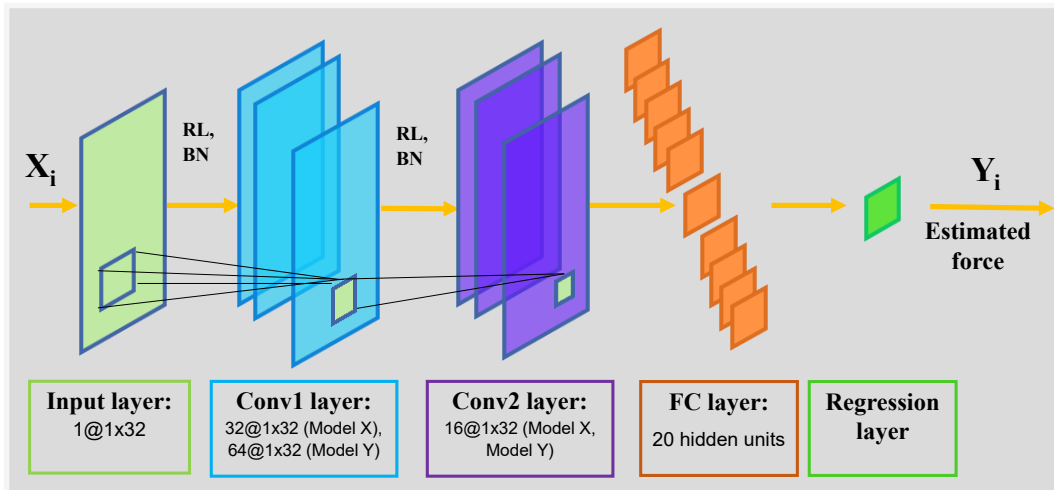


Figure 2.11. Proposed FMG-CNN architecture (Model X, Y). Reproduced from [58] with permission.



input layer of input size  $1 \times 32$  with “zerocenter” normalization was used. Both models had conv1 and conv2 convolutional blocks. Raw data was preprocessed using minmax scaling before passing to the input layer. In each convolution block, the conv layer was followed by a Relu and a batch normalization layer. For Model X, 32 filters were used in the conv1 block, while 64 filters were used for Model Y. The conv2 layer had 16 filters in both models. A fully connected layer with 20 connections followed the conv layers, and finally, a regression layer was used to map the instant force. Batch normalization helped to alleviate the internal covariance shifting present during training, as changes happened in input distributions of layers due to parameter changes in previous layers. Filters sized  $3 \times 3$  with a stride of 1 and a padding of 1 were used. During evaluation, fine-tuning occurred in the final fully connected layer. For both pretraining and fine-tuning, stochastic gradient descent (SGD) was implemented as the optimizer. Stochastic gradient descent helped to find the model parameters that corresponded to the best fit between predicted force and actual force. It’s an imprecise but powerful technique and was found suitable for our regression problem. A learning rate (LR) of  $1E-04$  and maximum epoch (E) of 40 were used in pretraining, while  $LR = 1E-05$  with  $E = 60$  was used during evaluation. MSE loss was used for validation of the training process.

In objective 3, an FMG-based deep convolutional neural network (FMG-DCNN) architecture was proposed for pretraining a transfer learning model with cross-domain generalization (TL-CDG). For FMG-based HRC in 3D, three separate models (Model X, Y and Z) were pretrained for predicting applied forces in that direction. For pHRI in 1D (either in X, Y or Z direction), only one relevant model was developed using MATLAB code and pretrained. Input data was normalized (minmax scaling) and passed to the input image layer [image size  $1 \times 34$  with ‘zerocenter’ normalization]. Few convolutional blocks were customized “in house” particularly for this problem using MATLAB code and were implemented sequentially where each block had a conv2d layer followed by a ReLu and a batch normalization layer. For Model X and Y, two convolutional blocks (conv1 and conv2) were used while three blocks (conv1, conv2 and conv3) were used in Model Z. 32 and 16 filters in Model X, 64 and 32 filters in Model Y and 32, 16, 8 filters in Model Z were used in the consecutive convolution layers, respectively. Two fully connected layers (FC1 and FC2) with 20 and 10 connections followed the conv blocks in consecutive order. A final regression layer mapped the instant force from the incoming feature spaces. The  $3 \times 3$  filters with a stride of 1 and a padding of 1 were used in each conv2d layer. For

optimization, stochastic gradient descent (SGD) was implemented with a learning rate (LR) of 1E-05 for maximum 60 epochs during pretraining.

## B. Unsupervised learning

Unsupervised and semi-supervised learning techniques were implemented in objective 4. Here we studied pHRI scenarios where labelled data were scarce, or data were unlabeled. To address such a real-world problem, we used unsupervised and semi-supervised approaches that required no labels or very few labels. The unsupervised, generative adversarial network (GAN) [70] model was implemented in this study. For the semi-supervised learning, a weakly supervised self-training approach was implemented.

### *i) Generative adversarial network*

In the GAN architecture, two separate models were engaged as discriminator (model D) and generator (model G). The model G was engaged in generating fake FMG signals while model D was employed to learn the discriminative feature distributions of both real and fake signals and classify them accordingly. We used this architecture to generate real-like synthetic FMG data and accumulate adequate training data for pretraining a transfer learning model. For model G, inputs were either noise signals ( $N_s \in \{X_N\}$ ) or transformed FMG signals ( $T_s \in \{X_{Ts}\}$ ) with shapes of (1, 100, 1), or aggregated noise and transformed signals. Model D received real FMG signals ( $D_c \in \{X_{C1}, X_{C2}\}$ ) and fake FMG signals/synthetic data ( $D_{sj} \in \{S_D\}$ ) generated by model G, where both inputs to model D were shapes of (1,16,1).

### *Model G Architecture*

Three successive convolutional 2D transposed (conv2DTranspose) layers [no. of filters: 128, 64, 1 and filter size: (1, 5), (1, 10), and (1, 5)] were implemented with strides of (1, 1), (1, 4), and (1, 2) and the 'same' padding. Each conv2DTranspose layer was followed by a batch normalization layer and a leaky ReLu layer. For the final output of fake generated signal ( $S_D$ ) of a shape of (1,16, 1), the tanh activation function was used. This architecture was used in 1D-X, Y and Z dimensions.

### *Model D Architecture*

Two convolutional (conv) blocks were implemented via Python code sequentially where each block had a conv2D layer followed by a leaky ReLu and a dropout layer with

a rate of 0.3 to reduce overfitting. Convolutional 2D (conv2D) layers were implemented with strides of (1, 2) and the 'same' padding. The number of filters used in the conv blocks for 1D-X dimension was 32, 16, 1, while it was 128, 64, 1 in 1D-Y and Z dimensions with the same filter sizes of (1, 5), (1, 10), and (1, 5) in each dimension. The convolutional blocks were followed by three dense layers of 20, 10 and 1 neurons for 1D-X while only one dense layer of 1 neuron was used for 1D-Y, and Z. A sigmoid function was used to classify the real input and the generated signals.

### *ii) Self-Training*

In this method, several steps were followed for semi-supervised learning where training data were mostly unlabeled. A few labeled training data were used in step 1 to pretrain the discriminator model (D). In step 2, this model was evaluated in predicting pseudo-labels for the large volume of unlabeled data. With the labeled and pseudo-labeled data, the model was retrained again in step 3. Finally, in step 4, the model was evaluated on target test data.

## **2.6.2. Data Driven Concepts and Approaches**

In this thesis paper, a few concepts were explored in developing data-driven models for practical implementations. Specially, model generalization was investigated as a viable solution in daily, regular usage of the FMG band. A generalized model that could estimate forces in dynamic motion for any participant or in any intended direction was desirable to simulate real-life applications. The generalized zero-shot learning method was studied because of transient nature of the FMG biosignals and was found effective for recognizing instantaneous signals. Real-world data scarcity was overcome by several transfer learning approaches. Such as, domain adaptation and domain generalization methods were studied during pHRI in 2D while cross-domain generalization was investigated for cross-platform pHRI application between 2D and 3D workspace. Hence, these methods gradually and successfully addressed step by step the practical limitations and difficulties associated with FMG-based HRI applications.

### ***A. Generalized zero-shot learning***

In machine learning, the ability of a trained model to fit unseen test data without compromising performance is essential for many real-world applications. To predict

categories or regressing new, unlearned test samples, zero-shot learning (ZSL) can be implemented where the trained model transfers knowledge learnt from the source (training) distribution to the target (test) distribution. Hence, in zero-shot learning (ZSL), a model trained with source distribution attempts to predict test samples from a target domain that it has never seen before (source distribution  $\neq$  target distribution) [71]. This approach allows a model to perform better with lower generalization error when the 'new input sample data' (test data) has some similarity to the model population data (training data) [72].

The generality to correctly predict such out-of-distribution (OOD) samples (test data) is doable when training data includes all possible distribution, which is practically not feasible. Specially, it was difficult to implement ZSL in practical FMG-based applications. As FMG was a transient, non-stationary time-series biosignal, and was affected by arm posture and motion of limb movements or physiological changes (sweats, tiredness), variations were always present in the streaming signal. Therefore, a generalized approach was followed in objective 2A that enabled both seen/learned source samples and unseen/unlearned test samples available during evaluation, hence known as generalized ZSL [73]. It bridged the gap between seen source domain and unseen target domain by leveraging their semantic information. Including few calibration data (target training data) with large volume of long-term multiple source distributions improved model's generality in predicting unseen target data.

## ***B. Transfer Learning Techniques***

Since an FMG biosignal is subjective-specific and sensitive to sensor position changes/band displacement each time a band is donned on a participant, it is treated as a different domain. To overcome such inherent challenges and to recognize unseen test data, domain adaptation, domain generalization and cross-domain generalization concepts were adapted, and codes were written in MATLAB or Python for implementing transfer learning in this thesis [74-76]. These methods have been successfully applied in image processing, but there are very few studies in bio-signal-based pHRI and hence were investigated.

### *i) Domain Adaptation*

Domain adaptation reuses part of a model pretrained with large pools of source

domains to predict different but related target domain where both domains have same feature spaces with different distributions. During test phase, this enables the model to predict similar, unseen, new target data. In objective 2B and 4, transductive transfer learning (few target data available/seen) via supervised domain adaptation (SDA) [77, 78] was investigated for inter-session (training and testing in different sessions) and intra-session (training and testing in same session) evaluations during interactions, respectively.

### *ii) Domain Generalization*

On the other hand, domain generalization uses a pretrained model with source domains and attempts to predict unseen target data [78]. It is particularly beneficial to mitigate gaps between different domains where knowledge about the target domain is absent [77, 78]. Inductive transfer learning (target data not available/unseen) via supervised domain generalization (SDG) for inter-participant evaluation was investigated in objective 2B.

### *iii) Cross Domain Generalization*

Cross domain generalization (CDG) can be promising for unrelated source and target data that allows a pretrained model to transfer knowledge between different platforms/systems. Furthermore, it generalizes beyond the source distributions [79-80]. Cross-domain generalization is studied in image classifications, vision system, natural language processing, medical diagnosis, machine fault detects, etc. and is found effective [81-84]. The CDG technique has been investigated in few studies conducted on human machine interfaces (HCI) and rehabilitations with surface electromyography (sEMG) or electro encephalography (EEG) biosignals [85-89]. Hence, it is studied in FMG biosignals based on HRI tasks for the first time in objective 3.

## **Transfer learning Process**

Transfer learning is the state-of-the-art technique that enables pretraining a model by learning discriminative features of source distributions to predict unseen target tasks by using the learnt knowledge via fine-tuning. A brief approach for transfer learning followed in objective 2B is shown in Figure 2.12. In this framework, the model learned discriminative features of the multiple source domains during pretraining. While fine-tuning, the last three layers of the saved model helped in adapting to converge quickly in

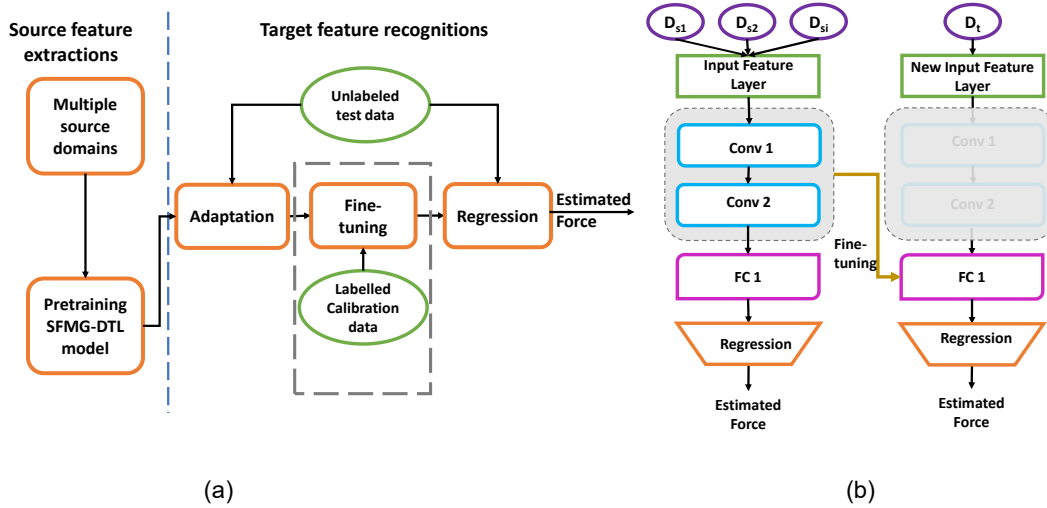


Figure 2.12. FMG-based transfer learning: (a) estimating applied interactive forces via SDA and SDG and (b) fine-tuning process of the pretrained SFMG-DTL model. Reproduced from [58] with permission.

recognizing target distribution. During evaluation, fine-tuning occurred in the final fully connected layer.

#### a) Pretraining a deep learning model

In objective 2B and 3, long-term multiple source distributions from the 2D-pHRI platform were used in pretraining a transfer learning model. In objective 4, the discriminator of the GAN model was pertained with real and synthetic data. These models were developed in MATLAB and Python code.

#### b) Fine-tuning

Fine-tuning the last layers of the pretrained model with few ‘target training data’ (calibration data) was used in adapting in recognizing target domain. Using few calibration data, these models were evaluated in recognizing inter-session and inter-participant target data (objective 2B), inter-domain target data (objective 3) and intra-session target data (objective 4). Table 2-IV shows the pretrained models and their hyper parameters during fine-tuning processes.

Transfer learning via domain adaptation and generalization has been studied in image processing mainly. For this thesis, as we have discussed, we modified these techniques to study FMG biosignal based HRI, which was far more challenging. We introduced cross-domain generalization in HRI studies for the first time. We also adapted a modified version of generalized zero-shot learning that helped knowledge transfer

Table 2-IV. Transfer Learning

Research Objective	Pretrained Model	pHRI	Hyper parameters & optimizers
Objective 2B	FMG-CNN for domain adaptation and generalization Tr. time: ~30-45 min	2D-pHRI: Model X Model Y	SDG optimizer LR = 1E-05 Epoch = 60
Objective 3	FMG-DCNN for cross domain generalization Tr. time: ~1 Hr.	3D-pHRI: Model X Model Y Model Z	SDG optimizer LR = 1E-05 (X, Z), LR = 1E-06 (Y) Epoch = 60
Objective 4	Self-trained FMG-DCGAN Tr. time: ~1 Hr.	1D-pHRI: Model X Model Y Model Z	Adam optimizer LR = 1E-04 Epoch = 500

among unrelated source and target data.

## 2.7. Performance Matrices

Statistical tools [90] such as the co-efficient of determination ( $R^2$ ) and co-efficient of correlation (Coeff), root mean square error (RMSE), and normalized RMSE (NRMSE) were used to evaluate performances of the ML models.

Co-efficient of determination ( $R^2$ ) was obtained by:

$$R^2 = \frac{\text{Explained variation}}{\text{Total variance}} \quad (2.4)$$

It was used to determine the correlations or dependencies of the dependent variable on the independent variable.  $R^2$  values varied between 0 and 1 indicating how good the regression predictions could fit the test data.

Correlation coefficient (Coeff) was determined between the matrix of pairwise variables of the true and the predicted values incurred by the model such that:

$$R = \begin{pmatrix} 1 & \rho(A, B) \\ \rho(B, A) & 1 \end{pmatrix}, \quad (2.5)$$

where the Pearson correlation coefficient  $\rho$  was calculated between A and B variables. It had values between -1 and 1 indicating strong and positive relationship between the variables.

*RMSE* was calculated based on:

$$RMSE = \sqrt{\frac{1}{n} \sum_i (Y_{est} - Y_{true})^2} \quad (2.6)$$

where  $n$  was number of samples,  $Y_{true}$  was the true data and  $Y_{est}$  was the prediction made by the regression model at an instant  $i$ .

*NRMSE* was determined by the fraction of *RMSE* to the observed range of the measured data such that:

$$NRMSE = \frac{RMSE}{mean(Y)} \quad (2.7)$$

where  $Y$  was the measured data.

One-way ANOVA with single-factor and multivariate tests and two-way ANOVA [90] with repeated measures were performed (IBM SPSS 2.0, NY, USA) in objective 1. A single-factor ANOVA was used to observe the separability of FMG signals during arm flexions and extensions. A two-way ANOVA with repeated measures [41] was performed to assess if arm motion patterns significantly related to the accuracy of regression methods. Two one-sided test (TOST) [90], an equivalence test, was conducted in objective 2B. In objective 4, t-test was conducted to compare samples for the mean generated by two variables.

## 2.8. Summary

In this thesis, FMG-based pHRI was investigated via combinations of no. of FMG channels, regression models and data-driven approaches. Such as, 32-channels FMG signals from upper arm and forearm positions were used capturing maximum muscle contraction reading during interactions in 1D and 2D with the linear robot. In industrial applications, lesser no. of channels is appropriate for reducing design complexities. Therefore, during interactions with the Kuka robot in 1D, 2D, and 3D, a 16-channels FMG band was wrapped in forearm position that could read the necessary information. The forearm position was also suitable for easy wear and comfort for the human participant. The pHRI setup was a simple biaxial stage in the beginning while the complex 7-DoF serial robotic arm was chosen later to verify the proposed objectives and methods. Table 2-V summarizes the overall setup and methods implemented in the four objectives. The



selected algorithms and methods were simple in the beginning of the thesis and then progressively became complex, state-of-the-art techniques that were appropriate for real-world scenarios. All algorithms were developed from scratch for the studies conducted in this thesis using MATLAB and Python in Windows platform.

Table 2-V. Progressively selected experimental setups, methods, and techniques

	<b>Objective 1</b>	<b>Objective 2A</b>	<b>Objective 2B</b>	<b>Objective 3</b>	<b>Objective 4</b>
<b>FMG band</b>	Two bands on forearm and upper arm	Two bands on forearm and upper arm	Two bands on forearm and upper arm	Two bands on forearm and upper arm One band on forearm	One band on forearm
<b>Robotic platform</b>	2-DoF linear robot	2-DoF linear robot	2-DoF linear robot	2-DoF linear robot 7-DoF serial robot	7-DoF serial robot
<b>No. of participants</b>	10	15	6	6	1
<b>Regression algorithms</b>	Traditional ML algorithms: SVR, KRR, MSVR, GRNN	Traditional ML algorithms: SVR	Deep transfer learning: CNN	Deep transfer learning: CNN	Adversarial learning: GAN, self-training
<b>Data driven concepts</b>	Supervised learning	Supervised, Generalized zero-shot learning	Supervised, Transfer learning via domain adaptation, domain generalization	Supervised, Transfer learning via cross-domain generalization	Unsupervised, Semi-supervised, transfer learning
<b>Programming language</b>	LabVIEW interface with embedded MATLAB scripting	LabVIEW interface with embedded MATLAB scripting	MATLAB	MATLAB	Python
<b>Toolboxes &amp; Platforms</b>	LabVIEW 2014 & MATLAB 2018 with statistics and machine learning toolbox running on HP Zbook laptop with Intel Core i7	LabVIEW 2018 & MATLAB 2019 with statistics and machine learning toolbox running on a desktop PC (Intel Core i7 processor and Nvidia GTX-1080 GPU).	MATLAB 2020 with deep learning toolbox, neural network toolbox, image processing toolbox running on a desktop PC (Intel Core i7 processor and Nvidia GTX-1080 GPU).	MATLAB 2021 with deep learning toolbox, neural network toolbox, statistics and machine learning toolbox, signal processing toolbox, Kuka Sunrise toolbox running on a desktop PC (Intel Core i7 processor and Nvidia GTX-1080 GPU).	Python 3.7 and Tensorflow running on a desktop PC (Intel Core i7 processor and Nvidia GTX-1080 GPU).
<b>Performance metrics</b>	R <sup>2</sup> , NRMSE, one-way ANOVA test, two-way ANOVA with repeated measures	R <sup>2</sup> , NRMSE, two one-sided test (TOST)	R <sup>2</sup> , NRMSE, t-test	Coeff, R <sup>2</sup> , RMSE, NRMSE	R <sup>2</sup> , NRMSE, t-test

## **Chapter 3.**

### **Learning Human Intentions of Interactions in a certain direction**

The material presented in this chapter is reproduced, extracted, and modified with permission from the following paper:

[56] U. Zakia and C. Menon. (2020, Apr.). Estimating exerted hand force via force myography to interact with a biaxial stage in real-time by learning human intentions: a preliminary investigation. *Sensors*. 20(7), doi: 10.3390/s20072104.

Sections of this chapter are reprinted or adapted from the above article to fit the formatting and scope of this chapter.

#### **3.1. Chapter overview**

This chapter explains the study conducted towards fulfilling the first objective to assess possibility of using FMG signals in estimating applied forces during interactions with a linear robot (biaxial stage). A real-time admittance control with human biosignal via force myography in the loop was developed using SVR and KRR machine learning (ML) algorithms. Five different motion patterns that were statistically significant were investigated in this study to understand human intentions of interactions. Ten healthy participants wearing forearm and upper arm FMG bands interacted with the linear robot in real-time evaluations via estimated interactive forces in the intended motion and were found statistically significant.

#### **3.2. Introduction**

In physical HRIs (pHRIs), interactions between humans and robots mostly occur through hand activities such as object handling or transportation tasks in simple and fixed trajectories. These require dynamic arm movements, while force interactions occur with hands. Learning human intentions such as realizing human hand forces and arm motions have been studied extensively to facilitate these collaborative tasks [11–14]. There are few studies to estimate hand forces or positions via sEMG technique for improving

human–robot interactions. However, there is a gap in research for FMG-based HRI control. Therefore, our objective was to investigate recognising exerted hand forces in certain motion during collaboration with a simple linear robot via FMG signals.

In this study, real-time applied hand force estimation in dynamic two-dimensional (2D) arm motions using FMG was investigated for the first time. A variety of simple and complex isotonic arm movements were studied as intended motions that involved shoulder abduction/adduction and elbow flexion/extension. A novel scheme was implemented to interact with a biaxial stage via FMG-based force estimations in an intended arm motion. Learning human intention was defined as an exerted hand force in a motion in a desired path trajectory during interactions. In a real-time scenario, a participant wearing two FMG bands grasped a custom-made gripper mounted to a stage and interacted with an exerted force in an intended motion in the XY-plane. In addition, the biaxial stage adjusted its velocity with the estimated exerted hand force, so that the gripper would slide accordingly in the same trajectory, thus ensuring compliant collaboration. Among several supervised machine learning techniques (see Appendix A1), two well-established techniques such as the support vector regressor (SVR) and the kernel ridge regressor (KRR) with their selected features, were implemented and written in MATLAB code for force estimation from FMG readings, and their performances were observed separately.

### **3.3. Methodologies**

#### **3.3.1. Real-Time FMG-Based Integrated Control**

In this study, human robot collaboration was observed, as a participant interacted with a biaxial stage via applied force in an intended arm motion, as described in Section 2.4.2. Two wearable FMG bands on the upper extremity read muscles contraction during interactions. The collaborative task was defined as to manipulate the biaxial stage by grasping its gripper and apply forces while moving arm in an intended trajectory. Using an admittance control scheme, the biaxial stage would adjust its velocity proportionate to the applied force, and the gripper would slide in the same path. Five different 1-degree-of-freedom (1-DoF) and 2-DoF arm trajectories were selected as intended motions. For simplicity, the collaborative task would be termed as 1-DoF/2-DoF interactions throughout the chapter. Each arm motion with a grasping force had its unique characteristics

represented by multichannel FMG signals. Thus, to identify a variety of intended motion patterns, these signals could represent muscle groups active in interaction.

An interactive control using a supervised regression algorithm (developed in LabVIEW interface and MATLAB scripting) estimated an applied hand force in a dynamic arm motion with FMG signals, converted it to the speed and sent the estimated data to the biaxial stage (according to equation 2.1, 2.2), thus allowing participants to manipulate the stage by grasping its gripper in the same trajectory. For the supervised training, force sensor (mounted inside the gripper) data was used as a true label data generator. The data acquisition and design aspect of this proposed integrated control is shown in Figure 3.1. During the real-time data collection for training, the biaxial stage was manipulated by the force sensor reading of the exerted hand force. During the real-time test phase, the integrated controller allowed participants to manipulate the biaxial stage with FMG-based estimated hand forces. The user interface provided visual feedback to the participants about the target arm motion pattern and the exerted force to maintain muscle volumetric contraction (MVC) in certain ranges.

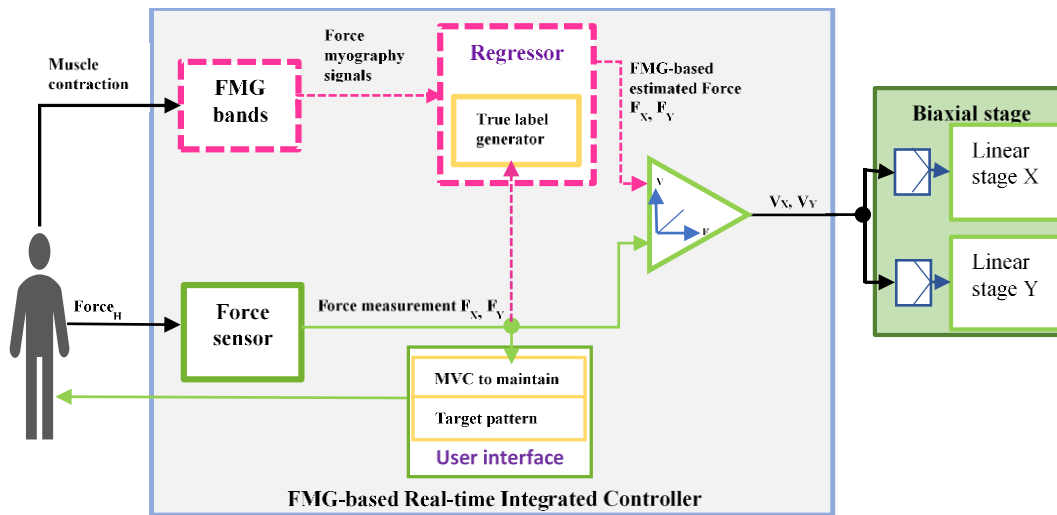


Figure 3.1. FMG-based real-time (RT) force control of a biaxial stage: the data collection and training phase are shown in green color, and the RT test phase is shown in magenta color. Reproduced from [56] with permission.

### 3.3.2. Dynamic Arm Motion Patterns

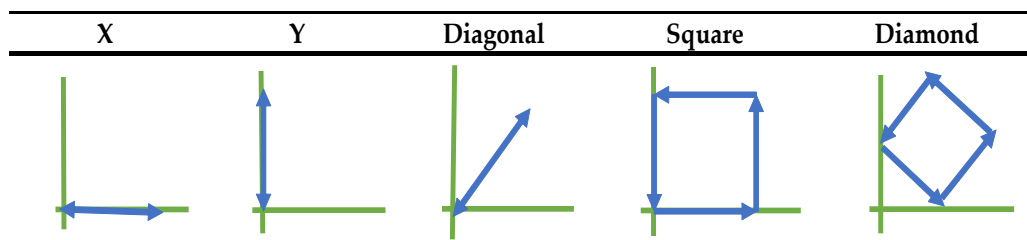
Five different dynamic arm motions (denoted as  $M_1, \dots, M_5$ ), i.e., “x-direction (X)”, “y-direction (Y)”, “diagonal (DG)”, “square (SQ)”, and “diamond (DM)” motions, in the

manipulator's cartesian space were considered as intended path trajectories for a participant to interact. These arm trajectory paths included both simple and complex arm movements and were chosen to cover the workspace of the biaxial stage. During interactions, a participant always kept his/her hand grasping the gripper with his/her elbow parallel to the horizontal plane with no specific instructions of grasp moment production. These interactions had 1-DoF and 2-DoF motions, such that the elbow and shoulder rotations were confined in the horizontal plane. The arm movements required shoulder abduction/adduction and elbow flexion/extension while his/her hand grasped the gripper, such that the wrist joint torque direction was in coincidence with the elbow joint torque. Each arm trajectory required unique combinations of elbow and shoulder movements and had spatial-temporal effects vary continuously with a changed direction of motion. For 2-DoF motions, more muscle contractions and expansions happened, while arm movements became progressively frequent, as described below. For data collection and evaluation, all arm motions were performed continuously for a certain time in a sinusoidal motion on the planar surface, with directions as indicated with arrows in Table 3-I.

#### Intended 1-DoF Arm Motion Patterns

For X motions, the participant grabbed the gripper/knob mounted on top of linear stage 1 and exerted a hand force in the X-axis only. For Y motions, the gripper was placed on top of the linear stage 2, and the participant grabbed the gripper and then an exerted hand force in the y-axis only. This intended interaction motion pattern required changing the hardware setup and dismounting linear stage 1 in the x-axis.

Table 3-I. Five interactive arm motion patterns. Reproduced from [56] with permission.



#### Intended 2-DoF Arm Motion Patterns

For DG, SQ, and DM interactive arm motions, the participant grasped the gripper and applied a hand force in one of these arm trajectories (Table 3-I). The applied force in a motion allowed the biaxial stage to adjust its velocity, and the gripper would slide in the

same path in the XY planar space. The interaction would continue anticlockwise for a certain time. Clockwise movements were not investigated because all participants were right-handed which facilitated easy interactions in anti-clockwise movements of their arms as they sat on the chair.

### **3.4. Protocol**

In this study, 10 participants interacted with the manipulator in five arm motion patterns separately. For each intended motion, there were a data collection phase, two training phases, and two testing phases, termed as a cycle and was described as Algorithm I in Table 6. Training and testing were performed twice for evaluating the two regression algorithms (SVR and KRR) separately. This process was repeated for all five interactive motions and required for around 1.5 hours to complete one cycle. Because of this time-consuming nature of the study, only few arm motions with limited directions were investigated. Intended interactions in a certain motion within participants were randomly chosen with periodical rests and controlled MVCs [91]. During training and test phases, regression algorithms were selected randomly. The randomization of motions and regressors helped to avoid observer-expectancy effects during investigation. During a cycle, the FMG bands were never removed, when interactions happened in one intended motion. As FMG signals were transient and nonstationary, removing the band would require data collection and training again, as the positions of the sensors would change.

#### **3.4.1. Data Collection Phase**

At the beginning of the data collection session, the participant sat comfortably on a specialized chair in front of the biaxial stage with his/her shoulder and back straight, while the chair was locked in position, as shown in Figure 3.2. Two custom designed FMG bands were placed on the forearm and upper arm positions of the participant's dominant right hand. The data collection phase started by measuring the maximum force that the participant could exert during an intended arm motion for 20 seconds. Based on this measurement, visual feedback alerted the participant to maintain MVCs above 30% and below 80% for both the x- and y-directions. Table 3-II shows the algorithm steps followed during the data collection phase that was written in LabVIEW and MATLAB.

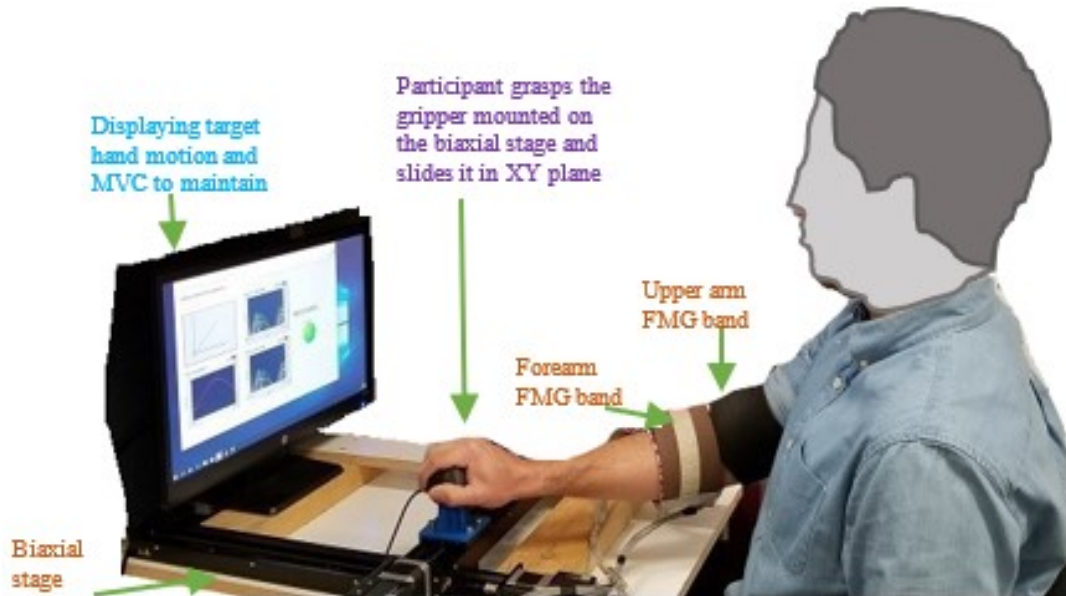


Figure 3.2. A participant wearing FMG bands interacts with the biaxial stage using an RT FMG-based integrated controller. Reproduced from [56] with permission.

The controller also provided visual feedbacks displaying target arm motion patterns to follow. Next, the participant exerted forces to the gripper to manipulate the biaxial stage in an intended motion pattern. This was repeated 5 times, while for each repetition 400 records (1 record:  $1 \times 32$  FSR channels and  $1 \times F_x$  or  $F_y$  in 1-DoF or both in 2-DoF of the label data) of raw data were collected without any filtering. Periodical rests between repetitions allowed the participants to comfort and relax their muscles. For each motion pattern, 2000 records (400 records \* 5 repetitions) of training data were collected and saved in comma-separated values (csv) files. In this phase, the biaxial stage was controlled by readings from the force sensor. This phase required around 15 minutes to complete (with periodic rests between repetitions), although the actual data collection duration was less than 10 minutes.

### 3.4.2. Training Phase

Once the data collection was done, the next step was to train models using the regression algorithms. The force sensor data were used as true labels for FMG-based force mapping. The collected FMG data were normalized and preprocessed before training using the min-max scaling method. For 1-DoF movements, each regressor generated one trained model (either model X or model Y) to estimate hand forces in one direction of an arm motion (X/Y). While for 2-DoF movements (DG/SQ/DM), each

Table 3-II. Algorithm 1: Logic flow of RT FMG-based integrated control. Reproduced from [56] with permission.

---

Real-time (RT) FMG-based admittance control of a biaxial stage by an estimated hand force in an intended arm motion pattern

---

**Input:** Forearm and upper-arm FMG signals,  $x = [x_1, x_2, \dots, x_{32}]$   
 True labels from a force sensor,  $y = [F_x, F_y]$

**Output:** FMG-based estimated force,  $y' = [F_x', F_y']$  to control the velocity of the biaxial stage

**Initialization:**  $z$  seconds,  $n$  data samples,  $r$  repetitions,  $m$  reg.model {SVR, KRR}

---

```

1: for z do
2:   Compute maximum voluntary contraction (MVC) in a planar surface
3: end for
4:   Target_forceH ← above MVCs of 30% and below MVCs of 80%
5:   Display ← (Target_forceH, Intended_motion)
6:   while (RT_Data_collection_phase == true) do
7:     r = 1;
8:     repeat
9:       for n samples do
10:        while ( exerted_force == true) do
11:          Collect x and y and save them in comma-separated values (csv) format
12:        end for
13:        r = r + 1;
14:      until r = 5;
15:    end while
16:    while (RT_Training_phase == true) do
17:      Select m reg_model
18:      Select r rep csv files
19:      Trained_model ← {x, y}
20:    end while
21:    while (RT_Test_phase == true) do
22:      Select m reg_model
23:      while (exerted_force == true) do
24:        FMG-based estimated force,  $y' \leftarrow$  Equation (2.1)
25:        Velocity of the biaxial stage ← Equation (2.2)
26:      end while
27:    end while

```

---

regressor generated two trained models for the x- and y-directions (both model x and model y) to estimate forces simultaneously. Models were trained online by calling MATLAB scripts in the LabVIEW interface (Figure 2.9) while the participant relaxed, and all trained models were saved; this usually required 2–3 minutes. Training accuracies and errors were displayed on the LabVIEW interface. The training process was conducted separately for both regressors and were selected randomly. Offline five-fold leave-one-out cross-validations (LOOCVs) were carried out later for comparing real-time test accuracies.



### 3.4.3. Test Phase

The test phase was followed immediately after training; and the trained models were evaluated to estimate forces in real time. Instantaneous test data (FMG data) arriving at the LabVIEW interface were normalized with the scaling values used in the training phase and sent to the regressor, and an exerted hand force was estimated in a dynamic arm motion. The same collaborative task was performed as before, i.e., participants manipulated the stage by grasping its gripper to slide it on the planar surface with an FMG-based estimated force in a certain arm motion and the biaxial stage followed the trajectory immediately. This phase lasted around 2 minutes, and 1000 records of the test data (labeled FMG signals and estimated hand forces) were collected. The test phase was conducted separately for both regressors. Figure 3.3 shows the actual exerted forces (true label generator from a force sensor reading) and the estimated force with FMG signals, while a participant was interacting with the stage in X and Y motions in real time with both regressors separately. These plots of real-time test evaluations (true vs. estimated forces) were visible in the control pane of the LabVIEW interface (Figure 2.9(a)). Table 3-III shows the training data used by the two regressors and the test data (estimated force) collected during the real-time evaluation of each of them.

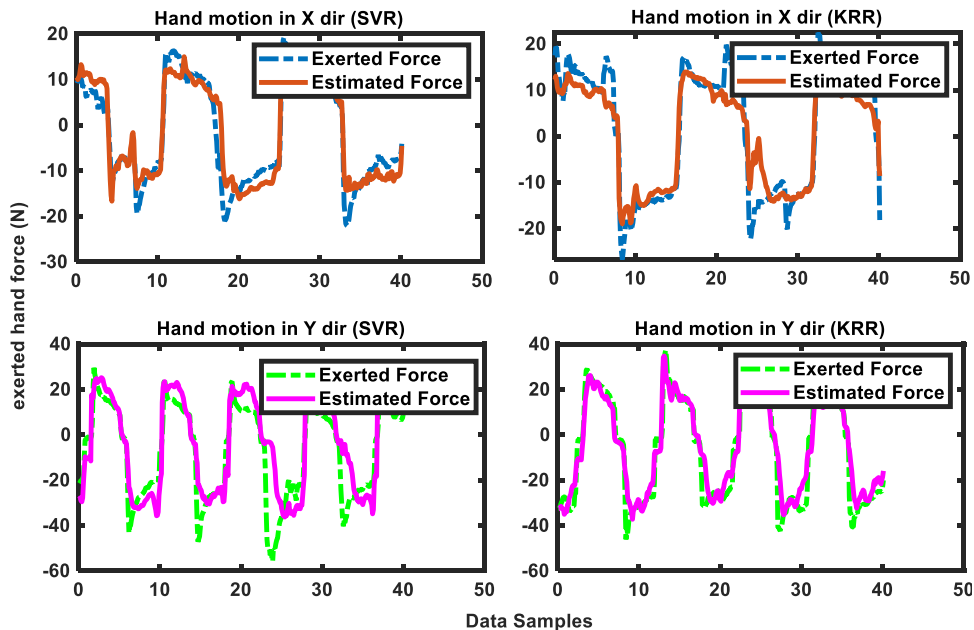


Figure 3.3. RT test phase, where a participant interacted with the biaxial stage by FMG-based estimated hand forces in intended X and Y arm motions with FMG signals. Reproduced from [56] with permission.

Table 3-III. Training data and test data (estimated forces collected during real-time interactions).  
Reproduced from [56] with permission.

Collaborative task	Training data (Labeled FMG signals)	Test Data (estimated forces and labeled FMG signals)
A participant interacting with the stage by sliding its gripper with an exerted hand force in an intended motion	2000 records or 68,000 data samples	1000 records or 36,000 data samples

### 3.5. Results

#### 3.5.1. Real-Time FMG-Based 1-DoF Interactions

Figure 3.4(a) shows the performance accuracies of the regressors in estimating hand forces in intended X interactive motions with FMG signals. The real-time test accuracies were around 94% and 92% for the SVR and the KRR, respectively, which were comparable with the cross-validation accuracies (around 95%). In intended Y motions, the cross-validation accuracies of hand force estimations were also above 95% for both regressors, although in real time the test accuracies were around 91% and ~90% for the SVR and the KRR, respectively, as shown in Figure 3.4(b). For both intended arm motions, the regressors obtained training accuracies higher than 95%.

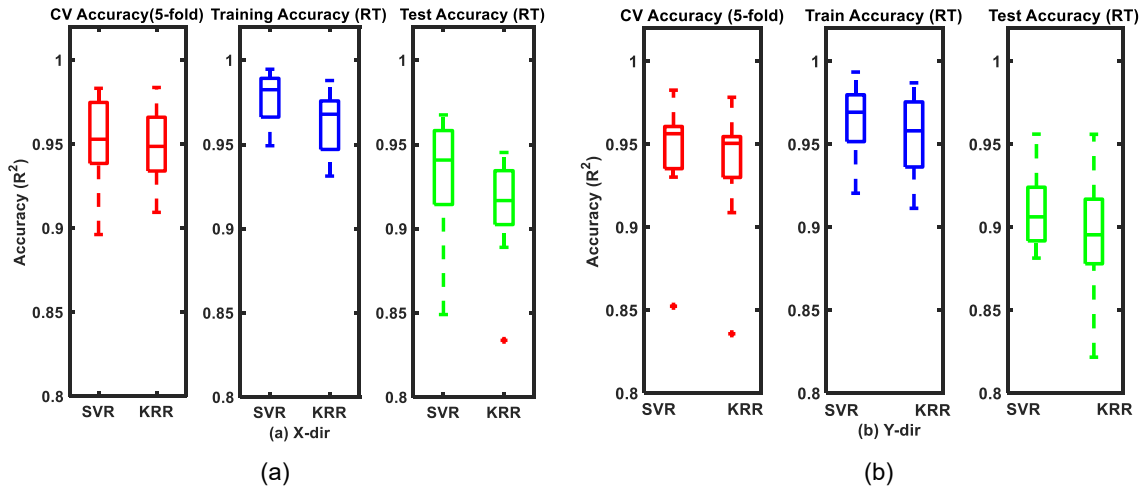


Figure 3.4. Performances of regressors estimating FMG-based hand forces during intended one-degree-of-freedom (1-DoF) arm motions: (a) x-direction only; and (b) y-direction only. Reproduced from [56] with permission.

### 3.5.2. Real-Time FMG-Based 2-DoF Interactions

Performance evaluations of the regressors in estimating hand forces during three different arm motion patterns (DG, SQ, and DM) for the participants (denoted as  $P_1, \dots, P_{10}$ ) are reported as box plots in Figure 3.5 (a–c), respectively, with training accuracies for all patterns higher than 90%. The accuracies of the cross-validations for the DG arm motion pattern were around 94% for both regressors, while the real-time test accuracies were 88% and 91% for the SVR and the KRR, respectively. For the SQ patterns, the accuracies of the cross-validations were 87–89%, while in real-time tests the accuracies were 84% and 86% secured by the SVR and the KRR, respectively. For the DM patterns, the real-time test accuracies of the SVR and the KRR were 82% and 85%, respectively; the cross-validation accuracies were approximately 88–92% for both the regressors.

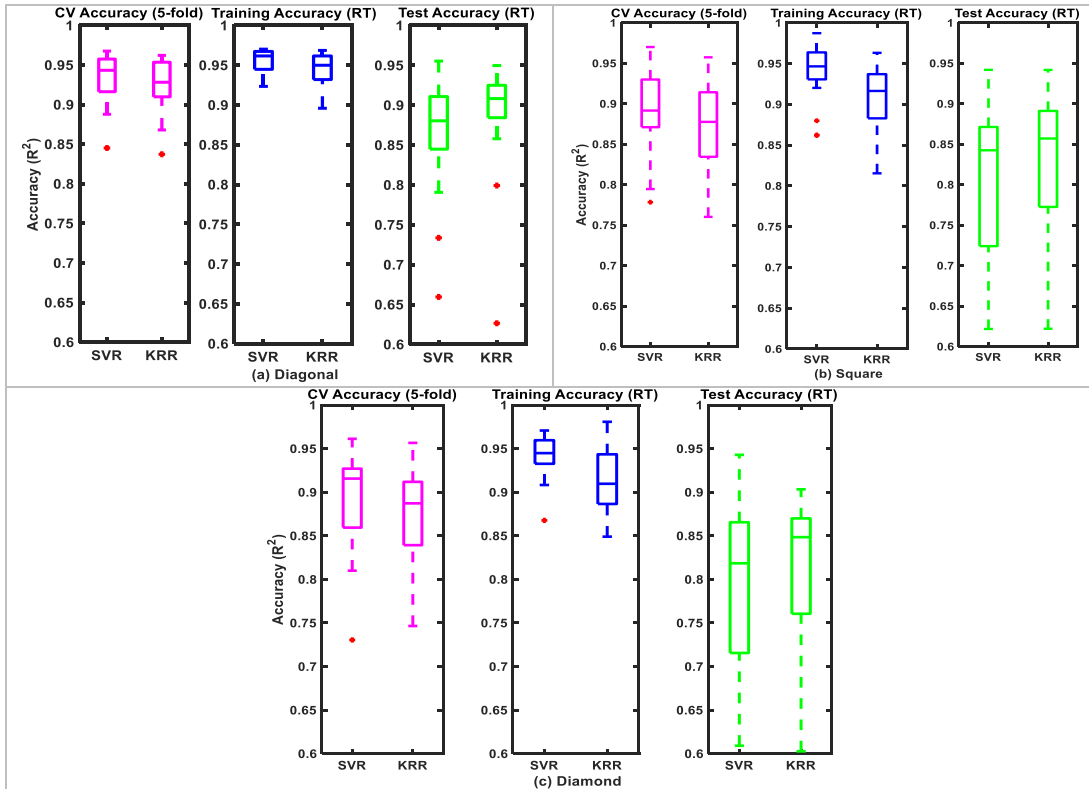


Figure 3.5. Performances of regressors estimating FMG-based hand forces during intended two-degree-of-freedom (2-DoF) arm motions: (a) diagonal; (b) square; and (c) diamond. Reproduced from [56] with permission.

Performance evaluation of the regressors during force estimation in the real-time test phase in terms of  $R^2$  and NRMSE are reported in Table 3-IV as median values (rounded to ceiling values), which were reasonably notable with higher accuracies and

Table 3-IV. Real-time performance evaluation:  $R^2$  and NRMSE. Reproduced from [56] with permission.

Data sample	ML model	Test accuracy ( $R^2$ )					Test error (NRMSE)				
		X	Y	DG*	SQ*	DM*	X	Y	DG*	SQ*	DM*
Tr: 2000 records	SVR	0.94±	0.91	0.88±	0.84	0.82	0.10±	0.11±	0.10±	0.10±	0.11±
		0.04	± 0.04	0.07	±	±	0.05	0.03	0.03	0.04	0.03
					0.09	0.09					
Te:1000 records	KRR	0.92±	0.90	0.91±	0.86	0.85	0.10±	0.12±	0.09±	0.10±	0.13±
		0.03	± 0.05	0.07	±	±	0.04	0.017	0.02	0.04	0.02
					0.09	0.10					

lower errors.

### 3.5.3. Comparison of Force Estimations in Dynamic Motions

Figure 3.6 shows the mean distributions of the test accuracies of the regression models in force estimations for five different motions. Both regressors (SVR and KRR) provided better estimation in 1-DoF arm motions ( $R^2 \geq 90\%$ ) than 2-DoF arm motions ( $R^2 \geq 82\%$ ). During the 1-DoF interactions, the SVR outperformed the KRR because of model simplicity. While for the 2-DoF interactions, the force estimations in the x- and y-directions were required simultaneously. This required high computational power, considerable memory allocation, and fast communication between the integrated controller and the biaxial stage. Moreover, lower accuracies obtained in the 2-DoF patterns compared to in the 1-DoF arm motions might be due to the increased level of the elbow and shoulder rotations resulting in faster muscle fatigue. For the 2-DoF interactions, the KRR slightly outperformed the SVR in DG and SQ trajectories, although the results were quite comparable. While the SVR required considering all the support vectors of the trained models to estimate, the KRR could provide better prediction with limited samples available in real-time force estimation [65]. Among the 2-DoF arm motion patterns, both the KRR and the SVR performed better in DG patterns because of simpler arm motions and fewer muscle contractions/expansions than in the other two patterns. Although the regressors had lower accuracies in the DM patterns compared to in the other two patterns, real-time force control was achievable with satisfactory accuracies.

With different demographic data, each participant manipulated the stage at his/her own comfortability during an intended motion. For a real-time environment, the regressors had estimated forces that varied among 1-DoF and 2-DoF motions ( $R^2 = 82\text{--}94\%$ ). The

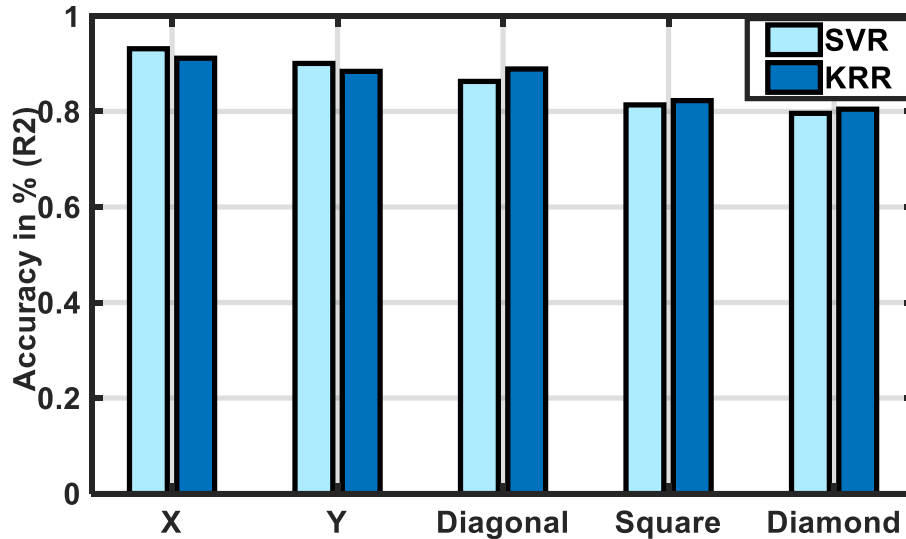


Figure 3.6. Performances (average  $R^2$ ) of the SVR and the KRR in estimating exerted forces with FMG signals during different arm motions. Reproduced from [56] with permission.

more complex the arm motion, the harder it became to estimate force in dynamic motions. Studies have shown that changing arm positions adversely influenced the performances of the regression algorithms over the population [92-93], as observed in this study.

The mean absolute error (MAE) shown in Table 3-V was also used to compare the regression algorithms' accuracies in force estimations. The lower the MAE was, the more accurate the regression model was. The MAEs of the SVR were higher than those of the KRR for the DG and SQ patterns, but that of the SVR was lower for the DM patterns compared with that of the KRR. The results indicated that the KRR and the SVR were comparable in the 2-DoF motions while the SVR slightly outperformed the KRR in the 1-DoF motions.

Table 3-V. Mean absolute errors (MAE) of regression models in different arm motions. Reproduced from [56] with permission.

	X	Y	Diagonal	Square	Diamond
SVR	0.1091	0.1114	0.1055	0.1092	0.1188
KRR	0.1174	0.1154	0.0997	0.1069	0.1262

### 3.5.4. Significance in Estimations

An investigation was done to study main effects if there was a significant relation between the arm motion patterns and the accuracies of the regressors. The within-subject-

effects tests for arm motion patterns showed statistical significance in different patterns ( $F(4,36) = 9.681, p = 0.000$ ). However, it was found that there was no significant difference between the regression models ( $F(1,9) = 0.0251, p = 0.877$ ), and no significant interactions between the arm motion patterns and the regression models ( $F(4,36) = 1.144, p = 0.352$ ). The post-hoc tests showed statistical significance as X arm motions had performance improvements of 10.3% and 12.1% than those of SQ and DM arm motions, respectively. Likewise, the performance of the Y patterns was 7.4% and 9.2% higher than those of SQ and DM motions, respectively. Pair-wise comparisons of X–SQ and X–DM were statistically significant, while those of Y–SQ and Y–DM were marginally significant, as observed from the corrected p-values reported in Table 3.VI.

The one-way ANOVA [89] showed that participants' ages did not significantly affect the performances of the regression models ( $F = 0.578, p = 0.875$ ). There was no relation between the FMG-based force estimation and the participant' age.

*Table 3-VI. Two-way repeated measures ANOVA. Reproduced from [56] with permission.*

Arm motion patterns	Mean difference	SD	Corrected p-value
X–SQ	0.103	0.013	0.000
X–DM	0.121	0.019	0.000
Y–SQ	0.074	0.022	0.048
Y–DM	0.092	0.026	0.049

Recognizing different arm motion patterns in two dimensions with real-time FMG signals was interesting and challenging because of the dynamic nature of motions and individual-specific muscle contractions. As a preliminary study, a simple interactive setup with a constrained protocol allowed investigating force estimations in a variety of complex motions with FMG signals. These motions were examined for understanding human intentions of manipulating a stage in any direction. The admittance control strategy implemented in this investigation utilized supervised machine learning methods. In many interactive control systems, complex human arm dynamics modeling is required [30]; while this study showed possible interactions without such modeling. Real-time evaluations were conducted for 10 participants interacting with the biaxial stage in 5 different intended motions using two different ML models. Hence, this study showed the viability of using FMG biosignals to estimate applied forces in dynamic motion during interactions with a planar robot. In addition, FMG-based force estimation could be beneficial in implementing

safe collaboration while working with a robot. If safety issues arise such as to avoid unwanted contacts or impact forces from the manipulator, participants can force the robot to move it further away in a certain direction. Therefore, using FMG biosignals as the only input in learning human activities appears promising.

## Chapter 4.

### Long-term FMG Model-based Force Estimation

The material presented in this chapter is excerpted, reproduced, and modified with permission from the following papers:

[57] © [2021] IEEE with permission. U. Zakia and C. Menon, "Toward Long-Term FMG Model-Based Estimation of Applied Hand Force in Dynamic Motion During Human–Robot Interactions," in *IEEE Transactions on Human-Machine Systems*, vol. 51, no. 4, pp. 310-323, Aug. 2021, doi: 10.1109/THMS.2021.3087902.

[58] U. Zakia and C. Menon, "Force Myography-Based Human Robot Interactions via Deep Domain Adaptation and Generalization," *Sensors*. 2022; 22(1):211. <https://doi.org/10.3390/s22010211>

Sections of this chapter are reprinted or adapted from the above two articles to fit the formatting and scope of this chapter.

#### 4.1. Chapter Overview

In this chapter, studies conducted to reach research objective 2 are discussed. The goal was to investigate generalization of a trained model with long-term data collected over a period several months. Generalized zero-shot learning and transfer learning via domain adaptation, domain generalization techniques were implemented with traditional SVR algorithm and state-of-the-art CNN algorithm. Several participants interacted with the linear robot in this 2D-pHRI platform.

#### 4.2. Introduction

Determining human intentions of applied forces in dynamic motion in objective 1 was found effective in real-time interactions with a linear robot. Although the study showed impressive results in recognizing applied forces in dynamic motion during HRI, it had a few shortcomings. First, a separate regression model was trained for predicting force applied by each participant for one specific motion. Second, separate training datasets



were needed if motions were different because of variations in muscle contractions. This required collecting adequate training datasets each time an individual interacted using a different motion (task) with the robot. Additionally, retraining from scratch was necessary occasionally when FMG bands were taken off and put back on later due to the non-stationary, transient, and individual-specific nature of FMG signals. Collection of another training dataset was time consuming and impractical for regular use. Moreover, intra-session FMG-based pHRI required collecting adequate labelled training data, which was biased and impractical in real scenarios. In addition, each session data was affected by transient, instantaneous signals, sensor position shift, physiological changes, limb motions, and postures each time an FMG band was donned. Such domain shifts and lack of adequate data severely limited inter-session or inter-participant performance evaluations.

Potential application of a wearable FMG band for human workers in industrial HRI workspaces would require general applicability to all workers for control and safety aspects. A trained model that can estimate dynamic hand force via FMG signals is preferable for all individuals in any intended motion during pHRI. However, obtaining such a trained model is feasible only with large volume of diversified population dataset. Therefore, in objective 2, two separate studies were conducted on generalization of a trained model feasible in FMG-based HRI applications. In study 1 (**Objective 2A**), multiple source domains collected during interactions between several participants and a linear robot in 5 different intended motions over long period of time was used to train a generalized model. This model was evaluated on real-time out-of-distribution target data to predict forces: *i) in unseen, unknown dynamic motion*, and *ii) applied by an unseen, unknown participant*. In the second study (**Objective 2B**), long-term source data were collected during interaction between one participant and the linear robot in an intended motion. A transfer learning model with domain adaptation and domain generalization was investigated for recognizing applied forces in certain motion for: *i) inter-session evaluation* (for the repeated user), and *ii) inter-participant evaluation* (for unseen, unknown participant).

### 4.3. Objective 2A

#### Study 1: Towards Long-term FMG Model-based Force Estimation during Human-Robot Interactions

To investigate generalization, a novel calibrated FMG-based model was proposed in this study where population data (multiple source domains) was collected over long period of time during real-time interactions between several participants and a linear robot (a biaxial stage). The viability of the proposed long-term calibrated FMG (LCFMG) model was based on the ability to recognize real-time (RT) unlearned ‘new input sample data’ (target domain) that were out-of-distribution (OOD) compared to the ‘learned’ population data. By ‘unlearned’, we meant estimating hand force either in ‘a new unlearned motion’ or for ‘a new unlearned participant’. By ‘learned’ we referred to the population data available to form a long-term ‘baseline dataset’ (aggregated multiple source distributions) for generalization. The proposed model was evaluated in estimating forces in a) scenario 1: unlearned/ unseen motion, and b) scenario 2: unlearned/ unseen participant. As real-time test data (target domain) in these scenarios were quite different from baseline dataset, few calibration data were required for practical evaluation of the model, thereby implementing a generalized zero-shot learning (GZSL) method for the proposed model [72, 73], as discussed in Sections 2.6.2.A and 2.7.1. Recognizing unseen scenarios using calibration data for domain adaptation is a relatively unexplored area in FMG-based HRI. These calibration data were distinct from the long-term population dataset and similar to test samples. In other words, the target training data or the calibration data were different than the source data and were similar to the target test data. Several combinations of population data and calibration data were used to train few long-term calibrated FMG-based (LCFMG) models. Performances of these LCFMG models were evaluated in real-time and compared to each other. A few models were also trained with ‘new input sample data’ only (no population data), as was mentioned in [56]. These models were termed as ‘specialized trained models (STMs)’ hereinafter and were compared with the proposed LCFMG models for performance evaluation.

Two main trends were considered for training the FMG-based regression models:

- 1) creating the proposed generalized long-term FMG-based calibrated regression models with minimum calibration data, LCFMGs, and

2) administering extensive data collection sessions to record FMG data from each new participants/new motion performing several repetitions to create specialized trained models, STMs.

### 4.3.1. Methodology

The proposed framework utilized a fully supervised multiple domain adaptation with a modified generalized zero-shot learning method where both source and target distributions were somewhat different but had the same feature spaces. In this study, our objective was to train a model with multiple source distributions [baseline dataset aggregated from a full/subset of ‘reference dataset’ only, and/or ‘learnt participant dataset’ only, (Section 4.3.2)] and evaluate new, unseen real-time test samples [target domain: unseen motion (scenario 1) / unseen participant (scenario 2)], as shown in Figure 4.1.

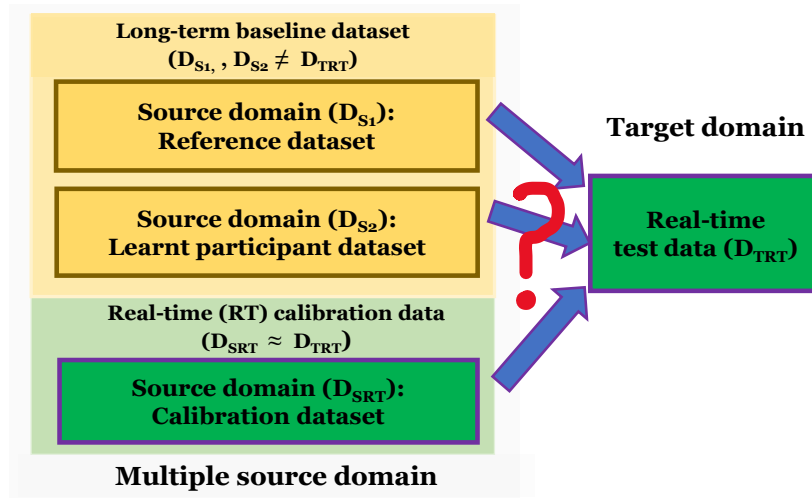


Figure 4.1. Implementing modified generalized zero-shot learning with multiple source domain adaptation in FMG-based HRI. Reproduced from [57] © [2021] IEEE with permission.

For FMG- based real-time interaction, instantaneous signals were required to represent muscle contractions. In recognizing unseen real-time test samples, a modified GZSL in adapting knowledge transfer helped where a few test samples were included in the aggregated multiple source distributions. Therefore, fewer ‘new input sample data’ or calibration data (applied force in an intended motion) was collected from a participant at the beginning of an evaluation period. These data were like the real-time test samples (target domain) and was aggregated with baseline source distribution for training purposes, as described in Section 4.3.2. As the seen calibration data was like the unseen RT test data, the model could learn what was expected from target domain and predicted

better. Therefore, the essence of the proposed framework was using real-time calibration data to fine-tune the training distribution. This special case of generalized ZSL of multiple domain adaptation framework bridged the gap between source and target distributions. Introducing few calibration datasets allowed the model to learn seen target samples to some extent; this provided the model with better predictability on unseen test samples captured from the target domain in real-time. A LabVIEW interface was developed for control and communication, and MATLAB code was written for training and evaluating the proposed model, i.e., a support vector regressor (SVR) model was created and evaluated on Windows platform. The SVR model was customized using the LIBSVM library and appropriate cost (C) and gamma (G) functions was determined using grid search.

### 4.3.2. Long-Term Calibrated FMG-based (LCFMG) Model

The ability of the proposed model to predict out-of-distribution (OOD) data was evaluated in, a) scenario 1 # unseen motion: a learned participant applying force in a ‘new, unlearned’ motion, and b) scenario 2 # unseen To verify the capability of the proposed framework, a 5-fold cross validation (CV) on the training dataset [baseline dataset augmented with calibration data] was conducted where the data set was split into 5 folds. participant: a ‘new, unlearned’ participant applying force in a learned motion. In this

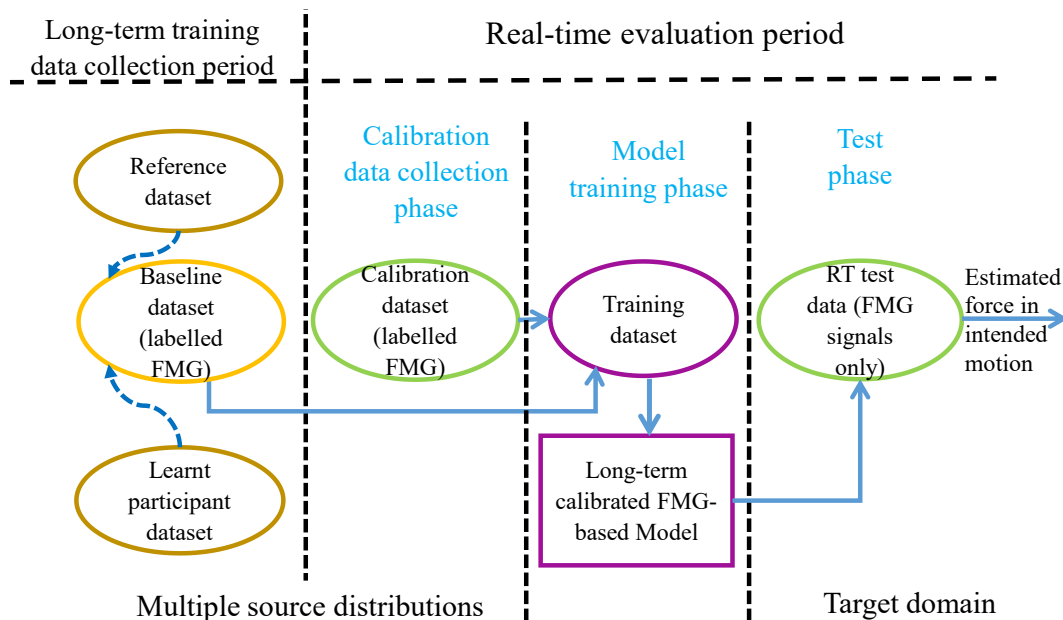


Figure 4.2. Proposed framework for Long-term calibrated FMG model. Reproduced from [57] © [2021] IEEE with permission.

context, 'learned' referred to the aggregated multiple source distributions acquired from a 'reference dataset' and/or a 'learnt participant dataset'. In the case of 'unlearned', no/negligible 'new input sample data' were included in the training dataset and referred to as the 'calibration dataset'. Figure 4.2 shows the proposed framework of the model.

In this study, a total of fifteen (15) participants ( $P_1$ - $P_{15}$ ) contributed voluntarily. Source domains collected from the first five participants ( $P_1$ - $P_5$ ) formed a 'reference dataset' for generalization. The other 10 participants ( $P_6$ - $P_{15}$ ) contributed to evaluate the proposed framework in real-time. Among them, three participants ( $P_6$ - $P_8$ ) contributed to collect 'learnt participant dataset' and to evaluate model performance in scenario 1; while the remaining seven participants ( $P_9$ - $P_{15}$ ) took part in scenario 2 for evaluation. To recognize unseen/unknown motion or unseen/unknown participant in the two scenarios [as described in Section 4.3.3.A and 4.3.3.B], a training dataset was formed using different source distributions:

### ***1. Long-term baseline dataset***

A 'long-term baseline dataset' or simply 'baseline dataset' (aggregated multiple source distributions) was accumulated from a 'reference dataset (subset/full)' only, and/or a 'learnt participant dataset (subset)' only.

- **Reference dataset  $D_{S1}$ :**

Multiple source domains were aggregated into a reference dataset. It was a collection of data from two FMG bands placed on the forearm and upper arm of five participants ( $P_1, P_2, P_3, P_4, P_5$ ) capturing muscle contractions during interactions with the linear robot. Participants applied forces in dynamic motions, namely X direction ( $M_1$ ), Y direction ( $M_2$ ), Diagonal ( $M_3$ ), Square ( $M_4$ ), and Diamond ( $M_5$ ) in the XY plane demonstrating both simple and complex planar motions. These diverse pools of multiple source domains offered better generalization in domain adaptation. The reference dataset (full/ subset) was used in both scenario 1 and 2 in recognizing unseen test samples.

- **Learnt participant dataset  $D_{S2}$ :**

To recognize unseen motion in scenario 1, a few source distributions were collected from volunteering participants ( $P_6$ - $P_8$ ). For each participant, a separate 'learnt participant dataset' was created during interactions in five different motions ( $M_1, M_2, M_3,$

$M_4, M_5$ ). This helped to generalize source domains collected from a participant for target domain adaptation. Participants ( $P_6$ - $P_8$ ) in scenario 1 were termed as 'learned' because some known or seen data from the 'learnt participant dataset' (subset of it) was used in training, as described in Section 4.3.3. A.

Both the 'reference dataset' and 'learnt participant dataset' were collected over a long period of time before the evaluation period; and hence 'long-term' was used to describe this model.

## ***II. Calibration dataset $D_{SRT}$***

The 'calibration dataset' was collected at the beginning of the real-time evaluation period of the framework. It was called the 'new input sample data' (0, 1 or 2 repetitions of 0, 400 or 800 samples data where a participant interacted with the robot for a certain time in each repetition). To evaluate the proposed models, force estimation in two intended motions: 'X direction ( $M_1$ )' and 'Diagonal ( $M_3$ )' were considered. So, either in scenario 1 or 2, calibration data collected from a participant ( $P_6$ - $P_{15}$ ) in an intended motion determined the real-time intended motion for interaction during evaluation via MATLAB code. SVR was customized, appropriate cost and gamma functions was determined using grid search

### **4.3.3. Training dataset formation**

To evaluate the proposed long-term calibrated FMG-based model implementing GZSL multiple domain adaptation, baseline dataset and calibration dataset were aggregated in various combinations to train few models and predict unseen test samples. Several cases were investigated to obtain a possible solution in real-world FMG-based HRI scenarios, as described below:

#### ***A. Scenario 1: Estimating Force in Unlearned Motion $M_U$***

In this scenario, the applied force in a new unlearned motion  $M_U$  ( $U=1,3$ ) was attempted by a learned participant  $P_L$  ( $L=6,7,8$ ) to interact with the biaxial stage, as shown schematically in Figure 4.3. 'New input sample data' from executions of such a motion were used to create a 'calibration dataset'. Two cases were considered in scenario 1:

### Case i # Intra-Participant:

The 'baseline dataset 1' for intended motion  $M_1$  was formed from a subset of a 'learnt participant dataset' i.e., FMG data of applied force in four motions:  $M_2, M_3, M_4, M_5$  by a participant,  $P_L$  ( $L=6,7,8$ ). Similarly, force exerted in  $M_1, M_2, M_4, M_5$  motions by a participant  $P_L$  ( $L=6,7,8$ ) contributed to the 'baseline dataset 1' for intended motion  $M_3$ . The Intra-Participant training dataset was formed by equation (4.1), and (4.2).

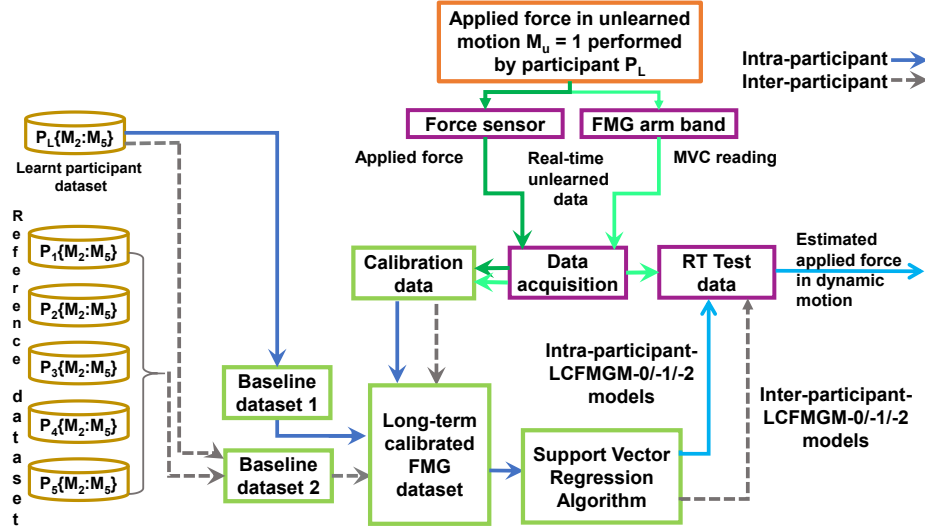


Figure 4.3. Schematic of scenario 1: long-term calibrated FMG-based model generation to recognize a new unlearned motion ( $M_1$ ) reproduced from [57] © [2021] IEEE with permission.

$$\text{Training dataset } [M_U=1] \leftarrow \{M_2, M_3, M_4, M_5\}_{P_L} \cup \{M_1\}_{P_L} \quad (4.1)$$

$$\text{Training dataset } [M_U=3] \leftarrow \underbrace{\{M_1, M_2, M_4, M_5\}_{P_L}}_{\text{Baseline dataset}} \cup \underbrace{\{M_3\}_{P_L}}_{\text{Calibration}} \quad (4.2)$$

### Case ii # Inter-Participant:

The 'baseline dataset 2' in this case was formed by augmenting 'baseline dataset 1' from Intra-Participant with a subset of reference dataset. Such as, for intended motion  $M_1$ , FMG data from five participants ( $P_1-P_5$ ) interacting in  $M_2, M_3, M_4, M_5$  motions were used. According to equation (4.3) and (4.4), Inter-Participant training datasets were formed.

$$\text{Training dataset } [M_U=1] \leftarrow \underbrace{\{M_2, M_3, M_4, M_5\}_{P_1, P_2, P_3, P_4, P_5, P_L}}_{\text{Baseline dataset}} \cup \underbrace{\{M_1\}_{P_L}}_{\text{Calibration}} \quad (4.3)$$

$$\text{Training dataset } [M_U=3] \leftarrow \underbrace{\{M_1, M_2, M_4, M_5\}_{P_1, P_2, P_3, P_4, P_5, P_L}}_{\text{Baseline dataset}} \cup \underbrace{\{M_3\}_{P_L}}_{\text{Calibration}} \quad (4.4)$$

In each case, no/few calibration data ('new input sample data':  $P_L$  interacting with the robot in unlearned motion  $M_U$ ) of zero, one, or two repetitions (0, 400, 800 samples) augmented with baseline datasets resulted in the LCFMG-0, LCFMG-1, LCFMG-2 trained models, respectively. To compare the performance of these models, specialized trained models (STM-1, STM-2, and STM-5) were generated with different repetitions (1, 2 and 5) of calibration datasets of an unlearned intended motion,  $M_U$  ( $U=1,3$ ), performed by  $P_L$  ( $L=6,7,8$ ).

### **B. Scenario 2: Estimating force for Unlearned Participant $P_U$**

In this scenario, a new unlearned participant,  $P_U$  ( $U=9,\dots,15$ ), with no prior information, interacted with the biaxial stage in a learned intended motion,  $M_L$  ( $L=1,3$ ). For generalization, the reference dataset (subset/full) was used. A 'new input sample data' from execution of the intended motion was used as the 'calibration dataset'. To construct the training dataset, two cases were considered:

#### **Case i # Intra-Motion:**

The 'baseline dataset 1' included a subset of the reference dataset of FMG data collected from five participants ( $P_1$ - $P_5$ ) applying force in an intended motion  $M_L$  ( $L=1,3$ ). The Intra-Motion training dataset was formed according to equations (4.5), and (4.6).

$$\text{Training dataset } [M_L=1] \leftarrow \underbrace{\{M_1\}_{P_1, P_2, P_3, P_4, P_5}}_{\text{Baseline dataset}} \cup \underbrace{\{M_1\}_{P_U}}_{\text{Calibration}} \quad (4.5)$$

$$\text{Training dataset } [M_L=3] \leftarrow \underbrace{\{M_3\}_{P_1, P_2, P_3, P_4, P_5}}_{\text{Baseline dataset}} \cup \underbrace{\{M_3\}_{P_U}}_{\text{Calibration}} \quad (4.6)$$

#### **Case ii # Inter-Motion:**

The full reference dataset was used as the 'baseline dataset 2'. According to equations (4.7) and (4.8), the Inter-Motion training dataset was formed.

$$\text{Training dataset } [M_L=1] \leftarrow \underbrace{\{M_1, M_2, M_3, M_4, M_5\}_{P_1, P_2, P_3, P_4, P_5}}_{\text{Baseline dataset}} \cup \underbrace{\{M_1\}_{P_U}}_{\text{Calibration}} \quad (4.7)$$

$$\text{Training dataset } [M_L=3] \leftarrow \underbrace{\{M_1, M_2, M_3, M_4, M_5\}_{P_1, P_2, P_3, P_4, P_5}}_{\text{Baseline dataset}} \cup \underbrace{\{M_3\}_{P_U}}_{\text{Calibration}} \quad (4.8)$$

Long-term calibrated FMG-based models for these cases were trained by including no/few calibration data ('new input sample data': unlearned  $P_U$  interacting with the robot in intended motion  $M_U$ ) of zero, one, or two repetitions (0, 400, or 800 samples) augmented



with the baseline dataset resulted in the LCFMG-0, LCFMG-1, LCFMG-2 models, respectively. A schematic of this scenario is illustrated in Figure 4.4. For performance comparison, specialized trained models (STM-1, STM-2, and STM-5) were generated using different repetitions (1, 2 and 5) of the calibration dataset in an intended motion  $M_L$  ( $L=1,3$ ) performed by a new participant  $P_U$  ( $U=9,\dots,15$ ).

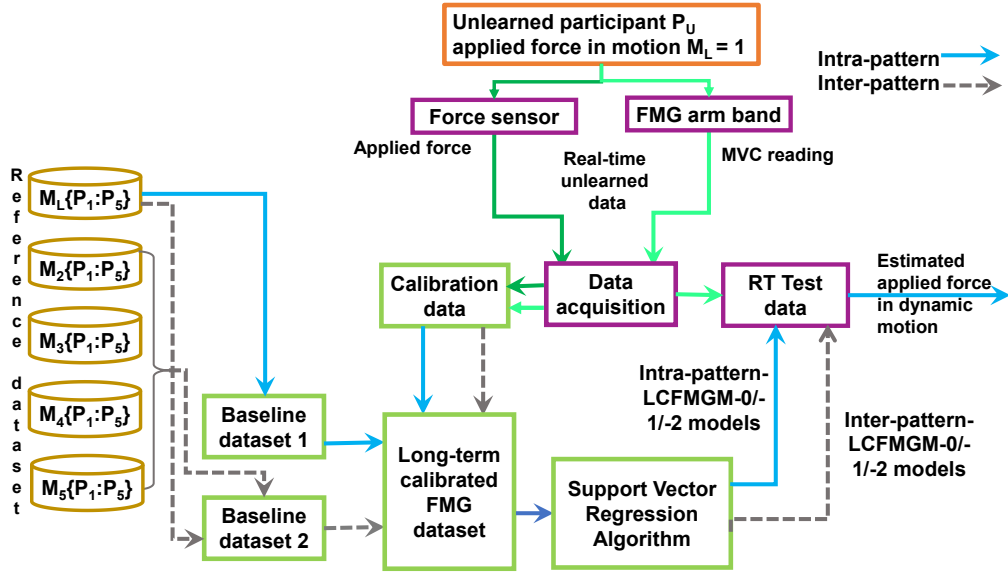


Figure 4.4. Schematic of scenario 2: long-term calibrated FMG-based model generation to recognize unlearned participant applying force in motion ( $M_1$ ). Reproduced from [57] © [2021] IEEE with permission.

#### 4.3.4. Study Protocol

The study spanned over two separate periods of a) 'long-term training data collection period', followed by b) 'real-time evaluation period' of the proposed models. Datasets collected in these two periods and formation of the training dataset is shown in Table 4-I for intended motion  $M_1$ .

##### A. Long-term training data collection period

The multiple source domains i.e., the baseline datasets ['reference dataset' from  $P_1$ - $P_5$  and 'learnt participant dataset' from  $P_6$ - $P_8$ ] required for different scenarios were collected in this period. These datasets were collected in multiple sessions over a few days where several participants ( $P_1$ - $P_8$ ) interacted with the robot. The baseline dataset was considered as the offline training dataset used for generalization and domain transfer knowledge. In this period, only the data collection phase was executed. In each training

data collection session, participant applied force in an intended motion during interaction and was considered as a separate source domain.

Table 4-I. Training datasets used in scenario 1 and 2 (intended motion:  $M_1$ ), reproduced from [57] © [2021] IEEE with permission

Long-term multiple source dataset collection phase			Real-time evaluation phase		
Reference dataset	Learnt participant dataset	Baseline dataset	Calibration dataset	Training Dataset	Real-time target data
<b>Scenario: 1</b> $R = \{\sum P_i \sum M_i\}^n$ [n =5] 5 participants ( $P_1$ - $P_5$ ) 5 motions $\{M_1$ - $M_5\}$ 2000 samples/motion for each participant	$Q = \{P_L \sum M_i\}^{n_i}$ 3 participants $P_L(P_6$ - $P_8)$ 5 motions $\{M_1$ - $M_5\}$ 2000 samples/motion for each participant 4*2000 samples/ $P_L$ $Q_1 \in Q$ [for $M_{i=1}$ ] $Q_2 \in Q$ [for $M_{i=3}$ ]	<b>Case 1: <math>B = Q_1</math></b> Here, $Q_1 = \{P_L \sum M_{i+1}\}^{n_{i+1}}$ 8000 samples/ $P_L$ [1 participant * 4 motions * 2000 samples/motion]	$C = P_L \{M_i\}$ $P_L(P_6$ - $P_8)$ Intended motion, $M_i = 1$ 0/ 400/ 800 samples	$D_s = B \cup C$	$D_T = P_L \{M_i\}$ $P_L(P_6$ - $P_8)$ Intended motion, $M_i = 1$ 600 samples (online)
		<b>Case 2: <math>B = A \in R \cup Q_1</math></b> Here, $A = \{\sum P_i \sum M_{i+1}\}_{i+1}^n$ [ $(P_1$ - $P_5)\{M_2$ : $M_5\}$ ] 48000 samples [5 participants * 4 motions * 2000 samples/motion + 8000 samples/ $P_L$ ]			
<b>Scenario: 2</b> None motion for each participant	None	<b>Case 1: <math>B = D \in R</math></b> Here, $D = M_{i=1} \{\sum P_i\}^n$ [ $(M_1) \{P_1$ : $P_5\}$ ] 10000 samples [ 1 motion * 5 participants * 2000 samples/motion]	$C = P_U \{M_i\}$ $P_U(P_9$ - $P_{15})$ Intended motion, $M_i = 1$ 0/ 400/ 800 samples	$D_T = P_U \{M_i\}$ $P_U(P_9$ - $P_{15})$ Intended motion, $M_i = 1$ 600 samples (online)	
		<b>Case 2: <math>B = R</math></b> 50000 samples [ 5 motions * 5 participants * 2000 samples/motion]			

\*\*samples collected per sensor/ FMG channel

At the beginning of a session, a participant wearing the two FMG bands sat comfortably on a chair in front of the biaxial stage with his/her shoulder and back straight on a chair locked in position. For compliant collaboration, the participant grasped the gripper and applied force in an intended motion and continued repeatedly until 400 data samples/sensor were collected; this was termed as one ‘repetition’. Five repetitions were performed to collect a total of 2000 samples of ‘source domain sample data’ from each sensor. Collected data were labeled and saved for later use in training the models. This phase lasted for approximately 12-15 minutes.

## **B. Real-time evaluation period**

Ten participants ( $P_6$ - $P_{15}$ ) contributed to the real-time evaluation of the proposed LCFMG models. During this period, a separate session was conducted for each participant in investigating a single scenario (two cases) for two intended motions ( $M_1$ ,  $M_3$ ), as shown in Figure 4.5. Six LCFMG models and three STM models were evaluated for one participant in a scenario (1 or 2) in one intended motion ( $M_1/M_3$ ). This required around 90 minutes to complete evaluation for each participant for the two intended motions. A calibration dataset was collected at the beginning of the evaluation period. To evaluate the proposed models in each motion, three phases were executed consecutively:

- calibration data collection phase in which participants interacted with the biaxial in an intended motion,
- model training phase in which several long-term calibrated FMG-based models were trained by merging different combinations of baseline and calibration datasets of acquired FMG data as described in Section 4.3.3 (A & B), and
- test phase in which the performance of the long-term calibrated FMG-based models were evaluated in real-time to estimate user-applied forces in dynamic motion.

### 1) Calibration Data Collection Phase

Labelled FMG data were collected same way as described in Section 4.3.4.A. For compliant collaboration, a participant sat comfortably with their arm parallel to the horizontal space, grasped the gripper of the robot, applied force in an intended motion ( $M_1$  or  $M_3$ ) and continued interaction repeatedly until 400 samples were collected in one 'repetition'. Five repetitions were executed to collect a total of 2000 samples of 'new input sample data' from each sensor. Among these, repetition 1 and 2 only were used as 'calibration data'. Collecting 2 repetitions of calibration data required approximately 5 minutes while the whole session was conducted in 12-15 minutes.

### 2) Model Training Phase

During this phase, several models were trained while the participant sat comfortably and relaxed with the FMG bands still wrapped around his/her arm. The training dataset for each model augmented the baseline dataset with 'calibration data' of 0, 400, or 800 samples of 'new input sample data'. Three separate long-term models

(LCFMG-0, LCFMG-1, LCFMG-2) were trained for each case in one scenario, as described in Section IV. For two cases in one scenario, six separate long-term calibrated FMG-based models (Scenario 1: Intra-Participant-LCFMG-0/1/2 and Inter-Participant-LCFMG-0/1/2, Scenario 2: Intra-Motion-LCFMG-0/1/2 and Inter-Motion-LCFMG-0/1/2) were trained. Also, three specialized trained models (STM-1, STM-2, STM-5) were generated using only ‘new input sample data’ (1, 2 and 5 repetitions or 400, 800, 2000 samples from calibration dataset) for performance evaluations. Table 4-II lists a detailed description of baseline and calibration datasets, number of samples collected from each sensor, and the model generated for each scenario and case.

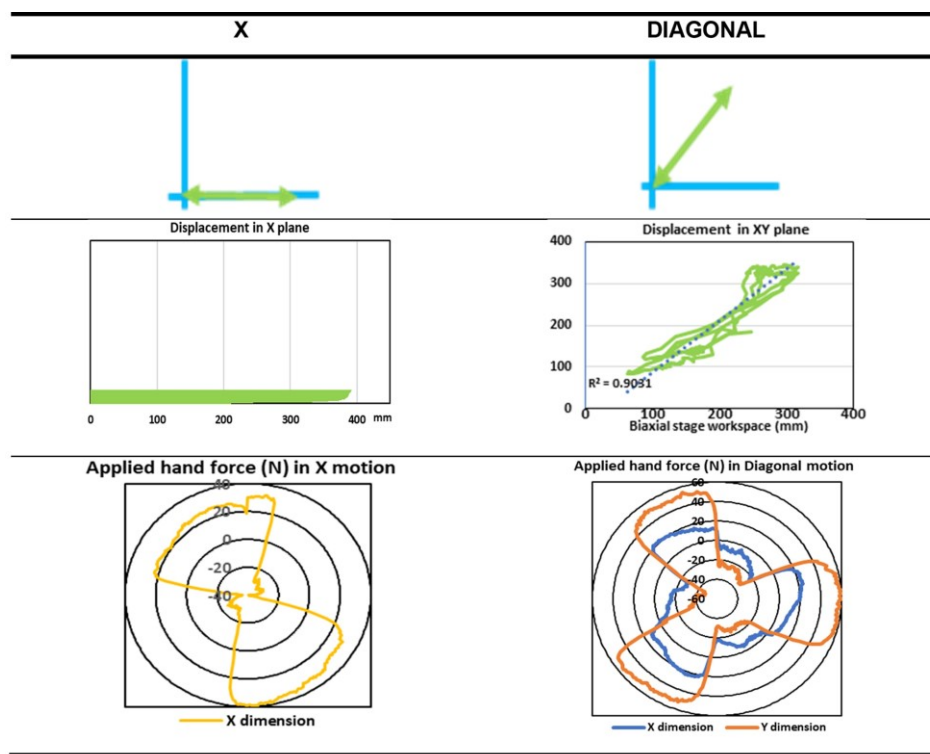


Figure 4.5. Applied forces and displacements during interaction between a contributing participant ( $P_6$ ) and the linear stage in real-time evaluation. Reproduced from [57] © [2021] IEEE with permission.

### 3) Test Phase

A block diagram of the real-time test phase summarizing the procedure followed to evaluate the performance of the trained models is shown in Figure 4.6 [also in Figure 4.3, 4.4]. After the models were trained, each of them (six LCFMG models and three STM models for one motion in a scenario) was evaluated separately, as listed in Table 4-II. During this phase, the robot was controlled by the estimated FMG-based applied force in motion predicted by the LCFMG model on incoming real-time test data. The estimated

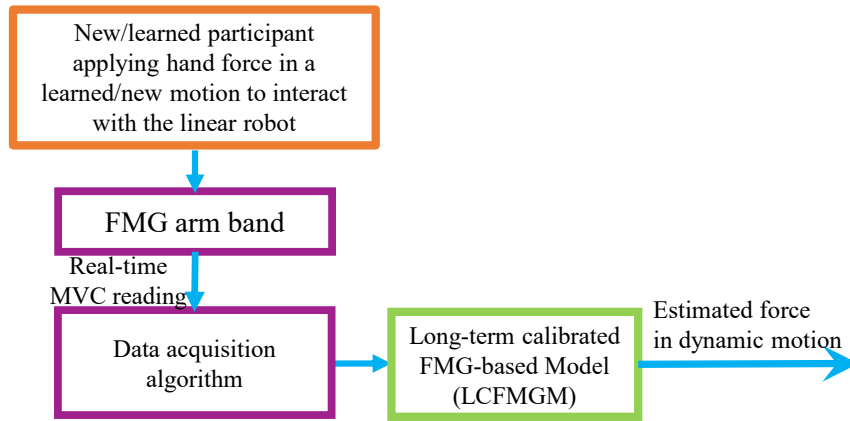


Figure 4.6. Real-time test phase evaluating a long-term calibrated FMG model in recognizing unlearned motion or unlearned participant reproduced from [57] © [2021] IEEE with permission.

force was mapped into displacements for the biaxial stage. This allowed compliant collaboration where the robot followed the same trajectory as the intended motion. Each trained model was evaluated approximately for 120 seconds.

### 4.3.5. Results

Two outcome measures: *co-efficient of determination* ( $R^2$ ) and *normalized root mean square error* (NRMSE) were used to evaluate the performance of the long-term calibrated FMG-based trained models. Performance of the different models in real-time test phases are reported in this section as box plots of  $R^2$  and NRMSE with median values in Figure 4.8-4.11 and listed in Table 4-II.

To verify the capability of the proposed framework, a 5-fold cross validation (CV) on the training dataset [baseline dataset augmented with calibration data] was conducted where the data set was split into 5 folds. In the initial repetition, the first fold was used for evaluating the model while the remaining folds were used to train the model. This process was repeated to test each fold individually. Cross validation was carried out for each participant ( $P_6$ - $P_{15}$ ) in each intended motion ( $M_1$  and  $M_3$ ). Inter-participant-2 and Inter-Motion-2 cases were considered where baseline datasets had larger labelled multiple source distributions (Table 4-II). Training data was shuffled for uniform distribution after aggregating baseline and calibration data. CV Accuracies ( $R^2$ ) in estimating force in each dynamic motion ( $M_1$  and  $M_3$ ) are reported separately in the boxplot shown in Figure 4.7. In both scenarios, median values of cross-validation accuracies were quite higher

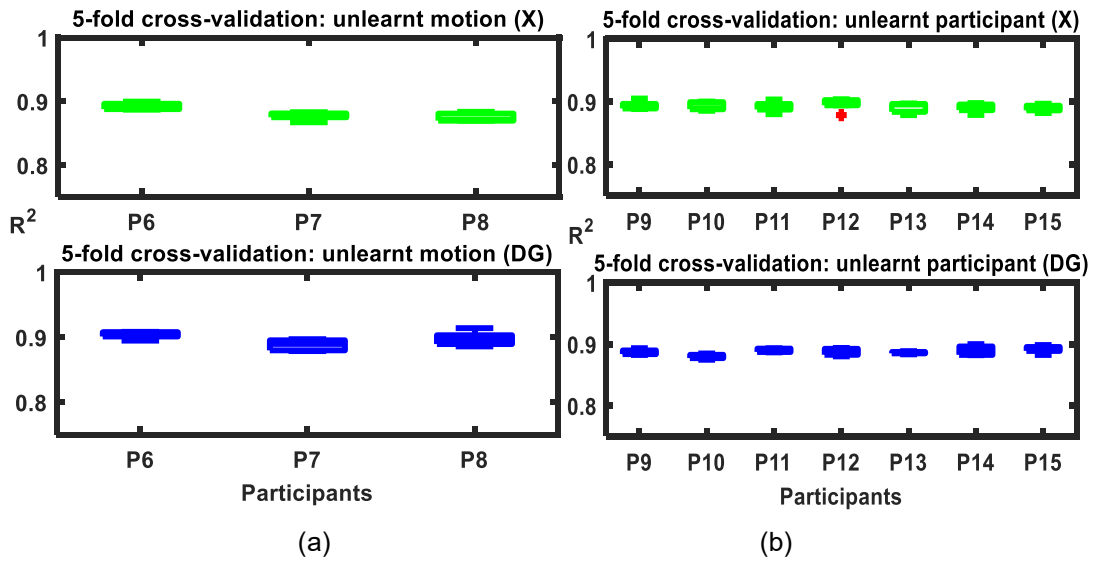


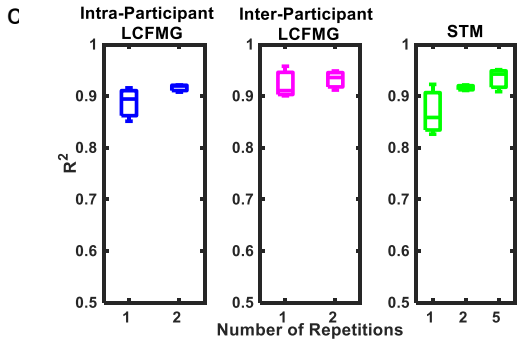
Figure 4.7. 5-fold cross validation accuracies on training dataset for: (a) Inter-Participant-2 in Scenario 1, and (b) Inter-Motion-2 in Scenario 2 reproduced from [57] © [2021] IEEE with permission.

( $R^2 \approx 90\%$ ) and approximately the same for both 'X' and 'Diagonal' motions across participants. This verified the applicability of generality and implementation of GZSL with domain adaptation in recognizing new, unseen, real-time test data.

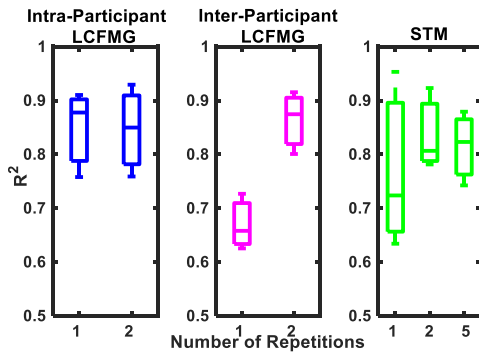
As explained in the previous sections, two different cases of Intra/Inter-Participant and Intra/Inter-Motion were considered in each scenario. During the real-time evaluation, the model LCFMG-0 trained with no calibration data, failed to estimate user-applied forces (average  $R^2 < 0.45$ , average  $\text{NRMSE} > 0.3$ ) in each case. Therefore, the Intra/Inter-Participant-LCFMG-0 and the Intra/Inter-Motion-LCFMG-0 models are not discussed in the following sections.

### A. Scenario 1: Unlearned Motion $M_u$

Real-time evaluation of the long-term models in scenario 1 showed that Inter-Participant-LCFMG-2 performed better in force estimation for both unlearned motions ( $M_1 = X$ -direction,  $M_3 = \text{Diagonal}$ ). Inclusion of two repetitions of calibration data boosted the performance (Figure 4.11); this was noticeable in the case of  $M_3$  ( $R^2 = 0.85$  with LCFMG-2 vs.  $R^2 = 0.67$  for LCFMG-1). Comparison of the performance of the long-term models with the specialized trained models showed competitive advantages of the proposed model. The Inter-Participant-LCFMG-2 outperformed STM-2 and was comparable with STM-5 in estimating user-applied forces in the 'X-direction' motion ( $M_1$ ). This long-term

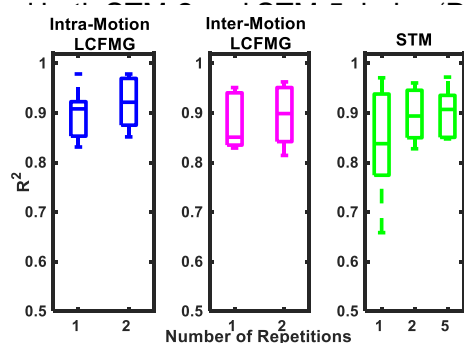


(a) Unlearned pattern: X direction ( $M_1$ )

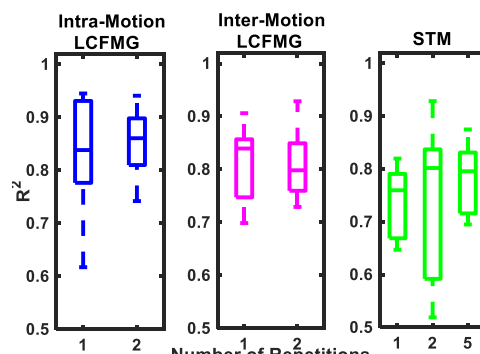


(b) Unlearned pattern: Diagonal ( $M_3$ )

Figure 4.11. Real-time evaluation of scenario 1: Co-efficient of determination ( $R^2$ ) values are reported for each trained model.

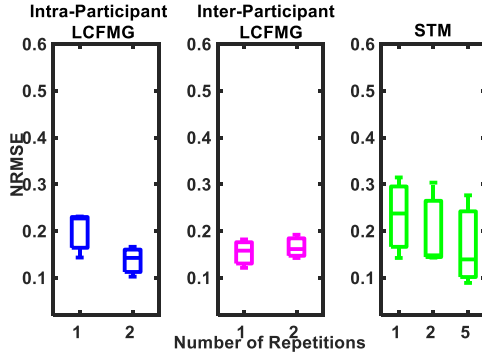


(a) Unlearned participant performing X ( $M_1$ ) pattern

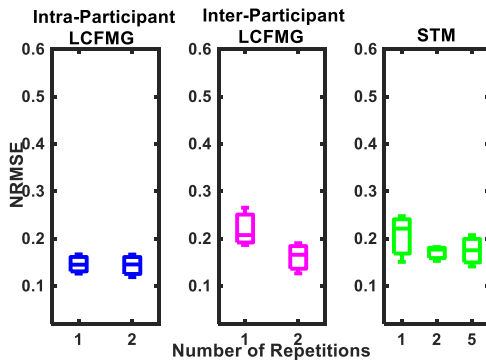


(b) Unlearned participant performing Diagonal ( $M_3$ ) pattern

Figure 4.11. Real-time evaluation of scenario 2: Co-efficient of determination ( $R^2$ ) values are reported for each trained model.

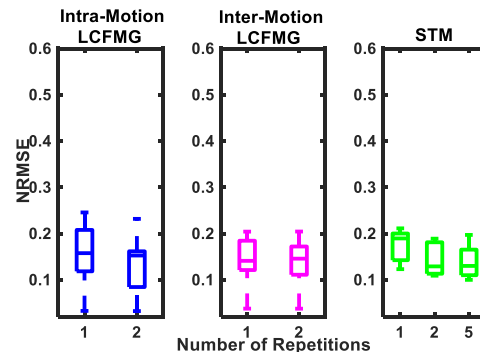


(a) Unlearned motion pattern: X direction ( $M_1$ )

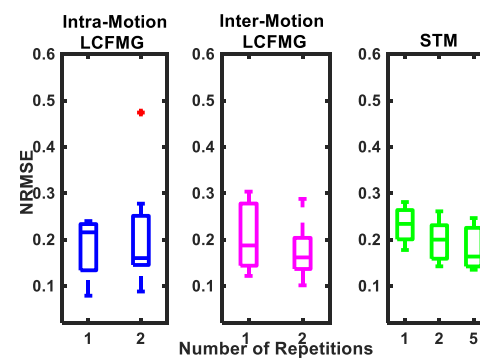


(b) Unlearned motion pattern: Diagonal ( $M_3$ )

Figure 4.11. Real-time evaluation of scenario 1: Normalized root-mean-square error (NRMSE) values are reported for each trained model.



(a) Unlearned participant performing X direction ( $M_1$ ) pattern



(b) Unlearned participant performing Diagonal ( $M_3$ ) pattern

Figure 4.11. Real-time evaluation of scenario 2: Normalized root-mean-square error (NRMSE) values are reported for each trained model.

motion ( $M_3$ ) (highlighted in 'gray' in Table 4-II).

Comparing the real-time performance of different models in both cases of this scenario showed that in most cases, LCFMG-2 outperformed LCFMG-1 as observed by a smaller average NRMSE (Table 4-II) and lower range of error variations (Figure 4.8). The Inter-Participant-LCFMG-2 model was superior to STM-2 and STM-5 in estimating the user-applied forces during the two intended motions  $M_1$  and  $M_3$  (Table 4-II). In addition, the range of variations of NRMSE with Inter-Participant-LCFMG-2 was less than that of the STM-2 model (Table 4-II) during  $M_1$ .

### ***B. Scenario 2: Unlearned Participant $P_u$***

Real-time evaluation results of Scenario 2 where unlearned participants interacted with the stage in the intended motions of  $M_1$  and  $M_3$  (X-direction, Diagonal) are illustrated in Figure 4.9. In both Intra- and Inter-Motion cases, LCFMG-1 and LCFMG-2 showed comparable performances, although LCFMG-1 did not perform well for all participants. In both intended motions, the Inter-Motion-LCFMG-2 model performed better and was comparable with specialized trained models STM-2 and STM-5, as observed in Table 4-II and Figure 4.9.

Calculating NRMSE in the real-time evaluation of this scenario showed similar results like scenario 1. In most cases, LCFMG-2 outperformed LCFMG-1, STM-2, and STM-5 with a lower NRMSE. These errors are presented in boxplots of Figure 4.10 and reported in Table 4-II.



Table 4-II. Summary of training datasets in Long-Term Calibrated FMG-based Model reproduced from [57]  
© [2021] IEEE with permission.

Scenario	Case	Contributing participant	Performed motion	Baseline dataset	Calibration dataset	Repetitions	Samples/sensor	LCFMG model	R <sup>2</sup>	NRMSE
Scenario 1: Unlearned motion	LCFMG Intra-Participant	P <sub>L</sub> (L=6,7,8)	M <sub>U</sub> (U=1,3)	In case of U=1: {M <sub>2</sub> , M <sub>3</sub> , M <sub>4</sub> , M <sub>5</sub> } <sub>P<sub>L</sub></sub>	{M <sub>1</sub> } <sub>P<sub>L</sub></sub>	0	8000	Intra-Participant-LCFMG-0	<0.45 <0.45	>0.30 >0.30
						1	8400	Intra-Participant-LCFMG-1	0.89 0.88	0.23 0.15
				2	8800	Intra-Participant-LCFMG-2	0.92 0.85	0.14 0.16		
	LCFMG Inter-Participant	P <sub>L</sub> (L=6,7,8)	M <sub>U</sub> (U=1,3)	In case of U=1: {M <sub>2</sub> , M <sub>3</sub> , M <sub>4</sub> , M <sub>5</sub> } <sub>P<sub>1</sub>, P<sub>2</sub>, P<sub>3</sub>, P<sub>4</sub>, P<sub>5</sub>, P<sub>L</sub></sub>	{M <sub>1</sub> } <sub>P<sub>L</sub></sub>	0	40000	Inter-Participant-LCFMG-0	<0.45 <0.45	>0.30 >0.30
						1	40400	Inter-Participant-LCFMG-1	0.91 0.67	0.16 0.21
				2	40800	Inter-Participant-LCFMG-2	0.94 0.85	0.16 0.17		
	STM	P <sub>L</sub> (L=6,7,8)	M <sub>U</sub> (U=1,3)	NA	In case of L=1: {M <sub>1</sub> } <sub>P<sub>L</sub></sub> In case of L=3: {M <sub>3</sub> } <sub>P<sub>L</sub></sub>	1	400	STM-1	0.86 0.81	0.24 0.21
						2	800	STM-2	0.92 0.87	0.15 0.17
						5	2000	STM-5	0.94 0.82	0.14 0.18
Scenario 2: Unlearned participant	LCFMG Intra-Motion	P <sub>U</sub> (U=9, ..., 15)	M <sub>L</sub> (L=1,3)	In case of L=1: {M <sub>1</sub> } <sub>P<sub>1</sub>, P<sub>2</sub>, P<sub>3</sub>, P<sub>4</sub>, P<sub>5</sub></sub>	{M <sub>1</sub> } <sub>P<sub>U</sub></sub>	0	10000	Intra-Motion-LCFMG-0	<0.45 <0.45	>0.30 >0.30
						1	10400	Intra-Motion-LCFMG-1	0.91 0.84	0.16 0.20
				2	10800	Intra-Motion-LCFMG-2	0.92 0.86	0.15 0.17		
	LCFMG Inter-Motion	P <sub>U</sub> (U=9, ..., 15)	M <sub>L</sub> (L=1,3)	{M <sub>1</sub> , M <sub>2</sub> , M <sub>3</sub> , M <sub>4</sub> , M <sub>5</sub> } <sub>P<sub>1</sub>, P<sub>2</sub>, P<sub>3</sub>, P<sub>4</sub>, P<sub>5</sub></sub>	In case of L=1: {M <sub>1</sub> } <sub>P<sub>U</sub></sub> In case of L=3: {M <sub>3</sub> } <sub>P<sub>U</sub></sub>	0	50000	Inter-Motion-LCFMG-0	<0.45 <0.45	>0.30 >0.30
						1	50400	Inter-Motion-LCFMG-1	0.85 0.84	0.14 0.17
						2	50800	Inter-Motion-LCFMG-2	0.90 0.80	0.15 0.16
	STM	P <sub>U</sub> (U=9, ..., 15)	M <sub>L</sub> (L=1,3)	NA	In case of L=1: {M <sub>1</sub> } <sub>P<sub>U</sub></sub> In case of L=3: {M <sub>3</sub> } <sub>P<sub>U</sub></sub>	1	400	STM-1	0.84 0.76	0.19 0.24
						2	800	STM-2	0.90 0.80	0.13 0.19
						5	2000	STM-5	0.91 0.74	0.13 0.17

Results corresponding to M<sub>1</sub> and M<sub>3</sub> are given in white- and grey-background cells, respectively.

### C. Comparative analysis

A comparison of the performance of different models is illustrated in Figure 4.12. The long-term calibrated FMG-based models generally acquired better prediction accuracies and lower standard deviations in contrast to the specialized trained models. This superior performance was clearly noticed when comparing LCFMG-2 models with the STM-2 and STM-5 models in Figure 4.12. The Inter-Participant-LCFMG-2 model in scenario 1 (recognizing new, unseen motion) and Intra-Motion-LCFMG-2 model in scenario 2 (recognizing new, unseen participant) performed better among the models. It is worth noting that the LCFMG-2 model obtained high prediction accuracies with limited information, i.e., only two repetitions of calibration of ‘new input sample data’.

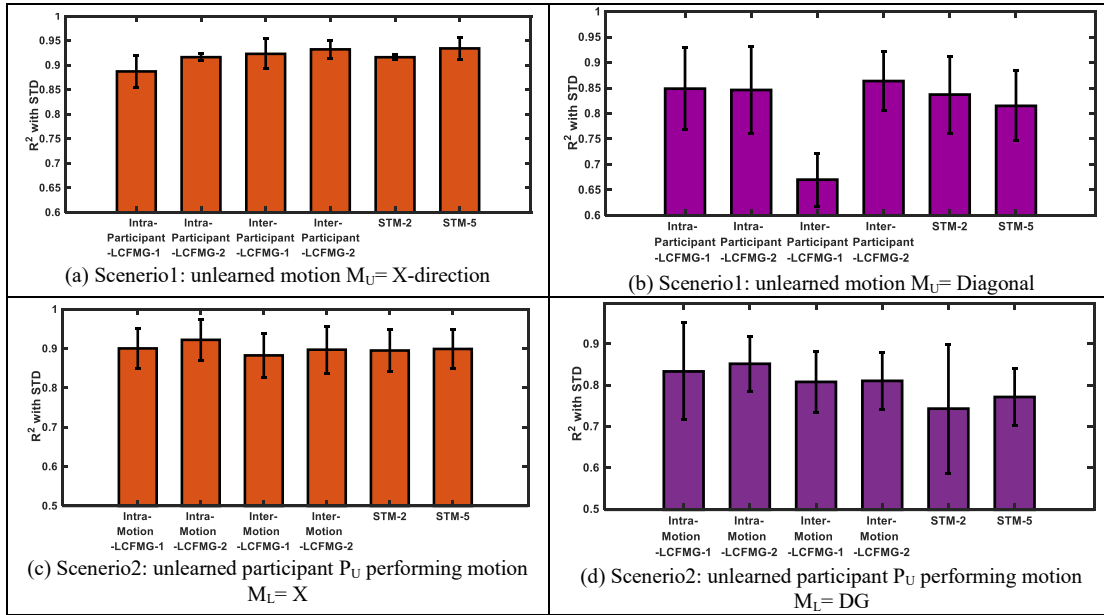


Figure 4.12. Comparison of performance of different models in estimating user-applied forces during different movement patterns. Reproduced from [57] © [2021] IEEE with permission.

The TOST equivalence test showed that Inter-Participant-LCFMG-2 was equivalent to STM-5 (scenario 1: ‘unlearned motion’) with hypothesized mean difference of 0.71 at 5% significance level. Similarly, Intra-Motion-LCFMG-2 was found equivalent to STM-5 (scenario 2: ‘unlearned participant’) with hypothesized mean difference of 0.707 at 5% significance level. However, it was difficult to be conclusive with a smaller population size, as in this study.

In both scenarios for ‘Diagonal’ intended motion, the Inter-Participant/Intra-Motion-LCFMG-1 model did not perform well, as indicated in Figure 4.13. To interact in a

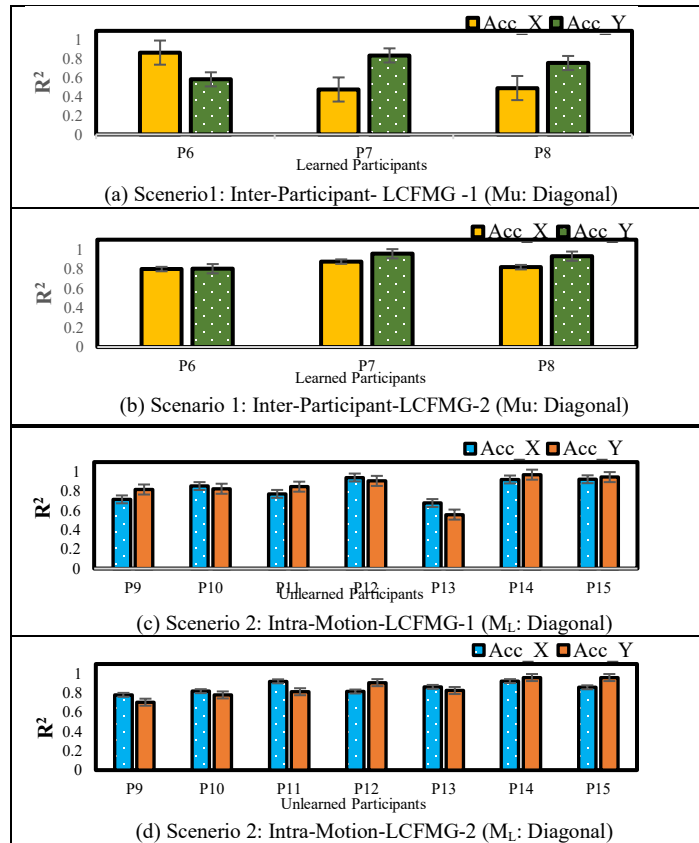


Figure 4.13. Effects of calibration dataset in estimating force in 'Diagonal' motion in Scenario 1 and 2 (reported for best models only) reproduced from [57] © [2021] IEEE with permission.

'Diagonal' motion pattern, a participant had to apply enough force to cause displacements in both X and Y dimensions. Recognizing applied force in a 'Diagonal' motion in the planar space required simultaneous predictions from two models (Model X: applied force in X dimension, and Model Y: applied force in Y dimension) from same real-time observations. For compliant collaboration, substantially higher estimation accuracies were required in each dimension; otherwise, the participant might lose control of the gripper. With a lower calibration dataset (400 samples), recognition became relatively tricky during real-time test phase because slight deviations in applied forces, arm motion speed or posture affected the model performance due to uncertainties involved during interactions. Therefore, a model trained with too little calibration data might fail to learn possible motions. In scenario 1, the Inter-Participant-LCFMG-1 model obtained quite low accuracies in the X-dimension ( $R^2 \approx 50\%$ ) for two participants (P<sub>7</sub>, P<sub>8</sub>), and the average accuracy across participants was only 67%. Also, the Intra-Motion-LCFMG-1 model did not well work for each contributing participant in scenario 2. Observations showed that for at least one participant (P<sub>13</sub>), the model estimated poorly in the Y-dimension ( $R^2 \approx 60\%$ ).

Therefore, the LCFMG-1 model might lead to uncomfortable interactions as it occasionally failed to obtain significant estimation accuracies in both X, Y dimensions during 'Diagonal' motion.

In both scenarios in any intended motion, the LCFMG-1 model obtained lower performance accuracy compared to the LCFMG-2 model. Including 1 repetition of calibration data was good in few instances, but 2 repetitions were better with improved estimation accuracies ensuring smooth interactions in both 'X' and 'Diagonal' motions. Considering the good performance of the LCFMG-2 models being comparable to the STM-5 model, it was decided that there was no need to include more calibration data. Although extending training dataset with more calibration data might further improved the estimation accuracy, it would require a longer data collection session; this might compromise real-time functionality. So, minimal usage of the calibration data was also pursued in this study for faster training in practical situations without compromising user comfort while acquiring higher estimation accuracies.

It was worthy to acknowledge that the real-time performance of an FMG based model varied greatly due to its inherent subject-specific nature. During the real-time evaluation period, continuous inbound test data was subject to individual variances such as sudden deviations in arm motion, posture or changed applied forces. Also, it was noticed that physiological attributes (arm length, forearm and upper arm perimeter, sweats, skin hair, fatigue) affected each participant's muscle contraction readings (better/poor observations in calibration and test data samples). Variations in the calibration data in the intended motion ('X', 'Diagonal') along with these phenomena impacted model performance; hence larger deviations were seen, as depicted in Figure 4.13. Using a small calibration dataset, the model worked well for most unlearned participants, while showed moderate performance for a few others. But when compared to STM-2, the Inter-Participant/Inter-Motion-LCFMG-2 model was superior.

In all scenarios, the Inter-Participant/Inter-Motion-2 model was more generalizable compared to the Intra-Participant/Intra-Motion-2 model. Aggregating calibration data with these diverse multiple sources provided a versatile and unique training dataset, applicable to the contributing participant only. Furthermore, calibration data in the 'X direction' and 'Diagonal' intended motions were quite different. It was the calibration data that determined which intended motion the model would recognize. In scenario 1 for the Inter-

Participant-2 model, although a same reference dataset was used for all participants, training data became different because of the unique 'learnt participant dataset' and calibration data. The 'learnt participant dataset' provided enough seen data from a contributing participant. Similarly, during recognition of unseen participant motion, Inter-Motion-2 model used two repetitions of calibration data (800 samples) aggregated with a large, diversified reference dataset for training. Apart from the calibration data, this trained model had no data from a new, unseen participant. Although CV accuracies were  $\approx 90\%$  in 'X' or 'Diagonal' for both Inter-Participant-2 and Inter-Motion-2 models, the real-time accuracies were 94%, 90% in 'X' and 85%, 80% in 'Diagonal' motions, respectively. These gaps between the offline model performances with real-time evaluations (specifically in M3: 'Diagonal') were observed in another similar research project using sEMG biosignals [30]. It was interesting to note that for 'X' motion, the generalized trained model performed well because of a simpler computation in one dimension only. However, larger standard deviations were observed for 'Diagonal' motion because more complex predictions were required simultaneously in X and Y dimensions (Inter-Participant-2:  $85\pm 5\%$ , and Inter-Motion-2:  $80\pm 7\%$ ) across all participants ( $P_6$ - $P_{15}$ ). Results indicated that adding 'learnt participant dataset' in scenario 1 was worthy in recognizing unseen 'Diagonal' motion, however, it was practically not easy to collect.

On the contrary, Inter-Motion-2 model was more practical to implement. This approach allowed a new, unseen worker interacted with a robot without spending a longer training time in collecting large training data. The Inter-Motion-2 would be particularly useful in FMG-based applications for a first-time user. Therefore, the Inter-Motion-LCFMG-2 model is recommended for the real-world HRI environment. The model will allow any new worker interacting with a robot in an intended motion such as the 'X direction' or 'Diagonal'. This versatile model would work for other simple motions too. Interestingly, the model did not distinguish a repeated user from a new user, meaning that any worker (unseen or seen) would be treated as an unseen participant. This was realistic because even for a repeated user, new calibration data was required for domain adaptation between the source and target data. By aggregating calibration data from previous, repeated use, the Inter-Motion-LCFMG-2 can become personalized (converting gradually towards Inter-Participant-LCFMG-2) for an individual where human interactions with machines are desirable on a regular basis.

## 4.4. Objective 2B

### **Study 2: Estimating interactive forces via supervised domain adaptation and generalization**

In study 1 (objective 2A), inter-participant domain generalization via traditional support vector regressor (SVR) was investigated [56]. In that study, we did not investigate deep transfer learning or intra-session evaluations when a participant interacted with a robot on regular basis.

Therefore, in this second study, deep transfer learning was implemented where interactions were expected to occur on regular basis to overcome limitations of intra-session evaluation [76,77,94]. Transductive transfer learning (few target data available/seen) via supervised domain adaptation (SDA) for inter-session evaluation and inductive transfer learning (target data not available/unseen) via supervised domain generalization (SDG) for inter-participant evaluation was investigated. Domain adaptation reuses part of a model pretrained with large pools of source domains to predict different but related target domain where both domains have same feature spaces with different distributions. On the other hand, domain generalization uses a pretrained model with source domains and attempts to predict unseen target data. It is particularly beneficial to mitigate gaps between different domains where knowledge about the target domain is absent [74,78]. These methods have been success-fully applied in image processing, but there are very few studies in bio-signal-based pHRI because of transient and dynamic nature of bio feedback and hence needs to be investigated. In a repetitive FMG-based pHRI application between a participant and a robot, previous intra-sessions data could contribute building a large dataset. Due to the transient signal, sensors shift, and dynamic interactive environment, each session's data were unique even when the task (applied force in certain motion) was the same. Therefore, the focus of this study was to investigate whether these multiple-source data could improve the user experience in daily interactions utilizing domain adaptation by pretraining a model and fine-tune via transfer learning. We further investigated the impact of domain generalization for a different pHRI task between the robot and several other participants (applied interacting force in another motion) using the same pretrained model. Such cross-subject evaluation became more challenging due to signal variability between the target distribution and the multiple intra-sessions source distributions. Fine-tuning the pretrained model via transfer learning could leverage the gap

between the source and target domain. For both SDA and SDG, few calibration data (target training data) was used for fine-tuning the model to adapt instantaneous state of the signal captured during the dynamic interactions.

An FMG-based convolutional neural network (FMG-CNN) architecture was proposed to investigate pHRI between several human participants and a linear robot/stage via domain adaptation and generalization. This architecture was used as a nonlinear regression model to map applied forces from instantaneous FMG signals during interactions, as shown in Figure 4.14. For transfer learning, multiple source distributions were used to pre-train a unified supervised FMG-based deep transfer learner (SFMG-DTL) model during the training phase. These multiple sources of FMG distributions (source distribution:  $D_s$ ) were collected in several sessions during regular pHRI activities between one human participant and the linear robot while the participant applied hand forces in a certain dynamic SQ-1 motion (source task:  $T_s$ ). The SFMG-DTL model was assessed on separate cases during the evaluation phase on target domain 1 for supervised domain adaptation (case i: SDA) and on target domain 2 for supervised domain generalization (case ii: SDG). In case i, inter-session target domain 1 ( $D_{t-SDA}$ ) was evaluated where the same participant (intra-subject) interacted with the linear robot in SQ-1 motion ( $T_{t-SDA}$ ). While in case ii, inter-participant target domain 2 ( $D_{t-SDG}$ ) was assessed separately for five (5) other participants (cross-subject) interacting with the linear robot in SQ-2 motions ( $T_{t-SDG}$ ). In the beginning of evaluation for both cases, a few calibration data (target training data) were collected to fine-tune the pretrained model in recognizing target distribution. Intra-session evaluations on target domains (target training and target test data) were conducted using FMG-CNN architecture for comparing performances of SDA and SDG cases. Several machine learning algorithms, such as support vector regression (SVR) and multi-dimensional support vector regression (MSVR), were also used for performance comparison in domain adaptation.

Major contributions of this study were:

- Investigating feasibility of deep transfer learning technique in repetitive FMG-based pHRI applications utilizing inter-session FMG data for the first time,
- Proposing a unified transfer learner for both supervised domain adaptation and domain generalization,

- Leveraging periodical calibration as needed with less data than normally required, and
- Proposing a nonlinear FMG-CNN regression architecture for mapping applied force from FMG signals without requiring biomechanical modelling of the human arm.

The FMG-CNN model was written and developed in MATLAB code running on a Desktop PC (Intel Core i7 processor and Nvidia GTX-1080 GPU).

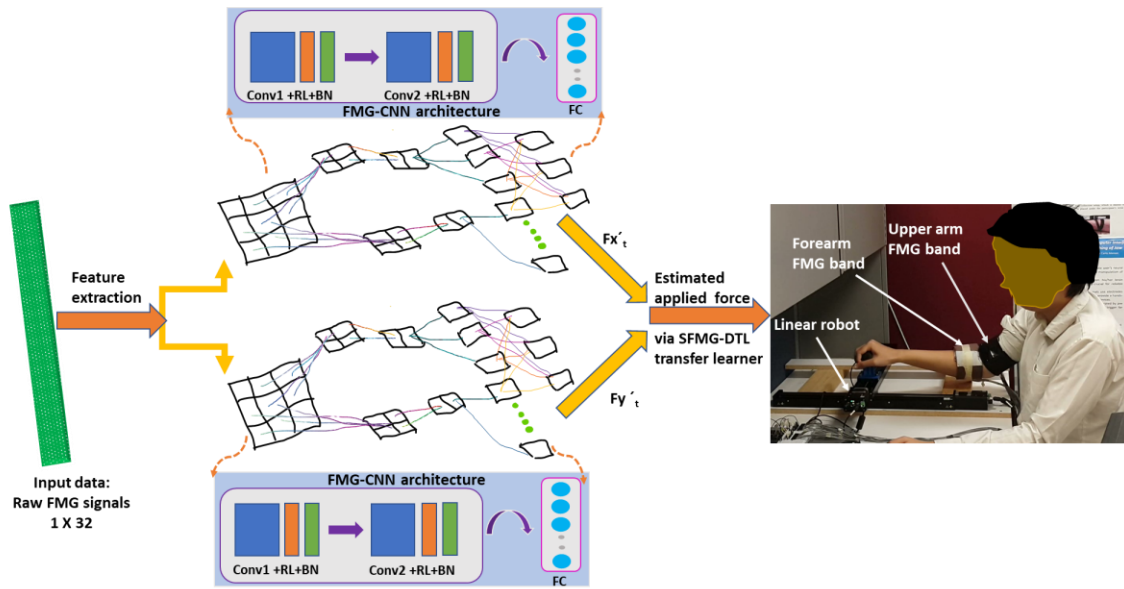


Figure 4.14. The proposed SFMG-DTL transfer learning model for estimating applied force during pHRI on a planar workspace with a linear robot. Reproduced from [58] with permission.

#### 4.4.1. Materials and Methods

##### A. Source and Target Domain

In this study, multiple source domains,  $D_{si} = \{i = 1, 2, 3\}$ , were used for pretraining a deep transfer learning model. Source domain  $D_{si} = \{\chi_{sj}, Y_{sj}\}$  had data matrix  $\chi_{sj} \in R^{N_{sj} \times S^c}$  such that  $i \in \{1, 2, 3\}, j \in \{1, 2, \dots, N_{sj}\}, S^c = \{c_1, \dots, c_{32}\}$  ( $c$ : 32 FMG channels,  $S^c$  = dimensionality of feature vectors, and  $N_{sj}$ : number of samples), and labels  $Y_{sj} = \{F_{sjx}, F_{sjy}, f(\cdot)\}$  [ $f(\cdot)$  was a predictive function, and  $F_{sjx}, F_{sjy}$  were label space of applied forces in X and Y dimensions such that  $f : \chi_{sj} \rightarrow F_{sj-x}$  and  $f : \chi_{sj} \rightarrow F_{sj-y}$ ]. All distributions were



homogenous and balanced. Target domain  $D_t = \{\chi_t\}$  had data matrix  $\chi_t \in R^{N_t} \times S^C$  [ $S^C$ : dimensionality of feature vectors, and  $N_t$ : number of samples in target domain]. Calibration data,  $C_d \in \{X_c, Y_c\}$  [ $Y_c = \{F_{cx}, F_{cy}, f(\cdot)\}$ ], a small subset of  $D_t$ , was used as target training data. A transfer learner pretrained with  $D_{si}$  and fine-tuned with  $C_d$  predicted force label spaces,  $Y_t = \{F_{tx}, F_{ty}, f(\cdot)\}$ , from target test distribution:  $\{\chi_t\} \in D_t$ . In case of domain adaptation, source and target domains were different, but source and target tasks of applied force estimations in SQ-1 motion were same ( $D_s \neq D_t, T_s = T_t$ ) ( $T_s, T_t$ : applied interactive forces in SQ-1 motion}). While in domain generalization, both source and target

Table 4-III. Acronyms used. Reproduced from [58] with permission.

Acronyms	Meaning	Acronyms	Meaning
SDA	Supervised domain adaptation	SQ-1	Interaction force in square motion with variable sizes in domain adaptation
SDG	Supervised domain generalization	SQ-2	Interaction force in square motion in domain generalization
Ds	Source domain	$D_{t-SDA}, T_{t-SDA}$	Target domain and target task in inter-session SDA
Dt	Target domain	$D_{t-SDG}, T_{t-SDG}$	Target domain and target task in inter-participant SDG
Ts	Source task	$D_{si}$	Multiple source domains
Tt	Target task	$F_{xt}'$	Estimated applied forces in X dimension
$C_d$	Calibration data	$F_{yt}'$	Estimated applied forces in Y dimension

domains and tasks were different ( $D_s \neq D_t$ , and  $T_s \neq T_t$ , where  $T_s$ : applied forces in SQ-1 motion and  $T_t$ : applied force in 'SQ-2' motion). Acronyms used in this article are listed in Table 4-III.

## B. Applied Interaction Force Estimation

At an instant of time,  $t$ , instantaneous raw input target test signals SC arriving at the model (with a  $\delta$  of  $\mu$  parameter set) with a probability  $P_t(S_t^C)$  mapped estimated applied force  $F_{xt}'$  and  $F_{yt}'$  (forces in X and Y dimensions) in a dynamic motion such that:

$$f_x(\cdot) = F_{xt}' = \delta, (s_t^C, \mu_1) \quad (4.9)$$

$$f_y(\cdot) = F_{yt}' = \delta, (s_t^C, \mu_2) \quad (4.10)$$

To find best parameter space  $\mu$ , loss function was computed:

$$\mu_1 = L(F_{xt}' - F_{xt}) = \arg \min_{\mu_1} \sum_{k=1}^t (F_{xk} - F_{xk}')^2 \quad (4.11)$$

$$\mu_2 = L(F'_{yt} - F_{yt}) = \arg \min_{\mu_2} \sum_{k=1}^t (F_{yk} - F'_{yk})^2 \quad (4.12)$$

Mean square error (MSE) was used to calculate average squared difference between estimated and real value. MSE for a single observation was:

$$MSE_x = \sum_{k=1}^R \frac{(F_{xk} - F'_{xk})^2}{R} \quad (4.13)$$

$$MSE_y = \sum_{k=1}^R \frac{(F_{yk} - F'_{yk})^2}{R} \quad (4.14)$$

where R was the number of responses; F<sub>xk</sub>, F<sub>yk</sub> were the target output; and F<sub>xk</sub>', F<sub>yk</sub>' were the network's prediction for response k.

### **C. The proposed SFMG-DTL model**

For transfer learning, a unified framework for SDA and SDG based on the FMG-CNN architecture (Figure 2.11). In this framework, the model learned discriminative features of the multiple source domains during pretraining. While fine-tuning, the last three layers of the saved model helped in adapting to converge quickly in recognizing target distribution.

During evaluation, fine-tuning occurred in the final fully connected layer (Figure 2.12). For both pretraining and fine-tuning, stochastic gradient descent (SGD) was implemented as the optimizer. A learning rate (LR) of 1E-04 and maximum epoch (E) of 40 were used in pretraining, while LR = 1E-05 with E = 60 was used during evaluation. MSE loss was used for validation of the training process.

#### **4.4.2. Experimental Setup**

A total of 6 participants (P<sub>1</sub>, ..., P<sub>6</sub>) volunteered in this study. FMG-based pHRI was investigated where a human participant collaborated with a linear robot/biaxial stage, as shown in Figure 4.16. Interactions occurred by applying force at the end-effector of the robot. Two FMG bands (32 feature space) were used to read muscle contractions during interactions. These bands were wrapped around the forearm and upper arm muscle belly.

### 4.4.3. Protocol

Figure 4.17 shows the training and evaluation phases followed in this study to investigate the proposed SFMG-DTL transfer learning model. Both source and target distributions and model hyper parameters used are summarized in Table 4-IV.

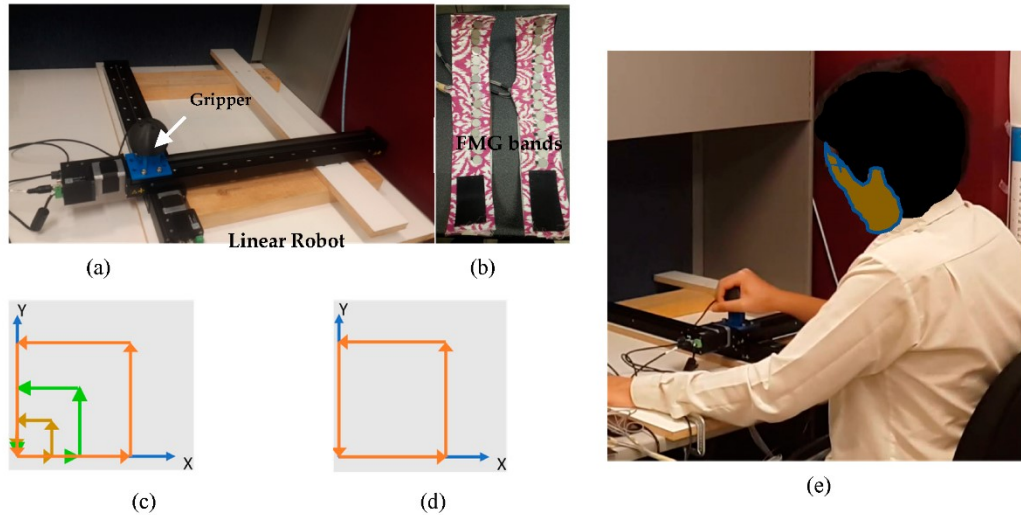


Figure 4.15. Setup used for data collection and evaluation of SFMG-DTL. Reproduced from [58] with permission.

(a) linear robot with gripper and end-effector on top, (b) two FMG bands, (c) interaction force in square motion SQ-1 with variable sizes in domain adaptation, (d) interaction force in square motion SQ-2 in domain generalization, and (e) participant P1 interacting with the robot by applying force in dynamic SQ-1 motion.

During the training phase, source distributions were collected and used for pretraining the model, while in the evaluation phase, separate target domains for SDA and SDG were collected and evaluated separately, as discussed below.

#### A. Training Phase

##### Multiple-Source Data Collection

Multiple training data collection sessions were conducted in three (3) different sessions during interactions between participant P<sub>1</sub> and the linear robot. The collaborative task was conducted by applying hand force in a dynamic square motion SQ-1 of varying sizes on the planar surface, as shown in Figure 4.16 (e). Participant P<sub>1</sub> sat in front of the linear robot/biaxial stage comfortably on a chair locked in position.

Two FMG bands were donned on the forearm and upper arm on the participant's dominant right hand [Figures 4.14 and 4.16(e)]. A total 14 cycles of data were collected during these sessions, where  $600 \times 32$  samples of data were collected in a cycle. In each cycle, participant grasped the gripper and applied interactive force in a dynamic square motion, defined as the source task (TSDA = applied force in SQ-1 motion). Applying forces in a non-uniform anti-clockwise square motion with gradually increasing displacement area on the planar surface [Figure 4.16(c)] were repeated continuously to complete one cycle.

### Pretraining Deep Learning Model

For domain adaptation and generalization, the proposed FMG-CNN architecture was used for pretraining the unified SFMG-DTL transfer learner model. The model was trained to predict applied forces in X and Y dimensions simultaneously from a distribution. Two separate models (Model X, Model Y) were generated for estimating forces in X and Y dimensions and saved as .mat file for use in evaluation sessions.

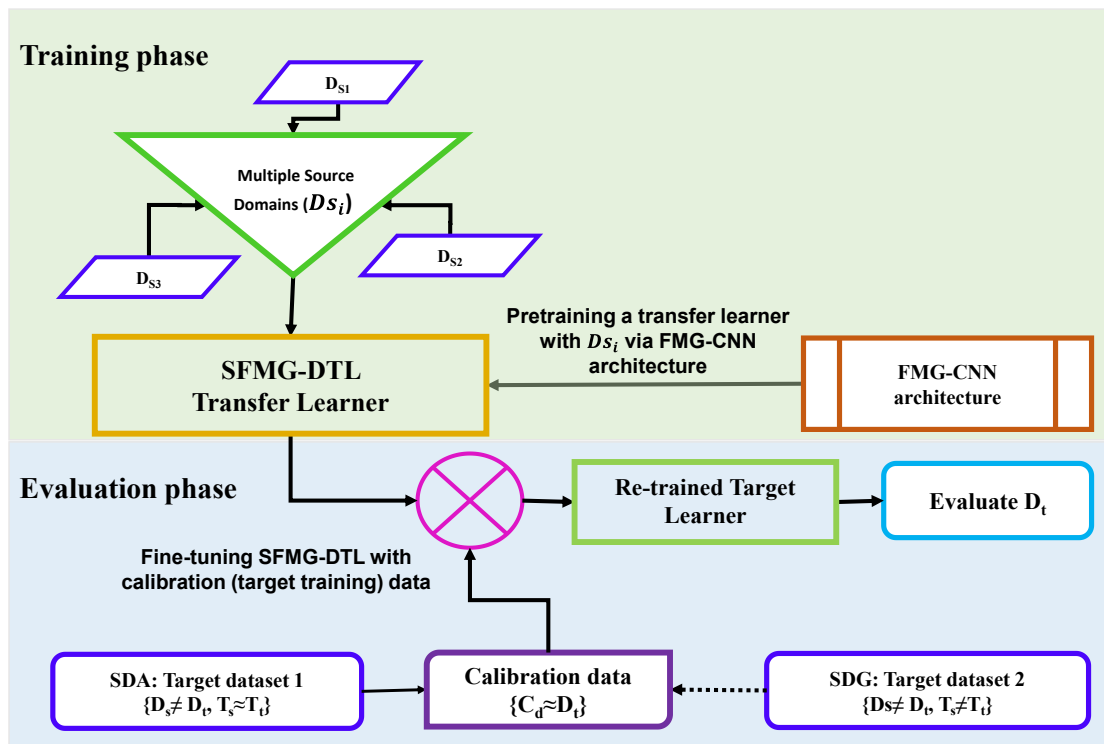


Figure 4.16. SFMG-DTL: unified transfer learning framework for SDA and SDG. Reproduced from [58] with permission.

## B. Evaluation Phase

Case i: evaluating intra-subject/inter-session target domain (Dt-SDA, Tt-SDA) via domain adaptation ( $D_s \neq D_t$ ,  $T_s \approx T_t$ )

Inter-session evaluation was investigated to see if multiple session data from a repetitive user (intra-subject/participant) could be useful in practical applications. In this target task, participant  $P_1$  interacted with the linear robot in similar motion speed and pattern SQ-1 following same source data collection protocol. For domain adaptation, first, a few calibration data were collected as target training data ( $1200 \times 32$  samples) for fine-tuning and formed target dataset 1. The transfer learner was thus retrained to adapt a new target domain. It was then evaluated on  $400 \times 32$  samples of target test data.

Case ii: Evaluating cross-subject/inter-participant target domain (Dt-SDG, Tt-SDG) via domain generalization ( $D_s \neq D_t$ ,  $T_s \neq T_t$ )

For domain generalization, five participants ( $P_2:P_6$ ) contributed to evaluate the pretrained SFMG-DTL model. Target distributions were collected from each participant during a collaborative task that allowed interaction with the robot applying force in a uniform square motion ( $T_{SDG}$  = applied force in SQ-2 motion), as shown in Figure 4.16 (d). For each participant, a total 4 cycles of target data ( $400 \times 32$  samples/cycle) were collected with similar source data collection protocol, and it was termed as target dataset 2. Leaving one out cross-validation (LOOCV) was implemented where 3 cycles were used as target training data for fine-tuning the SFMG-DTL model, and 1 cycle was used as target test data.

Table 4-IV. Source and target domains. Reproduced from [58] with permission.

Pretraining Phase		Evaluation Phase			
Source Domain	Hyper Parameters	Target Domain	Hyper Parameters	Fine Tuning	Target Test Data
$D_{S_i} = \{X_s, Y_s\} \{P_1\}$ , where, $D_{S_i} = \{D_{S_1} \cup D_{S_2} \cup D_{S_3}\}$ = $8400 \times 32$ samples, $T_{SDA}$ : applied force in SQ-1 motion	SGD Epochs: 40 LR: $1E-4$	case i. $D_{t-SDA} = \{X_s, Y_s\} \{P_1\}$ where $T_{SDA}$ : applied force in SQ-1 motion  case ii. $D_{t-SDG} = \{X_s, Y_s\} \{P_2, \dots, P_6\}$ , where $T_{SDG}$ : applied force in SQ-2 motion	SGD Epochs: 60 LR: $1E-5$	$C_d = \{X_c, Y_c\}$ $1200 \times 32$ samples	$D_t = \{X_t, Y_t\}$ $400 \times 32$ samples

#### 4.4.4. Results

For transfer learning in SDA and SDG, the SFMG-DTL pretrained model was evaluated with two separated target domains (in both cases, calibration data/target training data ( $1200 \times 32$  samples) and target test data ( $400 \times 32$  samples) were of same amount). Figure 4.17 shows plots of target domain 1: FMG test distributions and the model's performance of force estimations in X and Y dimensions during SDA.

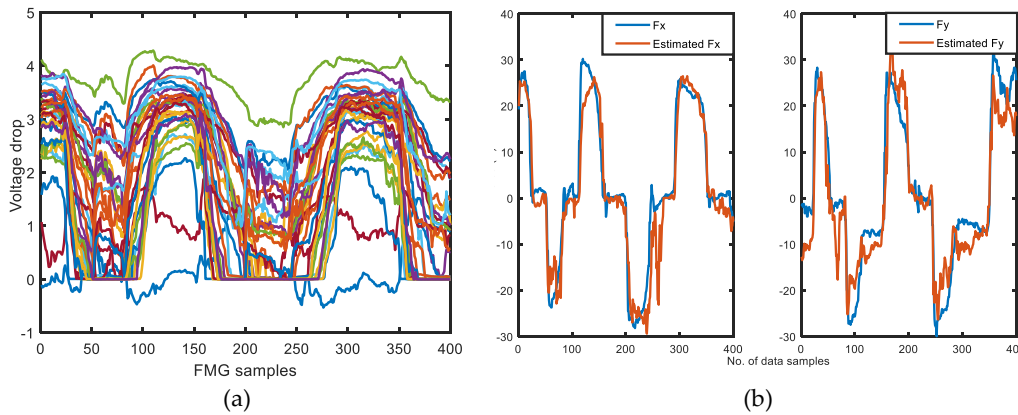


Figure 4.17. Target dataset 1 used in SDA. Reproduced from [58] with permission.

(a) target test FMG data; (b) true forces and estimated forces in X and Y dimensions estimated by the retrained SFMG-DTL learner.

#### A. Supervised Domain Adaptation

Supervised domain adaptation was investigated for inter-session FMG data for repetitive pHRI application with participant P<sub>1</sub>. The results obtained for  $R^2$  and NRMSE with the SFMG-DTL model along with other models are reported in Figure 4.18. The proposed deep transfer learner (MSE loss  $\approx 5.8$ ) outperformed in estimating force in the selected motion SQ-1 in terms of higher accuracies ( $R^2 \approx 89\%$ ) and lower error (NRMSE  $\approx 0.10$ ) than other algorithms, including intra-session baseline SDA (FMG-CNN model with target training data and target test data only). Among these models, MSVR performed poorly ( $R^2 \approx 52\%$ ) despite using a single model to predict force in both X and Y dimensions. Both baseline SDA and SVR showed similar results in predicting force ( $R^2 \geq 81\%$ ). Reported values were averaged for Model X and Model Y in estimation accuracies and losses.

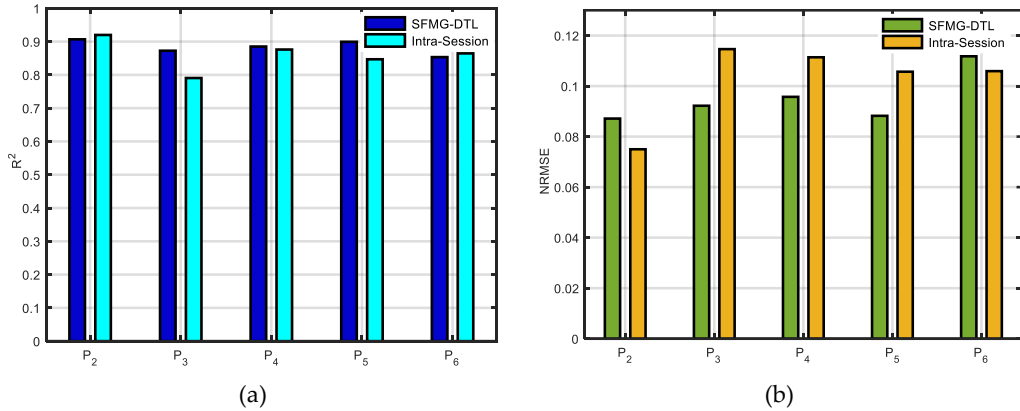


Figure 4.18. Performances of ML and DL models in case ii: on target dataset 2 (supervised domain generalization). Reproduced from [58] with permission.

(a) estimation accuracies ( $R^2$ ) and (b) error in estimation (NRMSE). Averaged values (Model X and Model Y) are reported for both intra-session and SFMG-DTL.

## B. Supervised Domain Generalization

Supervised domain generalization was evaluated for inductive transfer learning where the target distributions were unseen to the pretrained model. An inter-participant/cross-subject test was carried out for five participants (P<sub>2</sub>:P<sub>6</sub>) individually. For comparison, intra-session baseline SDG, using leave one out cross-validation (LOOCV) with target training data and target test data, was executed for each participant. The SFMG-DTL model obtained comparable estimation accuracies ( $R^2 \geq 88\%$ ) similar to the

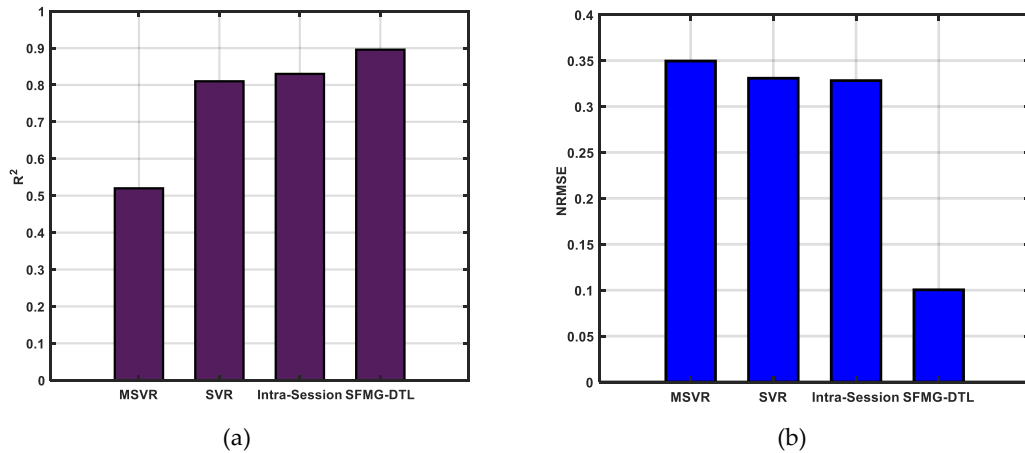


Figure 4.19. Performances of ML and DL models in case i: on target dataset 1 (supervised domain adaptation). Reproduced from [58] with permission.

(a) estimation accuracies ( $R^2$ ) and (b) error in estimation (NRMSE). Averaged values (Model X and Model Y) are reported for SVR, intra-session, and SFMG-DTL.

baseline SDG model ( $R^2 \leq 86\%$ ) across participants. Thus, performance with transfer learning obtained 2.4% improvement in estimating forces in dynamic SQ-2 motion. Moreover, the SFMG-DTL model encountered an error in estimation (NRMSE  $\approx 0.6$ ) that was 3.75% lower than the intra-session model across participants (mean MSE loss  $\approx 5.14\text{N}$ ). Individual results of  $R^2$  and NRMSE (averaged for Model X and Model Y) are reported in Figure 4.19 for all five participants.

### C. Viability of SDG

In this case, estimation accuracies and errors obtained by SFMG-DTL model were found comparable with intra-session evaluation of baseline SDG for participants  $P_2$  and  $P_6$ , while it performed better for  $P_3$ - $P_5$ . Although the overall performance improvement was limited, it was interesting that the SFMG-DTL model improved accuracies in estimating

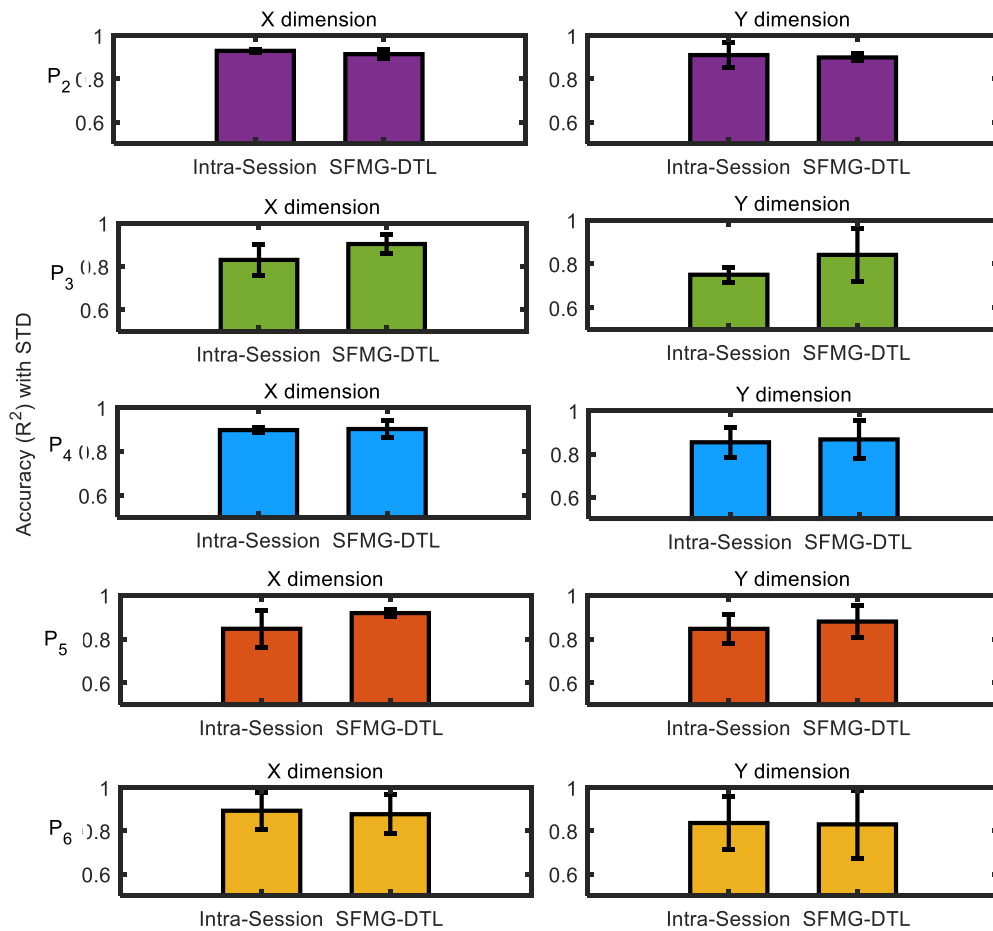


Figure 4.20. Comparing SFMG-DTL model with intra-session evaluation on case ii: target dataset 2 model in estimating forces in X and Y dimensions in domain generalization. Reproduced from [58] with permission.



force in the Y dimension compared to the baseline SDG model for some participants, as shown in Figure 4.20. A *t*-test was carried out with a 95% confidence level to compare performances of the intra-session and the SFMG-DTL model. Estimation accuracies ( $R^2$ ) in Y-dimension via the SFMG-DTL model were found statistically significant. This would improve designing FMG-based HMI in future practical applications.

## Chapter 5.

# Force Myography based Human Robot Collaboration in 3D

The material presented in this chapter is excerpted, reproduced, and modified with permission from the following paper:

[59] © [2022] IEEE with permission. U. Zakia and C. Menon, "Human Robot Collaboration in 3D via Force Myography based Interactive Force Estimations using Cross-Domain Generalization," *IEEE Access*, Mar. 2022, doi: 10.1109/ACCESS.2022.3164103.

Sections of this chapter are reprinted or adapted from the above article to fit the formatting and scope of this document.

### 5.1. Chapter Overview

This chapter discusses the study conducted to achieve research objective 3. The goal was to investigate interactive force estimation during a collaborative task with a Kuka robot in 3D. Cross domain generalization method was implemented in this study to transfer learnt knowledge from 2D-pHRI long-term multiple source domains to estimate interactive forces from 3D-HRC target data.

### 5.2. Introduction

A few studies are conducted recently where FMG biosignal was used for applied force estimations during physical human-robot interaction (pHRI) activities [56-58]. In [56], pHRI between several participants and a fixed linear robot was investigated using intra-session data. For each participant, a task-based ML model was trained with instantaneous applied force readings in a selected dynamic motion. Such individual-specific, intra-session biased model predicted interactive forces ( $94\% > R^2 > 82\%$ ) well in real-time during same session. Interestingly, pHRI with inter-session FMG data via domain adaptation and generalization in planar workspace were recently investigated and were found effective with improved force estimations [57, 58]. In these 2D-pHRI studies, a generalized model

trained with long-term FMG distributions could predict unseen target data in repetitive usage or during interactions with a new participant. The source and target domains in these studies had same interactive 2D-pHRI environment and system setup with 32 FMG channels on forearm and upper arm positions.

In this study, FMG-based pHRI with a 7-DoF Kuka robot was investigated by estimating grasping forces in dynamic motion for the first time. Initially, a cylindrical gripper attached as the end-effector (EEF) was used for hand grasps to interact in certain directions of 1D, 2D and 3D workspace. In each case, an intra-session convolutional neural network (CNN) model could estimate grasping forces in dynamic interactions. There are hardly any studies in literature conducting human robot collaborative task in 3D via FMG-based force estimations. Due to the dynamic nature of the task, tools involved and redundant resolution of human arm in 3D, force estimation via this transient biosignal is challenging. Hence, in this study, we mainly focused on investigating an HRC task of moving a wooden rod in collaboration with the Kuka robot. A 16-channel FMG band was used to capture the muscle readings during the task. Intra-session trained model in this 3D-HRC task moderately estimated forces during evaluation; and hence required further improvements.

In practice, a generalized trained model with reduced dependencies on intra-session data is more desirable. Having more participations or collecting more inter-session data during the HRC task with the Kuka robot was not possible or practical due to time constraints. On the other hand, a large volume of long-term data from the other pHRI platform, i.e., the biaxial stage, could be useful to reduce dependencies on intra-session data. Interestingly, cross-domain generalization (CDG) can be promising for unrelated source and target data that allows a pretrained model to transfer knowledge between different platforms/systems. Furthermore, it generalizes beyond the source distributions [79-80]. Cross-domain generalization is studied in image classifications, vision system, natural language processing, medical diagnosis, machine fault detects, etc. and is found effective [81-85]. The CDG technique has been investigated in few studies conducted on human machine interfaces (HCI) and rehabilitations with surface electromyography (sEMG) or electro encephalography (EEG) biosignals [86-89]. However, it is not studied in biosignals based on HRI tasks. Previously, FMG-based domain adaptation was examined with the same source and target platforms [58]. However, the platform-

independent FMG-based HRI via cross-domain generalization required further investigation [58].

Therefore, in this study, we conducted FMG-based HRC task of moving the wooden rod using the supervised CDG technique. Multiple long-term source data from a 2D-pHRI platform was used in pretraining a transfer learner with CDG (TL-CDG) and was evaluated on a target 3D-HRC task for the first time. In an initial ‘training phase’, the long-term source domains ( $D_{s_i}$ ) were collected when interactions occurred between several participants and a fixed linear robot via 32-channel FMG bands. In this 2D-pHRI platform ( $pHRI_{s_i}$ ), participant interacted by grasping a knob-like gripper/end-effector in the planar surface. In addition, a secondary pool of multiple source domains ( $D_{s_j}$ ) via 16-channel FMG-based 3D-pHRI platform ( $pHRI_{s_j}$ ) were also collected. In this 3D-pHRI, interactions occurred between a participant and a Kuka robot applying forces in 1D, 2D and 3D workspace while grasping a cylindrical gripper/end-effector. The secondary source data was used for comparative purposes only. Three separate TL-CDG models were pretrained with  $D_{s_i}$  data (TL-CDG-1),  $D_{s_j}$  data (TL-CDG-2), and aggregated  $D_{s_j}$  data (TL-CDG-3). These models were evaluated on two separate cross-platform ( $pHRI_t$ ) target domains where a participant interacted with the Kuka robot such that: case *i*) HRC task of moving a wooden rod in 3D environment (target domain  $D_{t_{3D}}$ ), as shown in Table 5-I, and case *ii*)

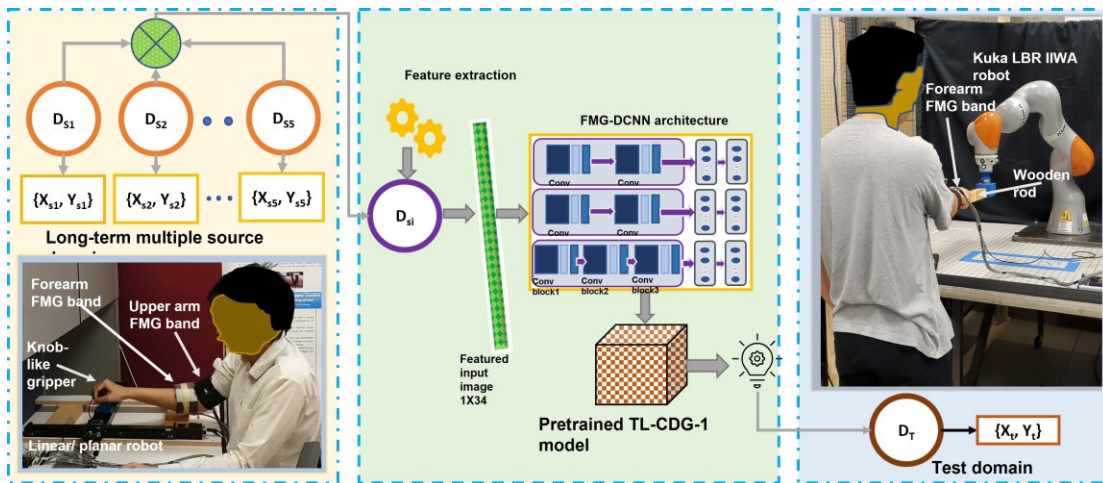


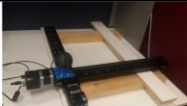
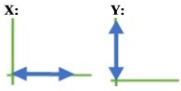
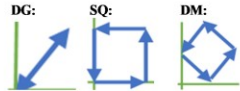

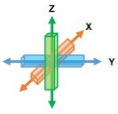
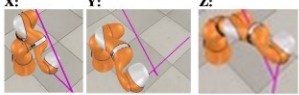
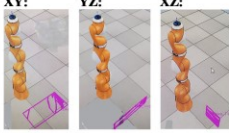


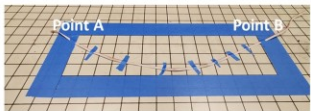
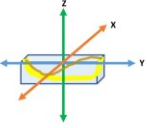
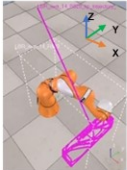



Figure 5.1. Cross-domain generalization via FMG-based TL-CDG-1 transfer learner in evaluating target HRC domain,  $D_{t_{3D}}$  (moving a wooden rod with Kuka robot in 3D). Reproduced from [59] © [2022] IEEE with permission.

HRI in 1D motions by grasping a cylindrical end-effector (target domain  $D_{tD-X,Y}$ ), as shown in Table 5-1.

The primary goal was to investigate the 2D-based TL-CDG-1 transfer learner’s ability to predict out-of-domain HRC target data from unseen 3D pHRI platform, as shown in Figure 5.1. Hence, all pretrained TL-CDG models were evaluated in case *i* while the TL-CDG-1 model was evaluated in case *ii* only. Therefore, the main focuses of this study were:

1. investigating FMG-based HRC with a Kuka robot in 3D,
2. investigating HRC activities using reduced FMG channels and reduced intra-session training data dependency, and
3. investigating FMG-based deep transfer learning with cross domain generalization in HRC for the first time where  $D_s \neq D_t$ ,  $T_s \neq T_t$ , and  $pHRI_s \neq pHRI_t$ .

Table 5-1. HRI/HRC Experimental Setup Reproduced from [59] © [2022] IEEE with permission.

pHRI	Experimental Setup	1D	2D	3D
HRI with a linear robot in 1D & 2D				NA
HRI with a Kuka robot in 1D, 2D & 3D	 	 For X# 0.4: 0.7 m(x), -0.3:0.2m(y), 0.4:0.42m(z) For Y# 0.6: 0.6 m(x), -0.35:0.2m(y), 0.4:0.4m(z) For Z# 0.6: 0.7 m(x), -0.3:0.2m(y), 0.25:0.7m(z)	 For XY # 0.45: 0.65 m(x), -0.3:0.2m(y), 0.4:0.42m(z) For YZ # 0.6: 0.62 m(x), -0.3:0.2m(y), 0.3:0.45m(z) For XZ # 0.45: 0.65 m(x), -0.1:0.25m(y), 0.3:0.5m(z)	 X Dimension: 0.2: 0.6 m Y Dimension: -0.5:0.5 m Z Dimension: 0.2:0.7m
HRC with a Kuka robot in 3D (moving a wooden rod from point A to point B)			 X Dimension: 0.2: 0.6 m Y Dimension: -0.5:0.5 m Z Dimension: 0.2:0.7m	
32-channel forearm & upper arm FMG bands		16-channel forearm FMG band		

## 5.3. Problem Statement

### 5.3.1. Transfer learning for Unseen Target Domain

In this study, transfer learning was investigated pretraining a cross-domain transfer learner using a primary set of five ( $i=1, \dots, 5$ ) different long-term source domains such that  $D_{si} \in \{X_{si}, Y_{si-X,Y,Z}\}$  ( $X_{si}, Y_{si-X,Y,Z}$  were 32 feature spaces, and true force labels in 3D, respectively) collected from a 2D-pHRI (pHRI<sub>si</sub>) platform. A secondary set of seven ( $j=6, \dots, 12$ ) source domains  $D_{sj} \in \{X_{sj}, Y_{sj-X,Y,Z}\}$  were also collected ( $X_{sj}, Y_{sj-X,Y,Z}$ : 16 feature spaces, and applied force labels, respectively) during interactions in a 3D-pHRI (pHRI<sub>sj</sub>) platform. Each source domain  $D_s$  had a feature space of  $X_s \in \mathbb{R}^{N_s \times \text{FMG}_C}$  where  $N_s =$  no. of samples,  $\text{FMG}_C = \{1, 2, \dots, C\}$  ( $C = 32, 16$  for  $D_{si}$  and  $D_{sj}$ ) and true force labels of  $F_{X_s}, F_{Y_s}, F_{Z_s}$  in X, Y, Z directions, respectively. Applying feature engineering, a new input feature space  $X_s^*$  was constructed such that:

$$\begin{aligned} X_{S_i}^* &= [X_{S_i}, \overline{X_{S_i}}, \sigma(X_{S_i})], \text{ for } D_{S_i}, \text{ and} \\ X_{S_j}^* &= [X_{S_j}, \gamma(X_{S_j}), \overline{X_{S_j}}, \sigma(X_{S_j})], \text{ for } D_{S_j} \end{aligned} \quad (5.1)$$

where  $\overline{X_S}$ ,  $\gamma(X_S)$  and  $\sigma(X_S)$  were the average, up sampled matrix, and variance of  $X_S$ , respectively. Therefore, all source domains became homogenous and balanced vectors ( $34 \times N_s$  for each domain) suitable for deep CNN architecture. Target domain  $D_t \in \{X_t, Y_{t-X,Y,Z}\}$  had feature space of  $X_t \in \mathbb{R}^{N_t \times \text{FMG}_C}$  where  $N_t =$  no. of samples,  $\text{FMG}_C = \{1, 2, \dots, C\}$  ( $C = 16$  FMG channels) and  $Y_{t-X,Y,Z}$ : true labels of applied forces in X, Y, Z directions ( $F_{X_t}, F_{Y_t}, F_{Z_t}$ ). For evaluation, a new feature space was reconstructed as:

$$X_t^* = [X_t, \overline{X_t}, \gamma(X_t), \sigma(X_t)] \quad (5.2)$$

where  $\overline{X_t}$ ,  $\gamma(X_t)$  and  $\sigma(X_t)$  were the average, up sampled matrix (up sampled to 32 channels) and variance of  $X_t$ , respectively. Hence, the target distributions had total feature spaces of ( $34 \times N_t$ ) like the source domains for force mapping during evaluation. Adding few more features increased data variabilities in the feature spaces for a deep learning model to learn discriminative features better.

For the source task  $T_s$ , true labels of applied interaction forces ( $Y_s$ :  $F_X, F_Y, F_Z$ ) were standardized according to:

$$Y_s^* = (Y_s - Y_s^{\sim})/\sigma(Y_s) \quad (5.3)$$

where  $Y_s^{\sim}$  and  $\sigma(Y_s)$  were the average and variance of  $Y_s$ , respectively. Due to the planar workspace of  $D_{s_i}$  domains,  $F_z$  was at minimal values (0.1N) as the force interactions were one-directional (1D) and two-directional (2D) only. A proposed deep transfer learning 'TL-CDG' model with a  $\phi$  of  $\Omega$  parameter based on a unique CNN architecture (Section 2.6.1) was used as feature extractor on  $\{X_s^*, Y_s^*\}$  and the trained model with learnt weights were saved to evaluate target domain  $D_t$ .

At an instant time,  $t$ , the pretrained TL-CDG model was used to evaluate target input  $FMG_C$  signals  $\{X_t^*\}$  which was split into calibration data  $\{X_C^* \subset X_t^*\}$  and validation data  $\{X_D^* \subset X_t^*\}$ . The calibration data (target training data)  $\{X_C^*, Y_{C-X,Y,Z}\}$  was used to retrain the model for target adaptation. Afterwards, for target task  $T_t \{Y'_{D-X,Y,Z}, f(\cdot)\}$ , a predictive function,  $f(\cdot)$  estimated interaction forces in the X, Y and Z directions on validation set (target test data)  $\{X_D^*\}$  at a time  $t$  such that:

$$f_x(\cdot) = F'_{XD} = \phi, (X_D^*, \Omega_1) \quad (5.4)$$

$$f_y(\cdot) = F'_{YD} = \phi, (X_D^*, \Omega_2) \quad (5.5)$$

$$f_z(\cdot) = F'_{ZD} = \phi, (X_D^*, \Omega_3) \quad (5.6)$$

The model attempted to find the best parameter space  $\Omega$ , which was determined by computing the loss function using force label space  $Y_{D-X,Y,Z}(F_{XD}, F_{YD}, F_{ZD})$  of target test data:

$$\Omega_1 = L(F'_{XD} - F_{XD}) = \arg \min_{\Omega_1} \sum_{q=1}^t (F'_{XD} - F_{XD})^2 \quad (5.7)$$

$$\Omega_2 = L(F'_{YD} - F_{YD}) = \arg \min_{\Omega_2} \sum_{q=1}^t (F'_{YD} - F_{YD})^2 \quad (5.8)$$

$$\Omega_3 = L(F'_{ZD} - F_{ZD}) = \arg \min_{\Omega_3} \sum_{q=1}^t (F'_{ZD} - F_{ZD})^2 \quad (5.9)$$

Root mean square error (RMSE) determined the average squared difference between the estimated and the real value. RMSE for a single observation was:

$$RMSE_x = \sum_{q=1}^W \frac{(F'_{XD} - F_{XD})^2}{W} \quad (5.10)$$

$$RMSE_y = \sum_{q=1}^W \frac{(F'_{YD} - F_{YD})^2}{W} \quad (5.11)$$

$$RMSE_z = \sum_{q=1}^W \frac{(F'_{ZD} - F_{ZD})^2}{W} \quad (5.12)$$

where  $W$  was the number of responses,  $F_{XD}, F_{YD}, F_{ZD}$  were the target force labels, and  $F'_{XD}, F'_{YD}, F'_{ZD}$  were the predicted forces for a response  $q$ .

### 5.3.2. The TL-CDG model

In this study, an FMG-based deep convolutional neural network (FMG-DCNN) architecture was proposed (as described in chapter 2) for pretraining a TL-CDG model. For FMG-based HRC in 3D, three separate models (Model X, Y and Z) were pretrained for predicting applied force in that direction using appropriate Equations (5.4) -(5.6). For pHRI in 1D (either in X, Y or Z direction), only one relevant model was pretrained. A homogenous matrix of 34 features was used as input for the model using Equation (5.1), as described in Section II.A.1. Input data was normalized (minmax scaling) and passed to the input image layer [image size  $1 \times 34$  with 'zerocenter' normalization]. For optimization, stochastic gradient descent (SGD) was implemented with a learning rate (LR) of  $1E-05$  for maximum 60 epochs during pretraining.

For transfer learning, each pretrained model was finetuned by reinitializing a fully connected layer before the final regression layer and retrained the model with target training data. The retrained model was evaluated on target test data with SGD optimizer, an LR of  $1E-05$  ( $1E-06$  for Model Y) for a maximum of 60 epochs. MSE loss [Equation (5.10) -(5.12)] was calculated to evaluate model performance in force estimations.



## 5.4. Protocol

A total of 6 participants volunteered as end-users in this study who had no prior knowledge about FMG technique. All participants were healthy, right-handed and their average age was  $33\pm 8$  years. In the supervised cross-domain generalization protocol, training phase of long-term FMG data collection was followed by evaluation phase as discussed below:

### 1. Training Phase

In this initial phase, multiple source domains were collected over a period of several months, and then several TL-CDG models were pretrained.

#### A. Long-term Multiple Source Data Collection

##### *i) Primary Source Domains $Ds_i \{i=1, 2, \dots, 5\}$*

Five participants ( $P_1, P_2, \dots, P_5$ ) wearing two FMG bands on their forearm and upper arm on the dominant hand interacted with a fixed linear robot. Participants sat in front of the robot on a fixed-positioned chair. Each participant interacted with applied forces in five dynamic motions (source tasks,  $Ts_i \{i = 1, 2, \dots, 5\}$ ) such as 1D 'X' ( $Ds_1$ ), 'Y' ( $Ds_2$ ), while 'Diagonal' ( $Ds_3$ ), 'Square' ( $Ds_4$ ) and 'Diamond' ( $Ds_5$ ) in 2D plane in separate sessions, as shown in Table 5-1. These interactions included arm flexions, extensions and arm abduction, adductions in the planar space. For interactions in the 2D plane ('Diagonal', 'Square' and 'Diamond' motions), forces  $F_x$  and  $F_y$  acted in X and Y directions with  $F_z$  being at a constant value in the Z direction. In 1D interactions, only  $F_x$  or  $F_z$  acted in 'X' or 'Y' direction. A total of  $50,000 \times 32$  FMG samples data were collected for the five source domains ( $Ds_1, Ds_2, \dots, Ds_5$ ). Each participant performed 5 'repetitions' (1 repetition: continuing interaction via applied force in a certain motion for approximately 1 min.) for each interactive task resulting in  $2,000 \times 32$  samples. More information on the data collected in this setup are available in [10]. All distributions and dynamic motions were different in these primary sources ( $Ds_1 \neq Ds_2 \neq Ds_3 \neq Ds_4 \neq Ds_5, Ts_1 \neq Ts_2 \neq Ts_3 \neq Ts_4 \neq Ts_5$ ).

##### *ii) Secondary source domains $Ds_j \{j=6, 7, \dots, 12\}$*

In these source data collections, participant ( $P_6$ ) wearing a 16 channel FMG band on dominant (right) forearm stood steadily in one position in front of the Kuka robot, grasped the cylindrical gripper and applied forces in 1D [ $Ds_6 = 'X', Ds_7 = 'Y'$  and  $Ds_8 = 'Z'$

dimensions], 2D [ $Ds_9 = 'XY'$ ,  $Ds_{10} = 'YZ'$  and  $Ds_{11} = 'XZ'$  plane] and 3D plane [ $Ds_{12} 'XYZ'$ ], as shown in Table 5-I. For compliant collaboration, trajectories of the Kuka robot were bounded by a 6-axis rectangular plane for an individual task [Table 5-I]. For each interaction in 1D, 2D, 3D, 5 repetitions of sample data were collected for training and evaluation purposes. Approximately, a total of  $44,000 \times 16$  FMG samples data were collected from these source domains where all distributions and tasks were different ( $Ds_6 \neq Ds_7 \neq Ds_8 \neq Ds_9 \neq Ds_{10} \neq Ds_{11} \neq Ds_{12}$ ,  $Ts_6 \neq Ts_7 \neq Ts_8 \neq Ts_9 \neq Ts_{10} \neq Ts_{11} \neq Ts_{12}$ ).

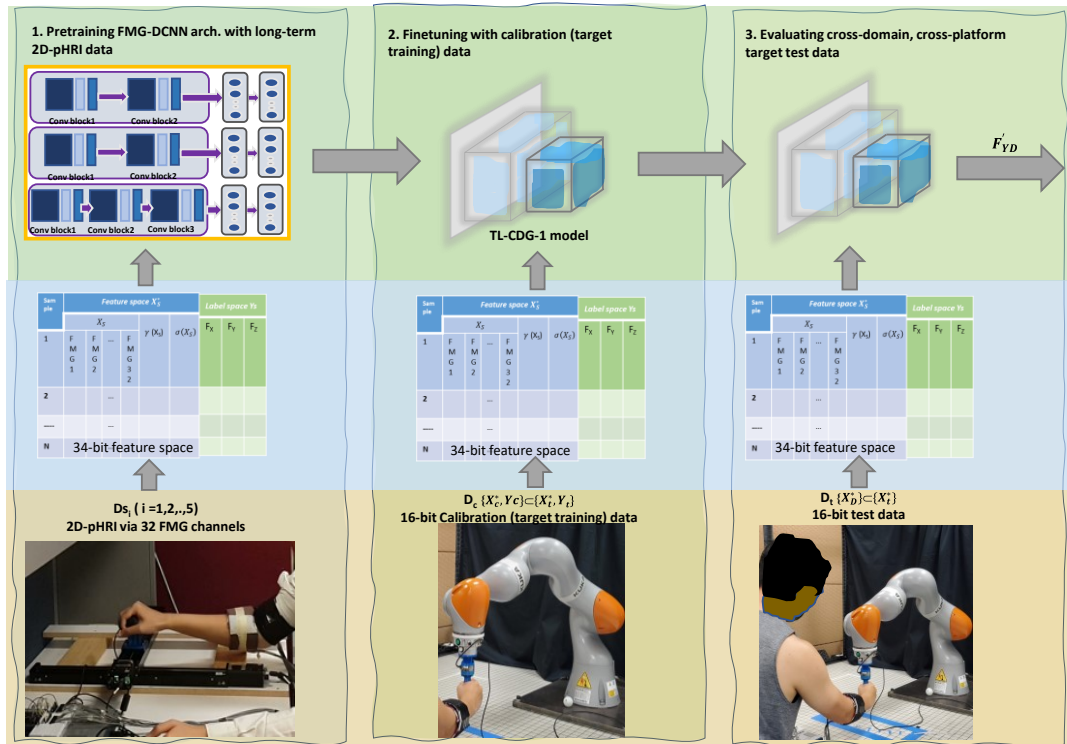


Figure 5.2. Transfer learning steps with TL-CDG-1 model for target domain,  $Dt_{1D-Y}$ : HRI in 1D-Y (traversing arm while grasping cylindrical EEF in right and left directions). Reproduced from [59] © [2022] IEEE with permission.

## B. Pretraining Deep Learning Models

For cross domain generalization, three deep learning TL-CDG models were pretrained using the FMG-DCNN architecture such that: a) TL-CDG-1: using  $Ds_i$  domains only, b) TL-CDG -2: using  $Ds_j$  domains only, and c) TL-CDG -3: using  $Ds_i$  and  $Ds_j$  domains ( $Ds_i \cup Ds_j$ ). All pretrained models had three separate models (Model X, Model Y, Model Z) for estimating interactive forces ( $F_x$ ,  $F_y$  and  $F_z$ ) in 3D motions, while only one model was

used in 1D (Model X for 1D-X, and Model Y for 1D-Y). These models were saved as .mat files for evaluation phase.

## **2. Evaluation Phase**

In this final phase, the two target domains: *case i*) HRC in 3D to move a wooden rod from point A to B ( $Dt_{3D}$ ), and *case ii*) pHRI in simple motions in 1D ( $Dt_{1D=X, Y}$ ) with cylindrical gripper were evaluated separately. In both cases, collected target data (5 repetitions:  $\sim 6,400 \times 16$  FMG data) were divided into target training data (first 4 repetitions) and target test data (last repetition).

### **A. Case i: Target domain, $Dt_{3D}$ (HRC in 3D)**

In each repetition, participant  $P_6$  wearing 16 channels forearm FMG band stood in front of the Kuka robot, grasped the free end of the wooden rod and moved it collaboratively with the robot from point A to B and from point B to A repeatedly. The movements continued for a certain time ( $\sim 2$  min.) for one 'repetition' in a half-circular 3D trajectory path as the participant applied forces within his comfort zone. This was carried on 5 times collecting 5 repetitions of data, as shown in Figure 5.1, and Table 5-I. All three pretrained TL-CDG models were finetuned with the target training data. The retrained target learner was then evaluated on target test data, thus resembling usual intra-session evaluation.

### **B. Case ii: Target domain, $Dt_{1D=X, Y}$ (pHRI in 1D)**

To observe how FMG-based generalization would impact pHRI with simple interactions, this special case was investigated with the TL-CDG-1 model only. This pretrained model was evaluated during pHRI between participant  $P_6$  with Kuka robot in 1D-X and 1D-Y directions separately. Source domains  $Ds_6$  and  $Ds_7$  ( $\sim 6,400 \times 16$  samples) were treated as  $Dt_{1D=X}$  and  $Dt_{1D=Y}$  where the first 4 repetitions were used for finetuning the TL-CDG-1 model, and the final repetition was used for model evaluation.

During the primary source distributions,  $Ds_i$ , the interactive task was done on the horizontal plane with the biaxial stage. The tasks in secondary source distributions,  $Ds_j$ , and the target distributions,  $Dt_{3D}$  or  $Dt_{1D=X, Y}$  were done in the vertical plane during interactions with the Kuka robot. This was clearly an example of transferring knowledge between two separate HRI platforms. Also, interactions with the Kuka were set within

certain boundaries in the 3D space which allowed dynamic or tilted arm movements instead of rigid, fixed motions.

## 5.5. Results

Pretraining the TL-CDG models and evaluations on target domain  $D_{t_{3D}}$  (*case i: HRC in 3D*) and  $D_{t_{1D-X, Y}}$  (*case ii: pHRI in 1D*) were carried out with MATLAB scripts using deep learning toolbox, neural network toolbox, statistics and machine learning toolbox, signal processing toolbox running on a desktop PC (Intel Core i7 processor and Nvidia GTX-1080 GPU). Force estimations in target domains were evaluated using  $R^2$  and *Coeff* while error in predictions was measured using *RMSE* and *NRMSE*, as reported of one minute evaluation for both *case i* and *case ii* in Table 5-II. Intra-session evaluation on the target domains (trained with 4 repetitions, tested on 5<sup>th</sup> repetition) were carried out using the baseline FMG-DCNN network to compare performances of the transfer learners in domain generalizations, as included in Table 5-II.

Table 5-II. Performances of TL-CDG Models. Reproduced from [59] © [2022] IEEE with permission.

Target domain	Pretrained Model	$R^2$	Coeff	RMSE	NRMSE	
<b>Case i</b> <i>D<sub>t<sub>3D</sub></sub>: HRC with Kuka in 3D</i> (moving a wooden rod from point A to point B)	TL-CDG-1	X: 0.70 Y: 0.59 Z: 0.59 63%	X:0.84 Y:0.76 Z:0.77 79%	X:6.26 Y:4.50 Z:3.12 4.6N	X:0.12 Y:0.13 Z:0.13 0.13	
	TL-CDG -2	X: 0.67 Y: 0.64 Z: 0.48 60%	X:0.82 Y:0.80 Z:0.70 77%	X:6.58 Y:4.13 Z:3.54 4.75N	X:0.13 Y:0.12 Z:0.15 0.13	
	TL-CDG-3	X: 0.68 Y: 0.55 Z: 0.61 61%	X:0.82 Y:0.74 Z:0.78 78%	X:6.41 Y:4.75 Z:3.03 4.73N	X:0.16 Y:0.15 Z:0.14 0.15	
	Baseline FMG-DCNN	X: 0.58 Y: 0.53 Z: 0.57 56%	X:0.76 Y:0.73 Z:0.76 75%	X:7.30 Y:4.76 Z:3.28 5.11N	X:0.13 Y:0.14 Z:0.14 0.14	
<b>Case ii</b> <i>D<sub>t<sub>1D-X</sub></sub>: pHRI with Kuka in 1D-X</i> (interacting by grasping the cylindrical gripper)	TL-CDG-1	86%	93%	3.58N	0.14	
	Baseline FMG-DCNN	77%	88%	4.72N	0.18	
	<i>D<sub>t<sub>1D-Y</sub></sub>: pHRI with Kuka in 1D-Y</i> (interacting by grasping the cylindrical gripper)	TL-CDG-1	79%	89%	5.79N	0.11
		Baseline FMG-DCNN	66%	81%	7.28N	0.14

### 5.5.1. Case i: HRC in 3D (Target domain $D_{t_{3D}}$ )

In this case, among the TL-CDG pretrained models, the TL-CDG-1 model was moderate in force estimation ( $R^2 \approx 63\%$ ,  $Coeff \approx 80\%$ ,  $RMSE \approx 4.6N$ ,  $NRMSE \approx 0.128$ ) while TL-CDG-2 and TL-CDG-3 models had similar accuracies (SDG-TL-2:  $R^2 \approx 60\%$ ,  $Coeff \approx 77\%$  and TL-CDG-3:  $R^2 \approx 62\%$ ,  $Coeff \approx 79\%$ ) in force estimations and losses (SDG-TL-2:  $RMSE \approx 4.8N$ ,  $NRMSE \approx 0.13$  and TL-CDG-3:  $RMSE \approx 4.7N$ ,  $NRMSE \approx 0.13$ ). These reported results were obtained by averaging corresponding values of Model X, Y, Z of each TL-CDG model. An intra-session baseline FMG-DCNN model with same target training and target test data obtained lower performance than the transfer learners ( $R^2 \approx 55\%$ ,  $Coeff \approx 75\%$ ,  $RMSE \approx 5.2N$ ,  $NRMSE \approx 0.14$ , where avg. values were obtained from X, Y, Z models). Hence, TL-CDG models clearly outperformed the baseline model with higher estimation accuracies and lower errors.

### 5.5.2. Case ii: pHRI in 1D (Target domain $D_{t_{1D}}$ )

In this case, TL-CDG-1 model was found effective in force estimations in X and Y dimensions once finetuned. Higher accuracies (X:  $R^2 \approx 86\%$ ,  $Coeff \approx 93\%$ , and Y:  $R^2 \approx 79\%$ ,  $Coeff \approx 89\%$ ) and lower losses (X:  $RMSE \approx 4.2N$ ,  $NRMSE \approx 0.165$ , and Y:  $RMSE \approx 6.8N$ ,  $NRMSE \approx 0.13$ ) were obtained by the TL-CDG-1 model than the intra-session baseline FMG-DCNN model (X:  $R^2 \approx 77\%$ ,  $Coeff \approx 88\%$ ,  $RMSE \approx 3.6N$ ,  $NRMSE \approx 0.14$ , and Y:  $R^2 \approx 66\%$ ,  $Coeff \approx 81\%$ ,  $RMSE \approx 5.8N$ ,  $NRMSE \approx 0.11$ ). Although the baseline model estimated forces well, but the TL-CDG-1 model performed surprisingly well by transferring knowledge learnt from the 2D-pHRI long-term distributions.

Observations showed that intra-session baseline FMG-DCNN model with 34 feature space could obtain  $R^2 \approx 56\%$  in 3D force estimations while the TL-CDG models moderately improved accuracies in estimations [ $R^2 \uparrow (2-8) \%$ ,  $Coeff \uparrow (2-7) \%$ ], with slight decrease in error [ $RMSE \downarrow \approx (0.2-0.5) N$ ]. Among the pretrained models, the TL-CDG-1 model performed comparatively better in both simple and complex interactions in 1D and 3D. Clearly, the TL-CDG-1 model achieved significant improvements in estimation accuracies in 1D-HRI [ $R^2$  in 1D-X ( $\sim 10\% \uparrow$ ), 1D-Y ( $\sim 12\% \uparrow$ )], and in complex 3D-HRC [ $R^2$  in 3D-XYZ ( $\sim 8\% \uparrow$ )]. Figure 5.3 shows target test FMG distributions during 1D and 3D interactions and the models' performances plotted in bar plot and boxplot for ease of visualization. Since TL-CDG-2 and TL-CDG-3 models were already pretrained with source

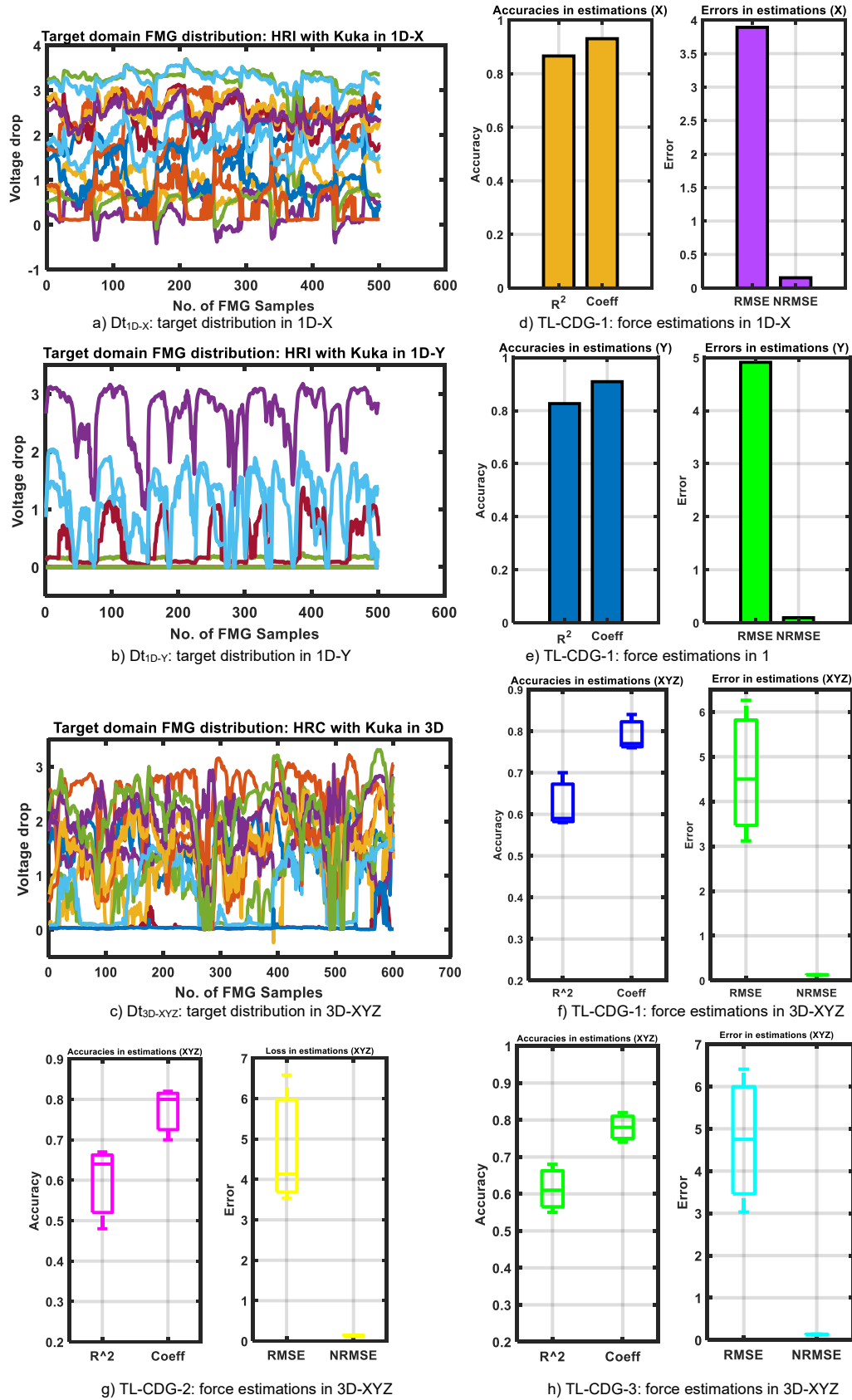


Figure 5.3. Few samples of target FMG distributions (a, c, e) and performances of the SDG-TL models (b, d: bar plot result for Model X and Y in 1D, and f, g, h: boxplot results for Model X, Y, Z in 3D).  
 Reproduced from [59] © [2022] IEEE with permission.

distributions of pHRI in 1D-X and 1D-Y, these were not investigated for *case ii*. HRI with Kuka in 1D-Z and 2D (XY, YZ, XZ) were not investigated due to time constraints. Furthermore, the constant Z dimension values in  $Ds_i$  restrained further exploration on this matter.

Source domains  $Ds_{i\{1,..5\}}$  and target domains  $Dt_{3D}$ ,  $Dt_{1D-X,Y}$  were different and the target data were totally unseen and out-of-distribution for the TL-CDG-1 model. Observations showed that this model could still predict OOD and unseen target data from a different HRI environment. Although, without fine-tuning with calibration data, the model would fail in estimating 3D-HRC task. Interestingly, the TL-CDG-1 model could predict simple 1D interactions fairly well. One reason could be that the source data used in pretraining this model had applied forces in arm flexion, extension, and arm abduction, adduction on the planar surface. Similar arm postures were also present in 1D-pHRI with Kuka robot. This phenomenon might help in the future design of an FMG-based HMI control system with safety mechanism. In a safety measures design, the TL-CDG pretrained model can be used for finetuning quickly with fewer target data for any participant. In a hazardous situation where human safety in pHRI might be breached, this can enable the participant to apply force on the robot and push away the robot from her/his proximity. Therefore, the proposed system can be implemented in human-robot safe collaborations in practical scenarios.

Initially, pHRI with Kuka robot by grasping the cylindrical gripper was investigated in this study using baseline FMGCNN architecture described in Section 2.4.3 and 2.6.1. Separate intra-session model was trained with first 4 repetitions and evaluated on last 5<sup>th</sup> repetition for 1D (X, Y, Z directions), 2D (XY plane, YZ plane, XZ plane) and 3D (XYZ plane). The intra-session models were examined training with source distributions of 34 channel extended feature space based on Section 5.3.1 and with raw 16 channel feature space to explore the effect of feature engineering. These results are summarized in Table 5-III. Although the baseline FMG-DCNN model could estimate similar with 16 or 34 feature space distributions, it was interesting to observe that the cross-domain TL-CDG-1 model with 34 feature space improved collaborative task performance of moving the wooden rod 3D, as well as improved grasping interactions in simple 1D-pHRI. Apparently, this TL-CDG-1 model could moderately improve grasping force estimation accuracies with lower errors during pHRI in 3D where cylindrical gripper was the end-effector (avg:  $R^2 \leq 57\%$ ,  $Coeff \leq 76\%$ ,  $NRMSE \leq 0.153$ ,  $RMSE \leq 8.1N$ ) with improvements. Including more features

Table 5-III. pHRI with Kuka: Intra-Session Evaluation with Baseline FMG-DCNN<sup>†</sup> model. Reproduced from [59] © [2022] IEEE with permission.

pHRI with Kuka (Grasping a cylindrical gripper)	Feature engineering	Intra-session models	R <sup>2</sup>	Coeff	RMSE	NRMSE
pHRI in 1D (X, Y, Z)	34 feature space	X: Model X Y: Model Y Z: Model Z	≥66%, ≤79%	≥81%, ≤89%	≥4.7N, ≤8.9N	≥0.14, ≤0.18
	16 feature space	X: Model X Y: Model Y Z: Model Z	≥78%, ≤81%	≥88%, ≤90%	≥4.0N, ≤8.0N	≥0.11, ≤0.16
pHRI in 2D (XY, YZ, XZ)	34 feature space	XY: Model X Model Y YZ: Model Y Model Z XZ: Model X Model Z	≥64%, ≤87%	≥80%, ≤ 93%	≥5.2N, ≤12.4N	≥0.12, ≤0.40
	16 feature space	XY: Model X Model Y YZ: Model Y Model Z XZ: Model X Model Z	≥64%, ≤87%	≥80%, ≤93%	≥5.6N, ≤12.2N	≥0.09, ≤0.16
pHRI with Kuka in 3D (XYZ)	34 feature space	XYZ: Model X Model Y Model Z	≥43%, ≤64%	≥65%, ≤80%	≥4.8N, ≤15N	≥0.13, ≤0.19
	16 feature space	XYZ: Model X Model Y Model Z	≥46%, ≤63%	≥68%, ≤80%	≥4.4N, ≤15.9N	≥0.12, ≤0.20
HRC with Kuka in 3D (XYZ) (Moving a wooden rod in collaboration)	34 feature space	XYZ: Model X Model Y Model Z	≥53%, ≤59%	≥73%, ≤77%	≥3.28N, ≤7.30N	≥0.13, ≤0.14
	16 feature space	XYZ: Model X Model Y Model Z	≥51%, ≤63%	≥85%, ≤90%	≥3.08N, ≤6.06N	≥0.12, ≤0.17

<sup>†</sup> Baseline FMG-DCNN model trained with 4 repetitions of target training data and evaluated on 5<sup>th</sup> repetition of target test data.

improved model performance during the collaborative target task of moving the wooden rod in 3D with the additional features, as described in Section 5.3.1. Also, having more features did not necessarily mean having unique features to improve the model learning process. This was observed in grasping interactions using a cylindrical gripper with comparative results using either 16 or 34 features. Collecting more inter-session training data from secondary sources could improve 3D-pHRI or 3D-HRC experiences for a shared task but requires more investigations in future.



In this study, cross-domain generalization was observed during human robot interactions via the force myography technique. Transfer learning allowed the FMG-based TL-CDG model to predict unseen, unrelated and out-of-domain target data ( $D_s \neq D_t$ ,  $T_s \neq T_t$ ) on a different workspace ( $pHRI_s \neq pHRI_t$ ). The source and target domains were distinctly dissimilar because of muscle readings captured by either 32 or 16 FMG channels positioned in different arm locations and separate HRI environments (different 1D/2D/3D workspaces, participant's body posture during interactions, knob/cylinder/wooden rod as end-effectors). Since the gripper orientation and shapes were different, grasping forces and arm postures became distinctive. Also, participants applied interactive forces within their comfortable ranges (usually within 15N-40N) which was not constant. During the sessions, FMG bands were put on approximately same positions but were not exact; hence, sensors position shifts were possible in different sessions. Also, winding forces to wrap the band around the limb was kept at the user's comfort. Furthermore, collecting 5 repetitions of intra-session data were proven sufficient in capturing enough variabilities present during the interactions. Also, time required for one session was approximately 12-20 minutes and one repetition of interactions was less than 2min; these reduced muscle fatigue and ensured participant's comfort. In addition to the discussions and observations made in this chapter, chapter 7 discusses the overall observations that helped in developing effective knowledge transfer during physical interactions with a robot.

## Chapter 6.

# Unsupervised, Semi-supervised Interactive Force Estimations via Generated Synthetic FMG Signals

The material presented in this chapter is reproduced, excerpted, and modified with permission from the following paper:

[60] © [2022] IEEE with permission. U. Zakia, A. Barua, X. Jiang, and C. Menon, “Unsupervised, Semi-Supervised Interactive Force Estimations During pHRI via Generated Synthetic Force Myography Signals,” IEEE Access, June 2022, doi: 10.1109/ACCESS.2022.3187115.

Sections of this chapter are reprinted or adapted from the above article to fit the formatting and scope of this chapter.

## 6.1. Chapter Overview

In this chapter, the investigation carried for objective 4 is discussed. In industrial physical human robot interaction (pHRI) applications, data is scarce, labels are usually unavailable or time consuming to generate. Semi-supervised learning can be useful because unlike the supervised learning which needs labeled data, it can work with a few labeled and mostly unlabeled data. Hence, in this study, we proposed a dual-phased algorithm based on semi-supervised adversarial learning where few training data were labeled. Then, this algorithm was used to estimate human applied forces during interactions with a Kuka robot in 1D-X, Y, Z directions via force myography, respectively.

## 6.2. Introduction

in real-world pHRI applications, obtaining enough training data, having more participants, or labelling all data are not always possible. In the case of unlabeled data, unsupervised learning can be an option which does not need labeled data. It learns latent feature distributions and may generate labels based on the learning process. Also, semi-supervised or weakly supervised learning can reduce the dependencies on labeled training data where only a few labeled training datasets are available. In recent pHRI

studies, there is a growing interest to use limited amounts of labeled data with large quantities of unlabeled data for realistic predictions [94-96]. Semi-supervised learning can be useful in such cases that utilizes few labeled training datasets to achieve similar performance like supervised learning with fully labeled data set. For scenarios where training data hard to collect or there is no previous data from other related sources are available, synthetic data could be a favorable alternative. The generative adversarial network (GAN), originally proposed by Ian Goodfellow [70] has been a proven technique in synthetic image generation, but not many biosignals are synthesized using this architecture. As a bio-signal, an FMG signal is transient, individual-specific, and each session's data are affected by control factors such as sensor position shifts, limb motions, and postures during activities. There are serious concerns if a reality gap occurs when the generated synthetic data do not follow the real domain data it is more challenging to generate synthetic FMG biosignals to control HRI because of higher risks associated with wrong predictions and hence, needs to be investigated. A domain randomization approach can be adapted to mitigate the reality gap [98-99]. This approach can make the simulated data as diverse as possible so that the real data would appear as another variation to the model [99, 100]. Data augmentation is a form of domain randomization that is applied on the collected data and performs certain refinements or transformations to render real-like environmental changes. Adapting carefully selected transformations that represent certain control factors affecting FMG signals can introduce wide variations in data and refine the synthetic data generation through the GAN making them more realistic [100].

In this study, we propose a two-phased 'unsupervised, self-trained FMG-based deep convolutional GAN (unsupervised, self-trained FMG-DCGAN)' algorithm where unsupervised adversarial learning was used for understanding the latent feature distributions followed by semi-supervised learning to evaluate intra-session test data. For the investigation, pHRI application between one participant and a Kuka LBR IIWA 14 robot in 1D (X, Y and Z dimensions) was considered. In its initial phase, an unsupervised FMG-based deep convolutional generative adversarial network (unsupervised FMG-DCGAN) model was implemented where both the generator and the discriminator were convolutional neural networks (CNNs). A set of transformation functions for data augmentation was used to implement domain randomization adding variabilities in the synthetic data. Employing cosine similarity as a benchmark score, each transformation function was investigated in generating real-like synthetic data and a GAN model was

saved for the next phase. In the final phase, each GAN model generated with different transformation functions was evaluated. The discriminator of each GAN with weights from initial phase was pretrained with a few real labeled training data and later was used to generate pseudo-labels for both unlabeled real training data and unlabeled synthetic data. The model was further trained with all real training (labeled and pseudo-labeled) and generated synthetic data (pseudo-labeled) and was called the self-trained FMG-DCGAN model. Finally, this model was evaluated on test data in estimating applied instantaneous forces during interactions. Using the cosine similarity score and generated synthetic data volume as decision criteria, the best model with the optimal transformation function was identified.

Major contributions in this study were:

1. investigating real-like synthetic FMG data generation using domain randomization via data augmentation, and obtaining the appropriate technique in this case,
2. investigating unsupervised and semi-supervised learning techniques where training data were scarce or large volumes of data were not available, and
3. implementing these techniques in challenging FMG-based pHRI using one FMG forearm band for user comfort and to reduce complexities of processing the data.

### **6.3. Protocol**

One healthy adult ( $P_1$ ) participated in this study with his written consent as approved by the Office of Research Ethics, Simon Fraser University, British Columbia, Canada. A 16 channel FMG band was donned on the participant's dominant forearm and was not removed during a session. For pHRI with the Kuka robot,  $P_1$  stood steadily in position in front of the robot, grasped the cylindrical gripper and applied interactive forces in simple dynamic 1D motions, as shown in Figure 6.1a. Separate sessions were conducted to interact in 1D 'X', 'Y' and 'Z' dimensions (Figure 6.1.b-d). In 1D-X, dynamic motion during applied force was front and back and vice versa (displacement in X: 0.4m); in 1D-Y, motion was from right to left and vice versa (displacement in Y: 0.55m); while in

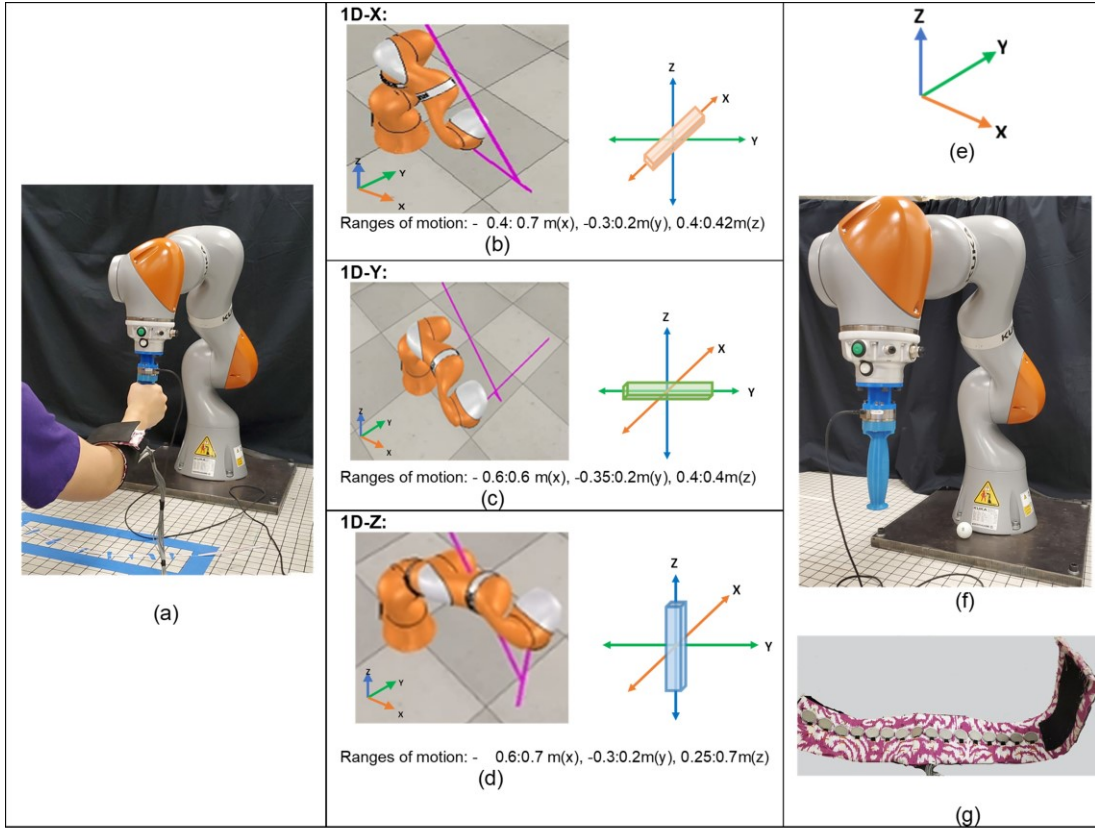


Figure 6.1. Experimental setup of the study. Reproduced from [60] © [2022] IEEE with permission.

a) pHRI between a participant and Kuka robot in 1D , b) dynamic interactions in 1D-X bounded by ranges of motions within a 6-axis rectangular area, c) dynamic interactions in 1D-Y bounded by ranges of motions within a 6-axis rectangular area, d) dynamic interactions in 1D-Z bounded by ranges of motions within a 6-axis rectangular area, e) directions of interactions in 3D, f) Cylindrical gripper and a 6-axis force/torque sensor attached to robot's flange via an adapter, g) custom-made 16-channel FMG band used on forearm during interactions. Reproduced from [60] © [2022] IEEE with permission.

1D-Z, motion was moving the gripper up and down and vice versa (displacement in Z: 0.45m). These motions required arm flexion, extension, abduction, and adduction, were continued for a certain time (approximately 90s of interactions without fatigue) while termed hereinafter as a 'repetition'. Dynamic motions during the interactions were confined in a 6-axis rectangular plane set through MATLAB script.

For each interaction session in 1D, 2 repetitions of sample data ( $D_C \in \{X_{C1}, X_{C2}\}$ ) were collected for training (source distribution  $D_C$ ) and 1 repetition ( $D_T \in \{X_T, Y_T\}$ ) for evaluation purpose (target distribution  $D_T$ ). All distributions of  $D_C$  and  $D_T$  had feature spaces of  $X \in \mathbb{R}^{N \times M}$  where  $N$  = number of samples and  $M$  = 16 FMG channels. Approximately, a total of  $4,000 \times 16$  FMG samples were collected for training and testing.

The source data were used for training the GAN and to calibrate the FMG signals for both generating the synthetic data and training the proposed model.

## 6.4. Unsupervised, Semi-supervised Self-trained FMG-DCGAN Algorithm

The proposed algorithm was developed in two consecutive phases where the final phase was dependent on the outcome of its initial phase, as shown in Figure 6.2. An *unsupervised FMG-DCGAN* architecture was introduced in phase I for real-like synthetic data generation. In phase II, a *self-trained FMG-DCGAN* model was investigated for estimating instantaneous applied forces.

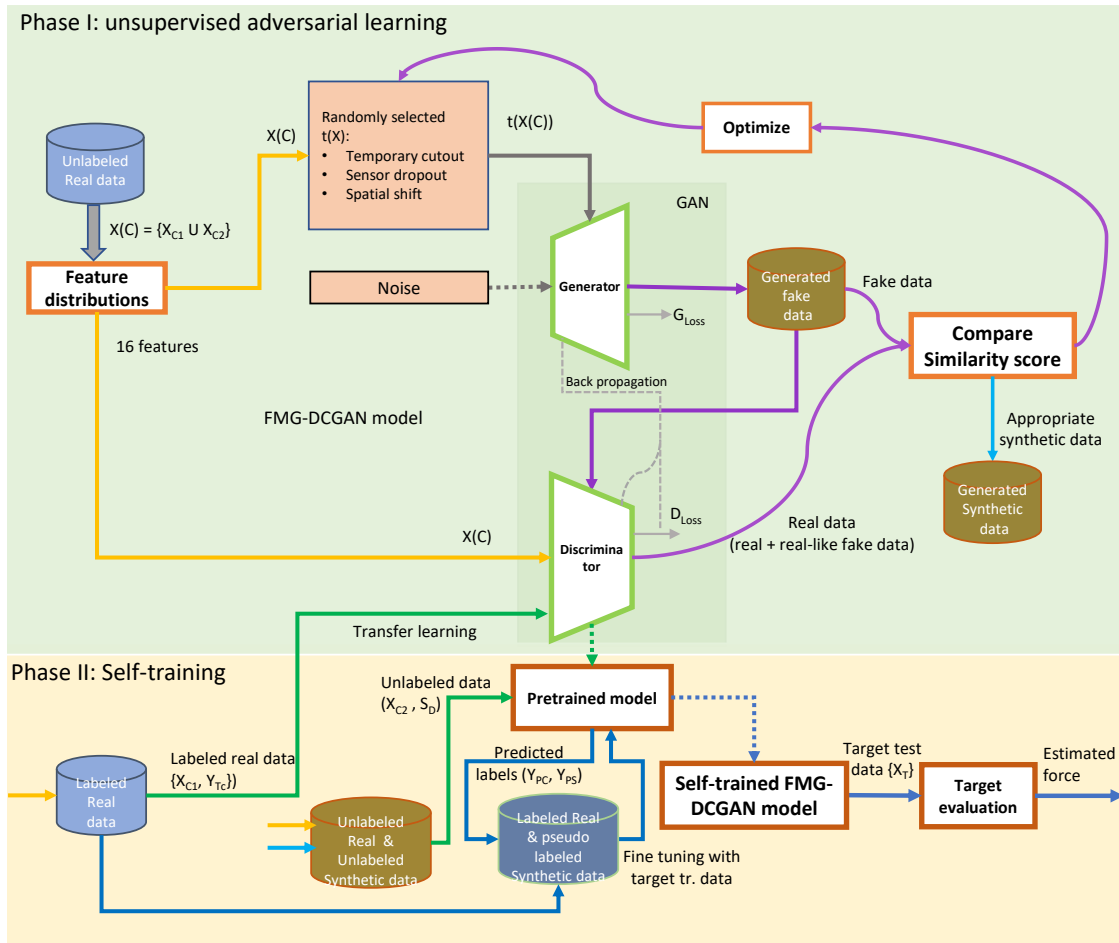


Figure 6.2. The proposed dual-phased unsupervised, self-trained FMG-DCGAN algorithm. Reproduced from [60] © [2022] IEEE with permission.

### 6.4.1. Phase I: Generating synthetic FMG data

The *unsupervised FMG-DCGAN* architecture had a generator (model G) and a discriminator (model D) where convolutional and convolutional-transpose layers were implemented respectively, similar to the original DCGAN architecture [101]. The *FMG-DCGAN* model was proposed for synthetic data ( $D_{Sj} \in \{S_D\}$ ) generation from unlabeled real FMG data ( $D_C \in \{X_{C1}, X_{C2}\}$ ) of  $3200 \times 16$  samples. A few techniques were adapted in this initial phase to reduce the reality-gap between the real and the synthetic data as much as possible and is discussed below.

- Domain Randomization via data augmentation

A variety of transformation functions  $t(x)$ s were generated that could potentially mimic situations where sensor position shifts, unused sensors or sensors that capture low signals could occur during the data collection process when an FMG band was donned on upper extremities. These are shown in Figure 6.3 and discussed below.

- *Temporal cutout,  $t(x_{tc})$* : a random contiguous section (consecutive any 3 channels) of the time-series signal (every 50ms of cutout window) was replaced with zeros.

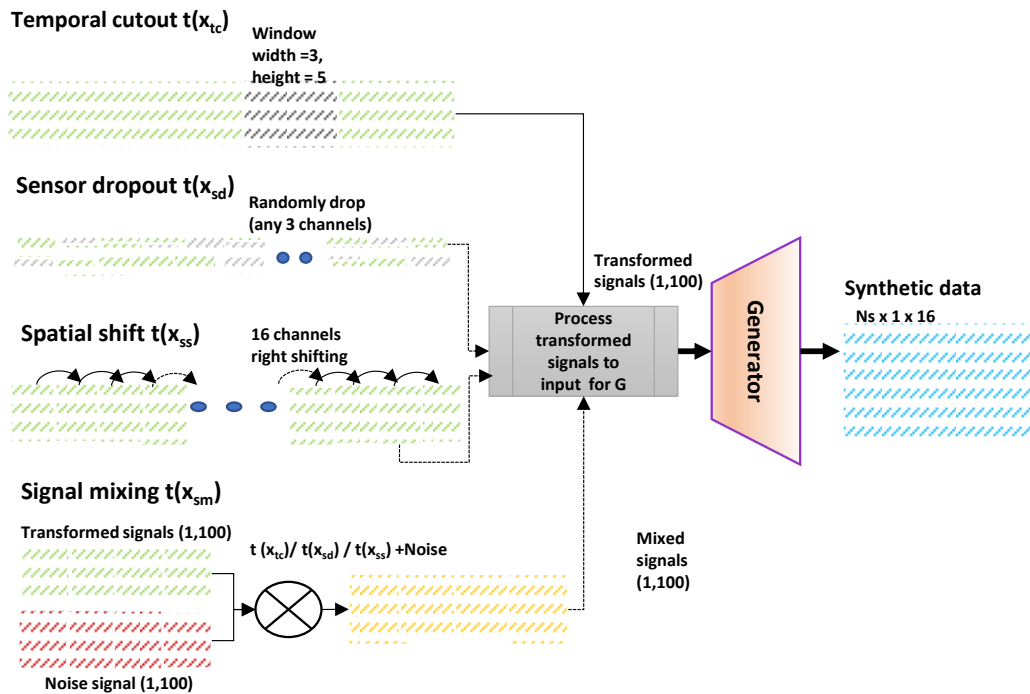


Figure 6.3. Domain randomization: a variety of transformation functions investigated. Reproduced from [60] © [2022] IEEE with permission.

- *Sensor dropout,  $t(x_{sd})$* : any random three FMG channels were set to zeros in every 10ms input of the time-series signal.
- *Spatial shift,  $t(x_{ss})$* : 16 FMG channels data were right-shifted by 1 for every 10ms input of the time-series signal.
- *Noise,  $t(x_n)$* : random zero-mean gaussian noise (3200, 100) was generated and used as input.
- *Signal mixing,  $t(x_{sm})$* : random noise  $t(x_n)$  was used in conjunction with  $t(x_{tc})$ ,  $t(x_{sd})$ , and  $t(x_{ss})$  to produce mixed signals  $t(x_{sm-ntc})$ ,  $t(x_{sm-nsd})$ ,  $t(x_{sm-nss})$ , respectively.

The transformation functions took real data of image shape of (1,16,1) as input, transformed the signal, and finally reshaped the transformed data as  $T_S$  (1,100,1) for input to model G. Padding with mean values of the corresponding 16 features was used for reshaping the transformed data. The other input was the noise signal (3200, 100), which was also reshaped as  $N_S$  (1,100,1) before feeding into model G.

- **Cosine similarity score  $\sigma(s)$**

Cosine similarity score measures the cosine of the angle between two n-dimensional vectors ( $D_C$  and  $S_D$ ) projected in a multi-dimensional space. Its range is between 0 to 1. It is defined as:

$$\sigma(s) = \cos(D_C, S_D) = (D_C \cdot S_D) / (\|D_C\| * \|S_D\|) \quad (6.1)$$

where  $D_C \cdot S_D$  is the dot product and  $\|D_C\| * \|S_D\|$  is the cross product of the lengths of the two vectors  $D_C$  and  $S_D$ . Higher values indicates more similarities between the vectors.

### ***i. The proposed FMG-DCGAN architecture***

In this architecture, model G was engaged in generating fake FMG signals while model D was employed to learn the discriminative feature distributions of both real and fake signals and classify them accordingly. For model G, inputs were either noise signals ( $N_S \in \{X_N\}$ ) or transformed FMG signals ( $T_S \in \{X_{T_S}\}$ ) with shapes of (1, 100, 1), or aggregated noise and transformed signals, as discussed in Section II.C.1. Model D received real FMG signals ( $D_C \in \{X_{C1}, X_{C2}\}$ ) and fake FMG signals/synthetic data ( $D_{S,i}$



$\in\{S_D\}$ ) generated by model G, where both inputs to model D were shapes of (1,16,1). Only those generated fake signals were considered as synthetic data for the next phase that obtained higher cosine similarity scores  $\sigma(s)$  along with greater generated-to-input-data ratio ( $\delta$ ).

### **Model G architecture**

Three successive convolutional 2D transposed (conv2DTranspose) layers [no. of filters: 128, 64, 1 and filter size: (1, 5), (1, 10), and (1, 5)] were implemented with strides of (1, 1), (1, 4), and (1, 2) and the 'same' padding. Each conv2DTranspose layer was followed by a batch normalization layer and a leaky relu layer. For the final output of fake generated signal ( $S_D$ ) of a shape of (1,16, 1), the tanh activation function was used. This architecture was used in 1D-X, Y and Z dimensions.

### **Model D architecture**

Two convolutional (conv) blocks were implemented sequentially where each block had a conv2D layer followed by a leaky relu and a dropout layer with a rate of 0.3 to reduce overfitting. Convolutional 2D (conv2D) layers were implemented with strides of (1, 2) and the 'same' padding. The number of filters used in the conv blocks for 1D-X dimension was 32, 16, 1, while it was 128, 64, 1 in 1D-Y and Z dimensions with the same filter sizes of (1, 5), (1, 10), and (1, 5) in each dimension. The convolutional blocks were followed by three dense layers of 20, 10 and 1 neurons for 1D-X while only one dense layer of 1 neuron was used for 1D-Y, and Z. Appropriate number of dense layers were obtained by trial and error due to the separate architectures of 1D-X, Y and Z models. A sigmoid function was used to classify the real input and the generated signals.

### **GAN Loss & Optimization**

Real data and fake data were labeled as 0 and 1 respectively to calculate losses of model D and model G using binary cross entropy (BCE) loss. The Adam optimizer with a learning rate (LR) of 1E-04 and Beta1, Beta2 = 0.9, 0.999 was used for both G and D models during training. An initial training was performed with model D. For training the FMG-DCGAN in generating real-like synthetic data, output from model D was expected to be 1 for real data and 0 for fake data. Therefore, the total loss for model D was calculated as the sum of the loss from the real data used in training model D and the loss from the synthetic data generated by model G. On the contrary, to maximize model G's

performance in convincing model D that the generated data were real,  $G_{Loss}$  was calculated and back propagated to improve G. Therefore,  $G_{Loss}$  had similar values with flipped labels.  $D_{Loss}$  and  $G_{Loss}$  were set up such that:

$$D_{Loss} = \log(D(x)) + \log\left(1 - D\left(G(t(x))\right)\right) \quad (6.2)$$

$$G_{Loss} = \log\left(D\left(G(t(x))\right)\right) \quad (6.3)$$

where,  $D(x)$  was the output from model D on an instance of training dataset  $x$  at time  $i$ ,  $G(t(x))$  was the generated data,  $D(G(t(x)))$  was the model D's output on the generated data at instant  $i$ , and  $t(x)$  was the transformed signal used as input to the Model G. The  $D_{Loss}$  and the  $G_{Loss}$  were back propagated to improve model D in discriminating better between real and fake signals and to improve model G in generating better quality signal that could fool model D, respectively. Both models were trained until they reached convergence when model D no longer could distinguish between the real and the fake data, and diversified data were generated where fake data were as good as real data by preventing mode collapse ( $1.5 > G_{Loss} > 0.8$  and  $0.7 > D_{Loss} > 0.5$ ).

### ***ii. Selecting optimal $t(x)$ via $\sigma(s)$ and $\delta$***

Cosine similarity score was implemented to compare the real data with the generated fake data from model G. Each fake data was compared with all real data,  $\sigma(s)$  was calculated, and the mean value of these scores was generated. Only those synthetic data were saved as future training data that obtained a score of  $\sigma(s) > 0.8$ , i.e., similarity between fake data and real data would be at least 80%. Data was normalized for score comparison between the real data and the synthetic data, where each synthetic data was compared with all  $3200 \times 16$  real samples,  $D_c$ . Transformation function that could generate more real-like synthetic data ( $\sigma(s) > 0.8$  with maximum  $\delta$ ) was used to optimize the model performance. Each transformation function was implemented separately, synthetic data was generated, performance was evaluated, and a model was saved with its weights for the next phase.

### **6.4.2. Phase II: Self-trained FMG-DCGAN model**

In this phase, calibration/target training data (few labeled real data, and a few unlabeled real data) and a large amount of generated real-like synthetic data (unlabeled) were used. This phase began by pretraining model D from phase I. A small amount of

labeled source data ( $D_{C1} \subset D_C$ ) and a large volume of unlabeled data (mainly synthetic data ( $D_{Sj}$ ) and few real data ( $D_{Si} \subset D_C$ )) were used in self-training. Finally, the model was evaluated on target test data,  $D_T$ . For finetuning, a fully connected layer was used to replace the last layer of model D for regressing force estimations. Several steps were followed in generating a *self-trained FMG-DCGAN* model using an Adam optimizer with learning rate,  $LR = 1E-04$  and epoch,  $E = 500$  to calculate mean squared error (MSE) losses, as discussed below.

### ***i. Pretraining Model D via Transfer Learning***

In step 1, the saved model D from phase I was finetuned with a few labeled ‘target training data’ or ‘calibration data’ ( $D_{C1} \in \{X_{C1}, Y_{TC1}\}$ ). This helped the model to adapt learning real target distributions and converge quickly and was termed hereafter as the ‘pretrained FMG-DCGAN’ model.

The pretrained FMG-DCGAN model was used in step 2 to generate pseudo labels  $Y_{PC}$  for the unlabeled real data,  $D_{Si} \in \{X_{C2}\}$  and pseudo labels  $Y_{PS}$  for unlabeled synthetic data,  $D_{Sj} \in \{S_D\}$ .

In step 3, the pretrained model was further trained with all true labeled and pseudo labeled real and synthetic data ( $D_{C1} \in \{X_{C1}, Y_{TC1}\} \cup D_{Si} \in \{X_{C2}, Y_{PC}\} \cup D_{Sj} \in \{S_D, Y_{PS}\}$ ) and was termed as the self-trained FMG-DCGAN model.

### ***ii. Estimating Interactive Force with Self-Trained FMG-DCGAN model***

The self-trained FMG-DCGAN model was used to predict interactive force on target test data ( $D_T \in \{X_T, Y_T\}$ ) of instantaneous FMG signals in every 10ms window size. At an instant time,  $t$ , target test input FMG signals  $\{X_T\}$  were used for validation purpose. Hence, for target task  $T_t \{Y_{Tt}, f(\cdot)\}$ , a predictive function  $f(\cdot)$  was used to estimate interaction forces in 1D such that,  $f: X_T \rightarrow F'_t$ .

$$f_x(\cdot) = F'_t = \gamma, (X_T, \varphi) \quad (6.4)$$

The model attempted to find the best parameter space  $\varphi$  from the proposed parameter set  $\gamma$  which was determined by computing the loss function using the true force label space  $Y_{Tt}$ :

$$\varphi = L(F'_{xt} - F_{xt}) = \arg \min_{\varphi} \sum_{q=1}^t (F'_t - Y_{Tt})^2 \quad (6.5)$$

## 6.5. Results

The performance of the proposed algorithm was evaluated using the mean cosine similarity score ( $\bar{\sigma}(s)$ ) and the generated-to-input-data ratio ( $\delta$ ) in phase I, while  $R^2$ , RMSE and NRMSE were used in phase II (using Python 3.7 and Tensorflow with GTX1060). For pHRI in 1D motions in X, Y and Z dimension, separate FMG-DCGAN model was implemented to generate synthetic data and evaluated on corresponding target distributions. Each FGM-DCGAN model (both Model D and G) with unique  $t(x)$  were saved as h5 files with their weights for future use in phase II. To compare the proposed model performance, a baseline CNN model using model D architecture employing supervised learning was generated using the same calibration/target training data,  $D_C (\{X_{C1}, Y_{TC1}\} \cup \{X_{C2}, Y_{TC2}\})$  with true labels (3200×17 samples) and was evaluated on same target test data,  $D_T$  (600×17 samples). Performance evaluations of 1D-X, Y and Z are reported in Table 6-I, 6-II and 6-III, respectively. Approximately  $E < 33$  epochs with a runtime of  $t(E) < 0.35$  seconds were required to generate synthetic data in each dimension.

## A. pHRI in 1D-X

In phase I, transformation functions,  $t(x_{tc})$ ,  $t(x_{sd})$ ,  $t(x_{ss})$ , and  $t(x_n)$  generated unlabeled synthetic data  $S_D$  in the ranges of  $2300 \times 16$  to  $3100 \times 16$  samples with  $\bar{\sigma}(s) > 88\%$ . In the case of signal mixing,  $t(x_{sm-ntc})$ ,  $t(x_{sm-nsd})$  and  $t(x_{sm-nss})$  generated synthetic data in the range of  $4600 \times 16$  to  $6300 \times 16$  samples with  $\bar{\sigma}(s) > 89\%$ . In phase II, for each transformation functions, a separate self-trained FMG-DCGAN model was pretrained and evaluated on the unseen target test data in 1D-X ( $600 \times 16$  samples). In all cases, it achieved impressive performances in force estimations ( $R^2 > 73\%$ , NRMSE  $< 0.175$  and RMSE  $< 3.5N$ ). The baseline model using supervised learning had  $R^2 > 81\%$ , NRMSE  $< 0.14$  and RMSE  $< 3N$ . These results are reported in Table 6-I.

Table 6-I. Model Performance in Force Estimations during pHRI in 1D-X. Reproduced from [60] © [2022] IEEE with permission.

pHRI	Phase I				Phase II			$R^2$	NRM SE	RMSE	
	T(x)	Input for GAN training (unlabeled)	Generated synthetic FMG data, $S_D$	Generated-to-input-data ratio, $\delta$	Cosine Similarity score, $\sigma^-(s)$	Calibration/target training data	Target test data				
1D-X	Temporal cut out	$t(x_{tc})$	Unlabeled real FMG data	2331×16 samples	0.73	91.76%	Labeled real data ( $D_{C1} \in \{X_{C1}, Y_{TC1}\}$ ) + pseudo-labeled real data ( $D_{S1} \in \{X_{C2}, Y_{PC}\}$ ) + pseudo-synthetic data ( $D_{S2} \in \{S_D, Y_{PS}\}$ ):	D <sub>T</sub> : 600×16 samples	77.15%	0.15	3.2N
	Sensor dropout	$t(x_{sd})$	2915×16 samples	0.91	88.13%	75.84%			0.17	3.3N	
	Spatial shift	$t(x_{ss})$	( $D_C \in \{X_{C1}, X_{C2}\}$ ): 3200×16 samples	3196×16 samples	0.99	90.76%			77.58%	0.16	3.2N
	Noise	$t(x_n)$	( $N_S \in \{X_N\}$ ): 3200×16 samples	3118×16 samples	0.97	92.09%			74.54%	0.17	3.4N
	Noise with temporal cut out	$t(x_{sm-ntc})$	Unlabeled real FMG data	5983×16 samples	0.93	90.76%			73.64%	0.17	3.5N
	Noise with sensor dropout	$t(x_{sm-nsd})$	( $D_C \in \{X_{C1}, X_{C2}\}$ ) + Noise ( $N_S \in \{X_N\}$ ): 6400×16 samples	4682×16 samples	0.73	92.18%			74.42%	0.17	3.4N
	Noise with spatial shift	$t(x_{sm-nss})$	6397×16 samples	6397×16 samples	0.99	89.50%			77.32%	0.15	3.2N
	<b>Baseline CNN model (supervised learning with model D arch.)</b>								<b>81.72%</b>	<b>0.14</b>	<b>2.9N</b>

## B. pHRI in 1D-Y

In phase I, transformation functions,  $t(x_{tc})$ ,  $t(x_{sd})$ ,  $t(x_{ss})$ , and  $t(x_n)$  generated unlabeled synthetic data  $S_D$  in the ranges of  $2300 \times 16$  to  $4200 \times 16$  samples with a similarity score of  $\bar{\sigma}(s) > 83\%$ . Signal mixing transformation functions,  $t(x_{sm-ntc})$ ,  $t(x_{sm-nsd})$  and  $t(x_{sm-nss})$  generated synthetic data in the range of  $5900 \times 16$  to  $6300 \times 16$  samples with  $\bar{\sigma}(s) > 84\%$ . In phase II, separate self-trained FMG-DCGAN model was pretrained and evaluated for each  $t(x)$  on the unseen target test data in 1D-Y ( $600 \times 16$  samples). The proposed model achieved good performances in force estimations ( $R^2 > 75\%$ , NRMSE  $< 0.16$  and RMSE  $< 6.0N$ ) while the baseline model had  $R^2 > 78\%$ , NRMSE  $< 0.15$  and RMSE  $< 5.6N$ , as reported in Table 6-II.

Table 6-II. Model Performance in Force Estimations during pHRI in 1D-Y. Reproduced from [60] © [2022] IEEE with permission.

pHRI	Phase I					Phase II						
	T(x)	Input for GAN Training (unlabeled)	Generated Synthetic FMG Data $\{S_D \times 16\}$	Generated-to-input-data ratio, $\delta$	Cosine Similarity score, $\bar{\sigma}(s)$	Calibration/target training data	Target test data	$R^2$	NRMSE	RMSE		
1D-Y	Temporal cut out	$t(x_{tc})$	Unlabeled real FMG data	$3129 \times 16$ samples	0.98	85.68%			75.17%	0.16	5.9N	
	Sensor dropout	$t(x_{sd})$	$(D_C \in \{X_{C1}, X_{C2}\})$ :	$2358 \times 16$ samples	0.74	84.52%	Labeled real data	D <sub>T</sub> : $600 \times 16$ samples	75.42%	0.15	5.8N	
	Spatial shift	$t(x_{ss})$	$3200 \times 16$ samples	$2388 \times 16$ samples	0.75	85.63%	$(D_{C1} \in \{X_{C1}, Y_{TC1}\}) +$		75.10%	0.16	5.9N	
	Noise	$t(x_n)$	$N_S \in \{X_N\}$ : $3200 \times 16$ samples	$3121 \times 16$ samples	0.97	83.98%	pseudo-labeled real data		77.94%	0.14	5.6N	
	Noise with temporal cut out	$t(x_{sm-ntc})$	Unlabeled real	$5985 \times 16$ samples	0.94	84.93%	$(D_{S1} \in \{X_{C2}, Y_{PC}\}) +$		76.13%	0.15	5.8N	
	Noise with sensor dropout	$t(x_{tc})$	FMG data $(D_C \in \{X_{C1}, X_{C2}\}) +$ Noise $(N_S \in \{X_N\})$ :	$4561 \times 16$ samples	0.71	81.59%	pseudo-synthetic data $(D_{Sj} \in \{S_D, Y_{PS}\})$ :		78.49%	0.15	5.5N	
	Noise with spatial shift	$t(x_{sd})$	$6400 \times 16$ samples	$6325 \times 16$ samples	0.99	84.78%	$1600 \times 17 + 1600 \times 17 + S_D \times 17$ samples		77.19%	0.15	5.7N	
	<b>Baseline CNN model (supervised learning with model D arch.)</b>								<b>78.15%</b>	<b>0.15</b>	<b>5.6N</b>	

## C. pHRI in 1D-Z

Transformation functions,  $t(x_{tc})$ ,  $t(x_{sd})$ ,  $t(x_{ss})$ , and  $t(x_n)$  generated unlabeled synthetic data  $S_D$  in the ranges of  $1500 \times 16$  to  $2600 \times 16$  samples with avg  $\bar{\sigma}(s) > 81\%$  in phase I. For signal mixing,  $t(x_{sm-ntc})$ ,  $t(x_{sm-nsd})$  and  $t(x_{sm-nss})$  generated synthetic data in the range of  $4800 \times 16$  to  $6100 \times 16$  samples with  $\bar{\sigma}(s) > 83\%$ . In phase II, for each transformation functions, the self-trained FMG-DCGAN model achieved impressive performances in force estimations ( $R^2 > 73\%$ , NRMSE  $< 0.175$  and RMSE  $< 3.5N$ ) on the unseen target test data in 1D-Z ( $600 \times 16$  samples). The reported results for the baseline model were  $R^2 > 88\%$ , NRMSE  $< 0.11$  and RMSE  $< 5.8N$ , as shown in Table 6-III.

Table 6-III. Model Performance in Force Estimations during pHRI in 1D-Z. Reproduced from [60] © [2022] IEEE with permission.

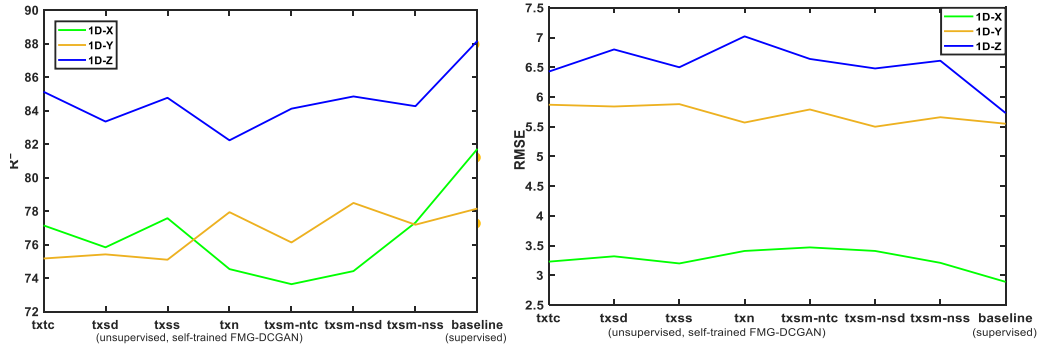
pHRI	Phase I				Phase II			$R^2$	NRM SE	RMSE	
	T(x)	GAN tr. FMG Data (unlabeled)	Generated Synthetic FMG data $\{S_D \times 16\}$	Generate d- to-input-data ratio, $\delta$	Cosine Similarity score, $\bar{\sigma}(s)$	Calibration/ Target Training Data	Target Test Data				
1D-Z	Temporal cut out	$t(x_{tc})$	Unlabeled real FMG data	$1541 \times 16$ samples	0.480	83.42%	Labeled real data ( $D_{C1} \in \{X_{C1}, Y_{TC1}\}$ ) + pseudo-labeled real data ( $D_{S1} \in \{X_{C2}, Y_{PC}\}$ ) + pseudo-synthetic data ( $D_{S2} \in \{S_D, Y_{PS}\}$ ):	D <sub>T</sub> : $600 \times 16$ samples	85.13%	0.11	6.4N
	Sensor dropout	$t(x_{sd})$	( $D_C \in \{X_{C1}, X_{C2}\}$ ):	$1763 \times 16$ samples	0.550	81.53%			83.35%	0.12	6.8N
	Spatial shift	$t(x_{ss})$	$3200 \times 16$ samples	$2704 \times 16$ samples	0.845	82.46%			84.77%	0.11	6.5N
	Noise	$t(x_n)$	$N_S \in \{X_{Nj}\}$ : $3200 \times 16$ samples	$1705 \times 16$ samples	0.532	84.10%	83.19%	0.12	6.8N		
	Noise with temporal cut out	$t(x_{sm-ntc})$	Unlabeled real FMG data	$5743 \times 16$ samples	0.897	85.70%	84.12%	0.12	6.6N		
	Noise with sensor dropout	$t(x_{sm-nsd})$	( $D_C \in \{X_{C1}, X_{C2}\}$ ) + Noise ( $N_S \in \{X_{Nj}\}$ ):	$4861 \times 16$ samples	0.759	84.76%	84.85%	0.11	6.5N		
	Noise with spatial shift	$t(x_{sm-nss})$	$6400 \times 16$ samples	$6134 \times 16$ samples	0.958	83.95%	84.3%	0.18	6.6N		
<b>Baseline CNN model (supervised learning with model D arch.)</b>							<b>88.17%</b>	<b>0.11</b>	<b>5.8N</b>		

## 6.6. Discussion

In this study, collecting training data (only a few were labeled) and evaluating test data with the proposed algorithm were conducted in the same session to simulate and compare to a situation where data collection in various sessions is costly, difficult, or impossible. Hence, the training data and test data had similar feature distributions, similar tasks, and the same sensor positions on the targeted limb. Therefore, domain randomization was implemented so that variations could be introduced such that it might become another session dataset for the model. During the adversarial training, real data that were transformed for generating synthetic data, were also used in pretraining the semi-supervised model. Due to the signal mix in phase I, investigated transformation functions modified and randomized the real distribution such that the model could learn better the latent features. Only during phase II, was the model introduced to the real feature distributions for pretraining. Therefore, implementing these functions helped reduce overfitting too.

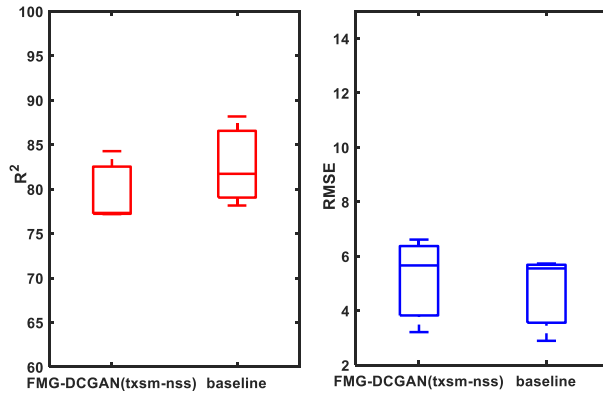
Observations showed that the FMG-DCGAN model generated more synthetic data when transformation functions  $t(x_{sm})$  based on signal mixing used. Specifically, signal mixing of noise with spatial shift ( $t(x_{sm-nss})$ ) generated a large volume of synthetic data ( $6400 \times 16 > S_D > 6100 \times 16$  samples) in each 1D interactions of X, Y and Z dimensions with greater generated-to-input-data ratio ( $99\% > \delta > 89\%$ ) and mean similarity score in the range of  $90\% > \bar{\sigma}(s) > 84\%$ . The volume of such synthetic data was almost double the calibration data collected during real-time interactions. A transformation function that used noise mixing with temporal cut out ( $t(x_{sm-ntc})$ ) also obtained impressive results ( $6000 \times 16 > S_D > 5700 \times 16$  samples,  $94\% > \delta > 89\%$ , and  $91\% > \bar{\sigma}(s) > 84\%$ ). Therefore, Transformation function  $t(x_{sm-nss})$  ranked highest, while  $t(x_{sm-ntc})$  ranked second in all pHRI scenarios. A statistical t-test was conducted to compare samples for the mean generated by the two functions  $t(x_{sm-nss})$  and  $t(x_{sm-ntc})$ . The selected transformation function  $t(x_{sm-nss})$  was found to be statistically significant ( $-4.75, 0.005$ ) at a 95% confidence level. Hence, it was obviously the better choice to optimize the model in generating maximum outcome. Figure 6.4 (a, b) shows the performance comparison of the proposed model for each transformation function with the baseline model in terms of the accuracies and error ( $R^2$  and RMSE).





(a)

(b)



(c)

Figure 6.4. Performance evaluation of unsupervised, self-trained FMG-DCGAN model with different transformation functions compared to the supervised baseline model. Reproduced from [60] © [2022] IEEE with permission.

a) plot of  $R^2$  in 1D-X, Y, Z, b) RMSE in 1D-X, Y, Z (pink dot: unsupervised self-trained FMG-DCGAN model with txsm-nss, yellow dot: supervised baseline model), and c) boxplot of self-trained FMG-DCGAN model with t(xsm-nss) in 1D-X, Y, Z compared to supervised baseline model in 1D-X, Y, Z ( $R^2$  & RMSE).

The baseline model was trained with labeled 3200x16 samples of real data while the self-trained FMG-DCGAN was trained with >9000x16 samples (1600x16 real labeled data aggregated with ~6200x16 pseudo-labeled synthetic data and 1600x16 real pseudo-labeled data). Therefore, the proposed model was trained with labeled data and pseudo-labeled data that had a ratio of approximately 1:4. Both the self-trained FMG-DCGAN and the baseline model were evaluated on the same target test data. For 1D-X, Y and Z, the baseline model achieved force estimation accuracies in  $R^2$  of 82%, 78% and 88%, respectively. On the contrary, the unsupervised, semi-supervised self-trained model with t(xsm-nss) accomplished impressive accuracies in 1D-X, Y, and Z as  $R^2$  of 77.32%, 77.19% and 84.27%, respectively, as shown in Figure 6.4 (c).

## Chapter 7.

### Observations & Concluding Remarks

The material presented in this chapter is excerpted, reproduced, and modified with permission from the following papers:

[56] U. Zakia and C. Menon, "Estimating Exerted Hand Force via Force Myography to Interact with a Biaxial Stage in Real-Time by Learning Human Intentions: A Preliminary Investigation", *Sensors*, vol. 20, no. 7, (22pp), Apr. 2020.

[57] © [2021] IEEE with permission. U. Zakia and C. Menon, "Toward Long-Term FMG Model-Based Estimation of Applied Hand Force in Dynamic Motion During Human-Robot Interactions," in *IEEE Transactions on Human-Machine Systems*, vol. 51, no. 4, pp. 310-323, Aug. 2021, doi: 10.1109/THMS.2021.3087902.

[58] U. Zakia and C. Menon, "Force Myography-Based Human Robot Interactions via Deep Domain Adaptation and Generalization," *Sensors*. 2022, 22(1):211. <https://doi.org/10.3390/s22010211>.

[59] © [2022] IEEE with permission. U. Zakia and C. Menon, "Human Robot Collaboration in 3D via Force Myography based Interactive Force Estimations using Cross-Domain Generalization," *IEEE Access*, Mar. 2022, doi: 10.1109/ACCESS.2022.3164103.

[60] © [2022] IEEE with permission. U. Zakia, A. Barua, X. Jiang, and C. Menon, "Unsupervised, Semi-Supervised Interactive Force Estimations During pHRI via Generated Synthetic Force Myography Signals," *IEEE Access*, June 2022, doi: 10.1109/ACCESS.2022.3187115.

Sections of this chapter are reprinted or adapted from the above articles for clarification and to fit the formatting and scope of the chapter.

## 7.1. Chapter Overview

This chapter discusses the observations made during the studies performed in this thesis. Future work and directions and practical applicability of the FMG-based human robot interactions are discussed in the concluding remarks.

## 7.2. Observations

The studies in objective 1-4 revealed some observations that might be useful in developing FMG-based real-world applications in future.

### 7.2.1. Forearm & upper arm FMG bands

Proper placement of the FMG bands to read the maximum useful information derived from muscle contractions (elbow and shoulder flexion/ extension/ adduction/ abduction) were selected in accordance with previous studies [102]. For the 2-DoF planar workspace, interactions with the biaxial stage required participants to perform a combination of elbow and shoulder rotations in the planar space. By positioning the bands on the upper-arm (biceps, triceps brachii muscles) and forearm (brachioradialis and extensor carpi radialis muscles), the reading of muscle movements was improved. It was observed in objective 1 that using one of the bands either on the upper-arm or forearm was not enough for force estimation of motions (efficiencies dropped to  $R^2 \leq 45\%$ ). The unique characteristics of each arm motion when performing a grasping force was better captured with more multichannel FMG signals. To recognize versatile complex arm motions in the experimental setup, the 32-multichannel FMG bands provided better estimations.

### 7.2.2. Impact of 32 vs. 16-channel FMG technique

For the target HRI studies using the Kuka robot, only one FMG band was used with a smaller number of channels (16 feature space) to compare the impact of knowledge transfer from source domains (32 feature space) that had more FMG channels. Mapping interaction force in 3D with one forearm FMG band with a small amount of training data was a challenging task, which was reflected in the intra-session evaluation in objective 3. However, the cross-domain generalization allowed the models to predict moderately well

in 3D motions and better in 1D motions, as shown in Table 5-III. Furthermore, including additional features improved discriminative feature learning process of the model. Such generalization also helped to reduce biases towards intra-session training data. A transfer learning model with cross domain generalization (TL-CDG model) trained with multiple source data can be more practical to use because it would leverage periodic finetuning with less FMG data. Additionally, the long-term multiple source data it reduced the need for collecting more labeled target training data and saved time. Therefore, cross-domain generalization via transfer learning could become an obvious choice for quick, practical FMG-based HRI implementation for safe collaboration.

### 7.2.3. Impact of band placements and winding force

During pHRI using the linear robot (objectives 1 and 2), both FMG bands of 32 channels were placed approximately at the same locations (forearm and upper arm positions) across participants and wrapped on arms snugly, but not tight enough to place constant pressure on the sensors. Figure 7.1 shows the winding forces with standard deviations (SDs) of the bands wrapped on the forearm and upper arm of the participants at an initial time ( $t = 0-100$  ms) as the participants were waiting to interact with the robot (the arm was at rest, while the hand grasped the knob).

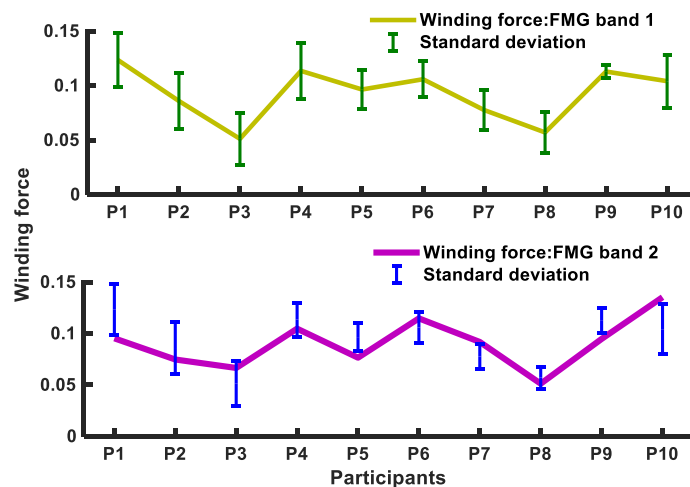


Figure 7.1. Winding forces of the FMG bands at the beginning of an interaction within participants. Reproduced from [56] with permission.

Group differences between the SDs of the two bands' winding forces were not found to be statistically significant ( $F = 4.49, p = 0.987$ ); meaning no difference in winding forces were present. As the reported results of the estimated forces in 1D were different

compared to the estimated forces in 2D motions (Figures 3.4 and 3.5) and the SDs varied significantly among the motions (Figure 7.3), it could be concluded that the winding forces (mean  $\leq 0.092$ ) did not significantly affect the estimation accuracies of the regressors for individuals due to individual variations in muscle contractions during interactions.

#### 7.2.4. Muscle voluntary contractions during an intended motion

Initially in objective 1, FMG signals were studied to evaluate separability of arm motion directions in a planar space. Data were collected for one participant performing isotonic muscle contraction of arm flexions and extensions for a certain period in the x- and y-directions, as shown in Figure 7.2(a). The FMG signals (forearm and upper-arm) were inputted into the K-means clustering algorithm with a Silhouette value of 1, which resulted in the clustered FMG signals in the x-direction and the y-direction, as shown in Figure 7.2(b). These FMG signals during flexion and extension (in x- and y- directions) were found to be statistically significant ( $p = 7.89 \times 10^{-51}$ ). More specifically, this result meant that FMG signals in the x- and y-axes corresponding to arm flexion and extension were distinguishable and revealed the potential of using FMG signals in recognizing arm motion patterns in a planar surface.

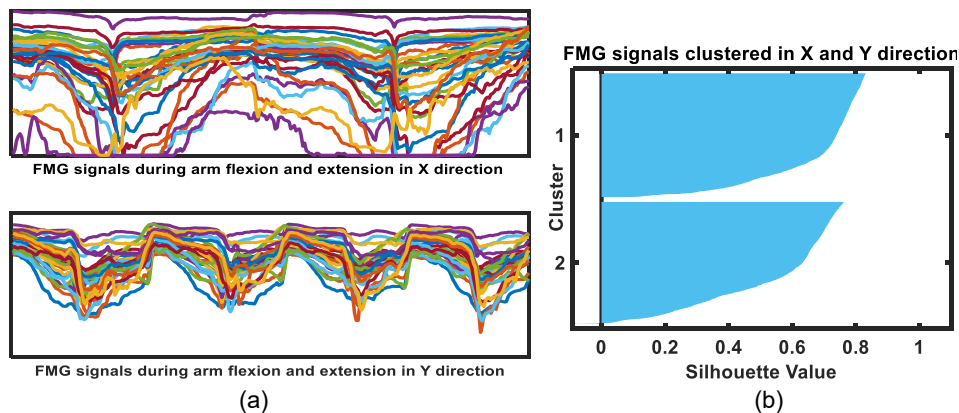


Figure 7.2. (a) FMG signals of arm motions in the x- and y-directions; (b) K-means clustering of FMG signals Reproduced from [56] with permission.

#### 7.2.5. Impact of intended motion

In objective 1, one trained model was required (biaxial stage moved along the X dimension only) for the 'X' intended motion, and two trained models performed simultaneous predictions in the X and Y dimensions for the 'Diagonal' intended motion.

For compliant collaboration, synchronous real-time conversions between applied force in motion and displacements in the linear stages were required. Due to the fundamental differences in arm posture, motion pattern or applied forces in the two intended motions, a model with the same baseline dataset (Inter-Motion-2/Inter-Participant-2) performed differently because the calibration data were different. Therefore, reported accuracies in real-time predictions [as shown in Figure 3.4, 3.5 and 7.1] were distinct and influenced by selection of the intended motion.

In objective 2A, interactions between participants and the linear robot in the 'X' intended motion, with the following parameters of applied forces: 20-30N, mean displacement: 400mm and average speed/motion:70~80mm/s, were observed. Interactions in the 'Diagonal' motion, with the following parameters of applied forces: 20-60N, mean displacement: 475mm and average speed/motion: around 60~90mm/s, were observed across participants. The intended motion used in the calibration phase allowed the model to predict the applied force in that motion. So, the applied force and motion speed in the calibration phase was expected to be maintained by a participant in the real-time test phase.

### 7.2.6. Average interactive applied forces

Figure 7.3 shows the observed average force estimations with standard deviations (SDs) using FMG signals from different arm motions from participants in objective 1. Participants applied hand forces (maximum voluntary contractions (MVC) between 30% and 80%), such that the estimated force range was between 20 and 60 N. Demographic

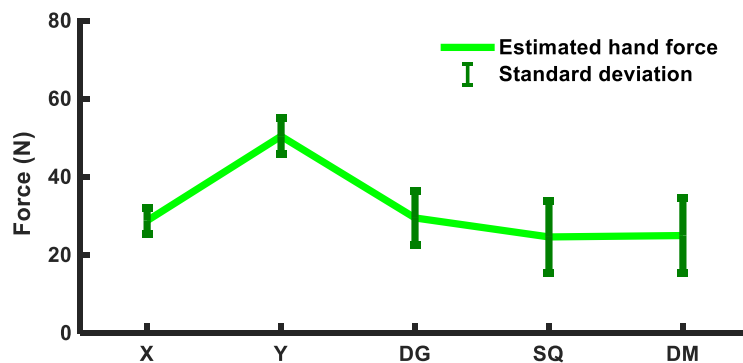


Figure 7.3. Averaged estimated hand forces and standard deviations (SDs) (within participants) in intended arm motions [X, Y, diagonal (DG), square (SQ), and diamond (DM) patterns].  
Reproduced from [56] with permission.

data such as height, arm length, arm perimeters, muscle contraction intensities, and interactions varied in widely among participants. For the 1-DoF interactions, the decreased change of directions introduced fewer variations in the DoF of the arm motions, and, hence, smaller SDs were observed.

However, for the 2-DoF interactions especially in the square and diamond motion patterns, changes in the arm motions and directions in the XY-plane were more frequent. This led to more variation among the participants in interactions in one motion pattern with their redundant choices of DoF. Thus, variations in SD were higher for the 2-DoF interactions.

### **7.2.7. Viability of calibration**

In Objective 2A, it was observed that the generalized zero-shot learning (GZSL) using a few calibration datasets allowed the long-term calibrated FMG (LCFMG) models: LCFMG-1 and LCFMG-2 to perform adequately. Therefore, any calibration data collected was valid during the period an individual continued wearing the FMG bands without doffing them. Thus, removing the bands and re-donning them, either by different users or by the same user, resulted in different FMG readings. Therefore, the need for collecting calibration data every time a participant wore the bands was essential and was revealed during testing with the LCFMG-0 model (average  $R^2 < 0.45$ ). It was not surprising that models trained without any calibration data failed in real-time testing and, hence, zero-shot learning could not be implemented using FMG signals.

Real-time model performance was governed by the calibration data. Introducing a few calibration datasets supported generalized ZSL with the multiple source domain adaptation technique where it tuned a model with the current state of FMG signals. These data simply transformed and applied the trained model distinctively to the participant performing the action in a real-time session. For effective applied force prediction in the test phase, motion pattern and interaction force were required to be like the calibration data. Therefore, the inclusion of calibration data during real-time evaluation was vital for i) involving a few test samples in training data to recognize unseen motion or an unseen participant using GZSL learning, ii) representing current states of muscle contraction and sensors positions, iii) selecting an intended simple motion, iv) reducing training time i.e.,

reducing fatigue, and v) allowing donning/doffing (on/off) of the band during longer time usage because new calibration data could be collected again.

With fewer calibration data, the model might lean towards multiple source distributions, predicting well for some participants while moderately predicting for others. But evaluation of the proposed model across participants indicated that even with bias towards multiple source domains, the proposed model predicted better when calibration data was used in training, thereby tuning the model towards the target domain.

In objective 2B, the pretrained supervised FMG deep transfer learning (SFMG-DTL) model was further retrained with a few calibration datasets to adapt to the target domain. The model worked well for both the supervised domain adaptation (SDA) and supervised domain generalization (SDG) once fine-tuned with calibration/target training data. To investigate the effect of calibration during SDA, the pretrained model was evaluated on target test data without fine-tuning towards target distribution. It was interesting that the pretrained model without fine-tuning could predict forces in the X dimension with higher estimation accuracy and lower error ( $R^2 \geq 89\%$ ,  $\text{NRMSE} \approx 0.09\%$ ), although it could not estimate well in the Y dimension ( $R^2 \leq 12\%$ ,  $\text{NRMSE} \geq 8\%$ ) with no adaptation to the target domain. For SDG, similar trends were observed in the X dimension ( $R^2 \geq 89\%$ ,  $\text{NRMSE} \approx 0.09\%$ ) and the Y dimension ( $R^2 \leq 25\%$ ,  $\text{NRMSE} \geq 6\%$ ). Muscle contractions in extension/flexion (X dimensions) and abduction/adduction (Y dimensions) affected FSR readings and the model's performance, although this requires further study. Therefore, it was revealed that fine-tuning with calibration data was mandatory for estimating forces in the 2D planar square motion with variable size: SQ-1 motion for SDA as well as in the square motion with fixed size: SQ-2 motion for SDG.

For compliant collaboration, applied forces in both dimensions needed to be estimated well simultaneously. Therefore, the proposed framework would not work without calibration data. The calibration data represented the instantaneous FMG data of muscle contraction during the interactions, and it was found an effective way to include the current state of muscle readings in certain activities during pHRI. Additionally, using fewer calibration datasets was helpful, as the model was calibrated within a few minutes.



### 7.2.8. Impact of long-term multiple source distributions

For generalization in objective 2A, the same multiple source distributions were used in training for recognition of the unseen test data, as described in Table 4-I. For instance, in scenario 1 (recognizing an unseen motion  $M_1$  or  $M_3$ ), although the 'learnt participant dataset' was distinct for each participant ( $P_6$ - $P_8$ ), the reference dataset was the same for all. Interestingly, in scenario 2, one baseline dataset (subset/full reference dataset) was used in recognition of unseen participants ( $P_9$ - $P_{15}$ ).

A model with the largest multiple source distributions, added more generality, diversity, and contribution to supervised transfer knowledge. The training dataset for the LCFMG-2 model was approximately 5 times greater than the LCFMG-1 model. Thus, the LCFMG-2 model was more generalized, although it required almost twice the training time. Generalized ZSL used in regressing FMG signals permitted generalization errors to be low and comparable with the supervised trained models (STMs). It was observed that the STM-1 and STM-2 models trained with a small amount of training data (calibration data of 400, 800 samples only) did not provide better estimates of real-time interactions. Whereas the long-term calibrated FMG-based models estimated real-time interactions quite well due to the multiple source distributions contributing to the transfer of knowledge.

## 7.3. Potential applications

The studies conducted in this thesis revealed that the force myography (FMG) technique can be a viable solution for pHRI applications by estimating interactive forces in dynamic motions. Identifying human intentions of applied force and directions during human and robot collaborations allowed implementing a control loop via data driven models. Compliant collaboration techniques showed that the robots will follow the trajectories of intended human interactions. Hence, the ability to predict human motions using FMG can prevent the human worker from getting injured or trapped by the robot in the industrial workplace. It was observed that transfer learning would be a better choice for the industrial workplace where a few calibration datasets would recognize interactive forces from instantaneous signals. Using multiple source distributions collected over a long period of time helped generalizing the model. It also enabled to bridge between different HRI platforms and could estimate interactive forces either via forearm or upper arm muscle readings for first-time or repeated user. An FMG-based transfer learning

technique can be more practical for domain adaptation to implement an FMG-based application either for one-time or periodic usage by overcoming sensor position shifts that occur with donning and doffing the FMG band on multiple elapsed days. Furthermore, generating real-like synthetic FMG source data and implementing self-training techniques can resolve real-world challenges of having an inadequate amount of labeled data. Hence, in everyday applications, these frameworks will allow faster adaptations of using an FMG band with a smaller amount of calibration data in practice. This will help reduce physiological effects of wearing an FMG band for a long period of time by retraining quickly when the band is taken off and put back again, which also avoids muscle fatigue for the wearer of the band. Therefore, the proposed methods showed that the FMG technique has a potential use in HMI, prosthetic, or safe collaboration during HRI for an individual where interactions with machines are required on a regular basis.

## **7.4. Limitations and Future Works**

In objective 2A, investigating different LCFMG models and a few STM models in real-time required approximately 1.5 hour for each participant. Due to the time-consuming nature of the study, only two motions were investigated to evaluate the proposed models. In a few instances, it was observed that the force and motion were governed by the large baseline dataset, which slightly limited the behavior of the real-time interaction.

In objective 2B, SDA and SDG showed potential improvements during offline analysis, and real-time implementation can be examined in future. The SFMG-DTL model performed well for domain generalization but was limited to a certain pHRI collaborative tasks. A pretrained model using more diversified source domains potentially could play a vital role in improving domain generalization and be extended to all other possible interactions.

In objective 3, pHRI with the Kuka robot was investigated via an FMG band with 16 channels to measure forearm muscle contractions. Investigating FMG signals of the upper arm in the future might provide better information for interactions in 3D. Due to time constraints, the proposed algorithm in objective 4 was evaluated during pHRI between only one participant and the Kuka robot in the 1D-X, Y, Z directions. Involving more participants and interacting in 3D would require further investigations. Also, implementing

domain generalization with the proposed unsupervised, self-trained FMG-DCGAN model can be studied in future.

Safe interactions were implemented via admittance control where the robot always complied. Hence, if a robot approached slowly in an undesirable direction towards a human worker, the methods presented here can be used to avoid collision with the robot. However greater speed or force applied by the robot towards the human worker might be hard to address.

## 7.5. Conclusion

Considering human activities in collaborative tasks where physical interactions happen between a human worker and a robot is vital for many reasons including efficiency and safety. Among many biosignals, the contemporary FMG technique can detect muscle contractions during contact forces during interactions with machinery. It can be a viable solution to use indirect measurements of hand forces to understand and predict human actions. Hence, estimating hand forces in motions during interactions with FMG signals can be useful for performing collaborative tasks with a robot.

In objective 1, we used an FMG band with 32-channels by the participant who interacted with a linear robot and showed that FMG-based force estimation achieved higher estimation accuracies ( $92\% \geq R^2 \geq 82\%$ ) during several 1D and 2D motions. The simple and complex intended motions indicated that a human worker could manipulate the robot in any intended trajectory. Objective 2 and 3 successfully investigated transfer learning via domain adaptation, domain generalization and cross-domain generalization techniques using 32 feature spaces long-term FMG source data (collected over a long period of time) with a small amount of instantaneous calibration data. These methods can leverage gaps between unrelated source and target data from unrelated HRI platforms. Long-term multiple source data collected over a long period of time helped improve interactions in simple motions ( $94\% \geq R^2 \geq 80\%$ ) for a new worker or a new intended motion, while it improved estimation accuracies ( $R^2 \geq 88\%$ ,  $\text{NRMSE} \leq 0.6$ ) for repeated usage. Conducting a 16-channel HRC task of moving a wooden rod in 3D with a serial robot using cross-domain generalization performed moderately well ( $63\% \leq R^2$ ), while obtaining improved performances in 1D-pHRI ( $86\% \geq R^2 \geq 79\%$ ). For practical applications where target data is inadequate or unlabeled, synthetic data with pseudo-labeling can resolve

these challenges. This was achieved in objective 4 via unsupervised and semi-supervised transfer learning ( $85\% > R^2 > 77\%$ ) using FMG signals from a 16-channel band in simple 1D.

Therefore, studies conducted in this thesis demonstrated that including human bio feedback in a robotic control scheme could improve safe collaboration between the human and robot in the workplace. These studies can provide viable solutions to interact with machines daily. The methods and techniques adapted in this thesis can be useful in developing other real-world applications using human bio feedback. The use of the wearable FMG bands capable of recognizing human activities can enhance pHRI quality in safe collaborations, rehabilitation applications, or prostheses control.

## References

1. E. Helms, M. Hägele, and W. Schaaf. Robot assistants at manual workplaces: effective co-operation and safety aspects. In the Proc. of 33rd Int. Symp. on Robotics (ISR), Oct. 2002, pp. 7–11.
2. A. D. Santis, B. Siciliano, A. D. Luca, and A. Bicchi. An atlas of physical human-robot interaction. *Mech. & Machine Theory*, 43 (3), pp. 253–270, 2008.
3. I. L. Matthias, S. Kock, H. Jerregard, M. Källman, I. Lundberg, and R. Mellander. Safety of collaborative industrial robots certification possibilities for a collaborative assembly robot concept. IEEE Int. Symp. Assembly and Manufacturing (ISAM), 2011, pp. 1–6.
4. E. N. Malamas, E. G. Petrakis, M. Zervakis, L. Petit, and J. D. Legat. A survey on industrial vision systems, applications and tools. *Image Vis. Comput.*, 21(2), pp. 171–188, Feb. 2003.
5. L. N. B. Bass, and E. Henry. Ultrasonic background noise in industrial environments. *J. Acoust. Soc. Am.*, 78(6), pp. 2013–2016, 1985.
6. C. Lee, H. Choi, J. Park, K. Park, and S. Lee. Collision avoidance by the fusion of different beamwidth ultrasonic sensors. *IEEE Sensors Journal*, pp. 985–988, 2007.
7. S. B. Niku. Introduction to Robotics Analysis, Systems, Applications. Prentice Hall Upper Saddle River, NJ 07458.
8. S. Haddadin, A. Albu-Schaffer, A. De Luca, and G. Hirzinger. Collision detection and reaction: a contribution to safe physical human-robot interaction. Int. Conf. on Intell. Robots and Systems (IEEE/RSJ), 2008, pp. 3356–3363.
9. M. G. Carmichael; D. Liu; K. J Waldron. Investigation of reducing fatigue and musculoskeletal disorder with passive actuators. Int. Conf. on Intell. Robots and Systems (IEEE/RSJ), Oct. 2010, Taipei, Taiwan, pp. 2481–2486.
10. N. A. Nelson; R. M. Park; M. A. Silverstein, and F. E. Mirer. Cumulative trauma disorders of the hand and wrist in the auto industry. *American Journal of Public Health*, 82(11), pp. 1550– 1552, 1992.
11. Y. Li, and S. S. Ge. Human–robot collaboration based on motion intention estimation. *IEEE/ASME Trans. on Mechatronics*, 19(3), pp. 1007–1014, June 2014.
12. H. C. Ravichandar, and A. P. Dani. Human intention inference using expectation-maximization algorithm with online model learning. *IEEE Trans. on Auto. Sc. & Eng.*, 14(2), pp. 855–868, Apr. 2017.

13. J. Owoyemi, and K. Hashimoto. Learning human motion intention with 3D convolutional neural network. Proc. of IEEE Int. Conf. on Mech. & Automation, Aug. 2017, Takamatsu, Japan pp. 1810–1815.
14. X. Yu, W. He, Y. Li, C. Yang, and C. Sun. Neural control for constrained human-robot interaction with human motion intention estimation and impedance learning. IEEE Chinese Auto. Cong., Sep. 2017 pp. 2682–2687.
15. S. C. Mukhopadhyay. Wearable sensors for human activity monitoring: a review. *IEEE Sensors Journal*, 15(3), pp. 1321–1330, Mar. 2015.
16. M. Cornacchia, K. Ozcan, Y. Zheng, and S. Velipasalar. A survey on activity detection and classification using wearable sensors. *IEEE Sensors Journal*, 17(2), pp. 386–403, Jan. 2017, doi: 10.1109/JSEN.2016.2628346.
17. Hu, Yu, et al. A novel attention-based hybrid CNN-RNN architecture for sEMG-based gesture recognition. *PloS one*, 13(10), Oct. 2018: e0206049.
18. F. Carlo, and P. Crenna. Multichannel SEMG in clinical gait analysis: a review and state-of-the-art. *Clinical Biomechanics*, 24(3), pp. 236–245, 2009.
19. S.H. Roy et al. A combined sEMG and accelerometer system for monitoring functional activity in stroke. *IEEE Transactions on Neural Systems and Rehabilitation Engineering*, 17(6), pp.585-594, 2009.
20. L. Zhijun et al. sEMG-based joint force control for an upper-limb power-assist exoskeleton robot. *IEEE journal of biomedical and health informatics*, 18(3), pp.1043-1050, 2013.
21. M.A. Oskoei, and H. Hu. Myoelectric control systems—A survey. *Biomed. Signal Process. Control*, 2(4), pp.275–294, Oct. 2007.
22. P. Geethanjali, and K. K. Ray. A low-cost real-time research platform for EMG pattern recognition-based prosthetic hand. *IEEE/ASME Trans. on Mechatronics*, 20(4), pp.1948–1955, Aug. 2015.
23. K. Gui, H. Liu and D. Zhang. A Practical and Adaptive Method to Achieve EMG-Based Torque Estimation for a Robotic Exoskeleton. *IEEE/ASME Transactions on Mechatronics*, 24(2), pp. 483-494, Apr. 2019, doi: 10.1109/TMECH.2019.2893055.
24. M. Yokoyama, R. Koyama, and M. Yanagisawa. An evaluation of hand-force prediction using artificial neural-network regression models of surface EMG signals for handwear devices. *Journal of Sensors*, 2017, 2017.
25. Q. Zhang, M. Hayashibe, P. Fraise, and D. Guiraud. FES-Induced torque prediction with evoked EMG sensing for muscle fatigue tracking. *IEEE/ASME Trans. on Mechatronics*, 16(5), pp. 816–826, Oct. 2011.

26. F. Duan et. al. sEMG-based identification of hand motion commands using wavelet neural network combined with discrete wavelet transform. *IEEE Trans. on Ind. Elect.* 63(3), pp.1923-1934, Mar. 2016, doi: 10.1109/TIE.2015.2497212.
27. U. C. Allard et. al. A convolutional neural network for robotic arm guidance using sEMG based frequency-features. In IEEE/RSJ Int. Conf. on IROS. pp. 2464–2470, 2016.
28. R. Meattini et. al. An sEMG-based human–robot interface for robotic hands using machine learning and synergies. *IEEE Trans. on Components, Pack. and Manu. Tech.* 8(7), pp. 1149-1158, July 2018, doi: 10.1109/TCPMT.2018.2799987.
29. Z.G. Xiao, and C. Menon. Towards the development of a wearable feedback system for monitoring the activities of the upper-extremities. *Journal of NeuroEng. Rehabil.* 11(2), 2014, doi:10.1186/1743-0003-11-2.
30. Z.G. Xiao, and C Menon. A Review of Force Myography Research and Development. *Sensors*, 19(20), Oct. 2019, doi.org/10.3390/s19204557.
31. A. Kadkhodayan,, X. Jiang, and C. Menon. Continuous prediction of finger movements using force myography. *Journal of Med. & Biological Eng.*, 36(4), pp. 594–604, Aug. 2016.
32. R. S. Chegani, and C. Menon. Regressing grasping using force myography: an exploratory study. *BioMedical Eng. OnLine*, 17(159), Oct. 2018, doi:10.1186/s12938-018-0593-2.
33. ML. Delva, M. Sakr, RS. Chegani, M. Khoshnam, and C. Menon. Investigation into the Potential to Create a Force Myography-based Smart-home Controller for Aging Populations. 7th IEEE Int. Conf. on Biomed. Robotics and Biomech. (BioRob), Enschede, The Netherlands, Aug. 2018, pp.770–775.
34. N. Ha, G.P.Withanachchi, and Y. Yihun. Performance of Forearm FMG for Estimating Hand Gestures and Prosthetic Hand Control. *Journal of Bionic Eng.* 2019(16), pp.88–98, doi.org/10.1007/s42235-019-0009-4.
35. A.K. Godiyal, H.K.Verma, N. Khanna, and D. Joshi. A force myography-based system for gait event detection in overground and ramp walking. *IEEE Trans. Instrum. Meas.*, 2018(67), pp.2314–2323, doi:10.1109/TIM.2018.2816799.
36. A.K. Godiyal, M. Mondal, and D. Joshi. Force Myography Based Novel Strategy for Locomotion Classification. *IEEE Transactions on Human-Machine System*, 2018(48), 648–657, doi:10.1109/THMS.2018.2860598.
37. T.B. Andersen, R. Eliassen, M. Jarlund, and B. Yang. Force myography benchmark data for hand gesture recognition and transfer learning. arXiv 2020, arXiv:2007.14918.

38. C. Ahmadizadeh et. al. Toward intuitive prosthetic control: solving common issues using force myography, surface electromyography, and pattern recognition in a pilot case study. *IEEE Robotics & Automation Magazine*, 24(4), Pp.102-111, 2017.
39. X. Jiang, L-K Merhi, and C. Menon. Force exertion affects grasp classification using force myography. *IEEE Transactions on Human-Machine Systems*, 48(2), pp. 219–226, Apr. 2018, doi: 10.1109/THMS.2017.2693245.
40. M. Sakr, and C. Menon. On the estimation of isometric wrist/forearm torque about three axes using force myography. IEEE Int. Conf. on Biomed. Robotics and Biomech. (BioRob), UTown, Singapore, June 2016, pp. 827–832.
41. U. Zakia, X. Jiang, and C. Menon. Deep learning technique in recognizing hand grasps using FMG signals. In Proceedings of the 2020 11th IEEE Annual Information Technology, Electronics and Mobile Communication Conference (IEMCON), Vancouver, BC, Canada, 4–7 November 2020; pp. 0546–0552, doi:10.1109/IEMCON51383.2020.9284893.
42. M. Anvaripour et.al. FMG- and RNN-Based Estimation of Motor Intention of Upper-Limb Motion in Human-Robot Collaboration. *Frontiers in Robotics and AI*, 7, pp.183, 2020, doi: 10.3389/frobt.2020.573096.
43. J. Sanford, R. Patterson, and D. O Popa. Concurrent surface electromyography and force myography classification during times of prosthetic socket shift and user fatigue. *Journal of Rehab. and Asst. Tech. Eng.*, 4, pp. 1–13, 2017.
44. X. Jiang, L. K. Merhi, Z. G. Xiao, and C. Menon. Exploration of force myography and surface electromyography in hand gesture classification. *Med. Eng. Phys.*, 41, pp. 63–73, 2017.
45. A. Belyea; K. Englehart, and E. Scheme. FMG Versus EMG: a comparison of usability for real-time pattern recognition based control. *IEEE Trans. on Biomed. Eng.*, 66(11), pp. 3098–3104, Nov. 2019, doi:10.1109/TBME.2019.2900415.
46. Statista Online. Available: <https://www.statista.com/statistics/728530/industrial-robot-market-size-worldwide/>
47. G. D. Kessler; L. F. Hodges, and N. Walker. Evaluation of the Cyber Glove as a Whole-Hand Input Device. *ACM Transactions on Computer-Human Interaction*, 2(4), Dec. 1995, pp. 263-283.
48. J. P. Wachs et.al. Vision-based hand-gesture applications. *Commun. ACM*, 54(2), pp. 60–71, Feb. 2011.
49. C. D. Mutto, P. Zanuttigh, and G. M. Cortelazzo. Time-of Flight Cameras and Microsoft Kinect. Briefs in Electrical and Computer Engineering, Springer, 2012.



50. O. C. Jenkins, G. González, and M. M. Loper. Tracking human motion and actions for interactive robots. 2nd ACM/IEEE International Conference on Human-Robot Interaction (HRI), Arlington, VA, 2007, pp. 365–372.
51. B. D. Argall, and A. G. Billard. A survey of Tactile Human–Robot Interactions. *Journal of Robotics and Autonomous Systems*, 58, pp.1159–1176, 2010.
52. J.W. Hart et. al. Developing Robot Assistants with Communicative Cues for Safe, Fluent HRI. *Studies in Systems, Decision and Control*, 117, Springer, Cham.
53. I. Ceballos. Learning Operator Intentions Using Supervised Learning for Safe Human-Robot Collaboration. Student project, Aalborg University, 2017.
54. J. DelPreto, and D. Rus. Sharing the Load: Human-Robot Team Lifting Using Muscle Activity. IEEE International Conference on Robotics and Automation (ICRA), 2019, pp. 7906–7912, doi: 10.1109/ICRA.2019.8794414.
55. L. Peternel, N. Tsagarakis and A. Ajoudani. Towards multi-modal intention interfaces for human-robot co-manipulation. IEEE/RSJ International Conference on Intelligent Robots and Systems (IROS), Daejeon, 2016, pp. 2663–2669.
56. U. Zakia, and C. Menon. Estimating Exerted Hand Force via Force Myography to Interact with a Biaxial Stage in Real-Time by Learning Human Intentions: A Preliminary Investigation. *Sensors*, 20(7), pp. 22, Apr. 2020.
57. U. Zakia, and C. Menon. Toward Long-Term FMG Model-Based Estimation of Applied Hand Force in Dynamic Motion During Human–Robot Interactions. *IEEE Transactions on Human-Machine Systems*, 51(4), pp. 310–323, Aug. 2021, doi: 10.1109/THMS.2021.3087902.
58. U. Zakia, and C. Menon. Force Myography-Based Human Robot Interactions via Deep Domain Adaptation and Generalization. *Sensors*, 22(1), pp.211, 2022. <https://doi.org/10.3390/s22010211>.
59. U. Zakia, and C. Menon. Human Robot Collaboration in 3D via Force Myography based Interactive Force Estimations using Cross-Domain Generalization. *IEEE Access*, Mar. 2022, doi: 10.1109/ACCESS.2022.3164103.
60. U. Zakia, A. Barua, X. Jiang, and C. Menon, “Unsupervised, Semi-Supervised Interactive Force Estimations During pHRI via Generated Synthetic Force Myography Signals,” *IEEE Access*, June 2022, doi: 10.1109/ACCESS.2022.3187115.61.
61. U. Zakia and C. Menon, ""Dataset on Force Myography for Human Robot Interactions", MDPI Data (submitted June 2022).
62. Tanzio Printed Electronics. Available online: <https://tanzio.co/collections/frontpage> (accessed on 27 January 2020).

63. Zaber Technologies Inc. Available online: <https://www.zaber.com/products/linear-stages/X-LSQ/details/X-LSQ450B> (accessed on 27 January 2020).
64. ATI Industrial Automation. Available online: [https://www.atia.com/products/ft/.ft\\_models.aspx?id=Mini45](https://www.atia.com/products/ft/.ft_models.aspx?id=Mini45) (accessed on 27 January 2020).
65. B. Komati et.al. Explicit force control vs. impedance control for micromanipulation. In ASME 2013 International Design Engineering Technical Conferences and Computers and Information in Engineering Conference, American Society of Mechanical Engineers Digital Collection: Portland, Oregon, USA, 4–7 August 2013, pp. 1–8.
66. KUKA Industrial Automation. Available online: <https://www.kuka.com/en-ca/products/robotics-systems/industrial-robots/lbr-iiwa/>
67. C. M. Bishop. *Pattern recognition and machine learning*, 4(4), New York: springer, 2006.
68. A. Pozdnoukhov, and S. Bengio. Semi-Supervised Kernel Methods for Regression Estimation. IEEE International Conference on Acoustics Speech and Signal Processing Proceedings, 2006, pp. V-V, doi: 10.1109/ICASSP.2006.1661341.
69. Y. LeCun, and Y. Bengio. Convolutional networks for images, speech, and time series. *The handbook of brain theory and neural networks*, 3361(10), 1995.
70. I. Goodfellow et.al. Generative adversarial nets. *Advances in neural information processing systems*, 3, pp. 2672–2680, 2014, doi:10.3156/jsoft.29.5\_177\_2.
71. Y. Xian et. al. Zero-shot learning—a comprehensive evaluation of the good, the bad and the ugly. *Trans. on Pattern Anal. and Machine Intel.*, 41(9), pp. 2251-2265, Sept. 2019, doi:10.1109/TPAMI.2018.2857768.
72. P. Zegers et. al. Systematic testing of generalization level during training in regression-type learning scenarios. IEEE Int. Joint Conf. on Neural Networks, July 2014, doi: 10.1109/IJCNN.2004.1381101.
73. W. L. Chao et. al. An empirical study and analysis of generalized zero-shot learning for object recognition in the wild. ECCV 2016. Lecture Notes in Comp. Sc., 9906. Springer, Cham, 2016, doi: 10.1007/978-3-319-46475-6\_4.
74. Q. Yang et. al. Transfer Learning. Cambridge University Press: Cambridge, UK, 2020.
75. L. Torrey, and J. Shavlik. Transfer learning. Handbook of research on machine learning applications and trends: algorithms, methods, and techniques. IGI global, pp. 242-264, 2010.

76. S. Pan, and J. Yang. A survey on transfer learning. *IEEE Transactions Knowl. Data Eng.*, 2009(22), pp. 1345–1359, 2009.
77. K. Wouter, and L. Marco. An introduction to domain adaptation and transfer learning. arxiv 2018, arxiv.org/abs/1812.11806.
78. S. Motiian et.al. Unified Deep Supervised Domain Adaptation and Generalization. IEEE International Conference on Computer Vision (ICCV), Venice, Italy, October. 2017, pp. 5716–5726, doi:10.1109/ICCV.2017.609.
79. J. Wang et.al. Generalizing to Unseen Domains: A Survey on Domain Generalization. Mar. 2021. arXiv preprint arXiv:2103.03097.
80. E. Otović et.al. Intra-domain and cross-domain transfer learning for time series data—How transferable are the features? Knowledge-Based Systems, pp. 107976, Dec. 2021.
81. J. Zheng et.al. Improving the Generalization Ability of Deep Neural Networks for Cross-Domain Visual Recognition. *IEEE Transactions on Cognitive and Developmental Systems*, 13(3), pp. 607–620, Sept. 2021, doi: 10.1109/TCDS.2020.2965166.
82. S. Paul et. al. Universal Cross-Domain Retrieval: Generalizing Across Classes and Domains. IEEE/CVF International Conference on Computer Vision, pp. 12056–12064, 2021.
83. J. Savelka et. al. Cross-domain generalization and knowledge transfer in transformers trained on legal data. Dec. 2021. arXiv preprint arXiv:2112.07870.
84. Z. Ding, and Y. Fu. Deep Domain Generalization With Structured Low-Rank Constraint. *IEEE Transactions on Image Processing*, 27(1), pp. 304–313, Jan. 2018, doi: 10.1109/TIP.2017.2758199.
85. Y. Gu et.al. Progressive Transfer Learning and Adversarial Domain Adaptation for Cross-Domain Skin Disease Classification. *IEEE Journal of Biomedical and Health Informatics*, 24(5), pp. 1379–1393, May 2020, doi: 10.1109/JBHI.2019.2942429.
86. D. -K. Han, and J. -H. Jeong. Domain Generalization for Session-Independent Brain-Computer Interface. 9th International Winter Conference on Brain-Computer Interface (BCI). pp. 1–5, 2021, doi: 10.1109/BCI51272.2021.9385322.
87. J. Qi et.al. Intelligent Human-Computer Interaction Based on Surface EMG Gesture Recognition. *IEEE Access*, 7, pp.61378–61387, 2019, doi: 10.1109/ACCESS.2019.2914728.

88. Y. Guo et.al. MCDGD: Multi-Source Unsupervised Domain Adaptation for Abnormal Human Gait Detection. *IEEE Journal of Biomedical and Health Informatics*, 25(10), pp. 4017–4028, Oct. 2021, doi: 10.1109/JBHI.2021.3080502.
89. Z. He, Y. Zhong, and J. Pan. An adversarial discriminative temporal convolutional network for EEG-based cross-domain emotion recognition. *Computers in biology and medicine*, pp.105048, 2021.
90. A. Field. *Discovering Statistics Using IBM SPSS*, 5th ed; Sage: Los Angeles, LA, USA, 2017.
91. Z. Ju, and H. Liu. Human arm motion analysis with multisensory information. *IEEE/ASME Transactions on Mechatronics*, 19, pp.456–466, 2014.
92. Y. Suzuki et.al. Human Operation with XY-Stages-Human Adaptive Mechatronics. IEEE International Conference on Systems, Man and Cybernetics, Taipei, Taiwan, Oct. 2006; pp. 4034–4039.
93. N. Jiang et.al. Effect of arm position on the prediction of kinematics from EMG in amputees. *Med. Biol. Eng. Comput.*, 51, pp.143–151, 2013, doi:10.1007/s11517-012-0979-4.
94. M. Ghifary et. al. Scatter Component Analysis: A Unified Framework for Domain Adaptation and Domain Generalization. *IEEE Trans. Pattern Anal. Mach. Intell.*, 39, pp.1414–1430, 2016, doi:10.1109/TPAMI.2016.2599532.
95. J. E. Van Engelen, and H. H. Hoos. A survey on semi-supervised learning. *Machine Learning*, 109(2), pp. 373–440, 2020.
96. I. Triguero, S. García, and F. Herrera. Self-labeled techniques for semi-supervised learning: taxonomy, software and empirical study. *Knowledge and Information systems*, 42(2), pp. 245–284, 2015.
97. X. Li et. al. Learning to self-train for semi-supervised few-shot classification. *Advances in Neural Information Processing Systems*, 32, pp. 10276–10286, 2019.
98. S. Höfer et. al. Sim2Real in Robotics and Automation: Applications and Challenges. *IEEE Transactions on Automation Science and Engineering*, 18(2), pp. 398–400, Apr. 2021, doi: 10.1109/TASE.2021.3064065.
99. J. Tremblay et. al. Training Deep Networks with Synthetic Data: Bridging the Reality Gap by Domain Randomization. IEEE/CVF Conference on Computer Vision and Pattern Recognition Workshops (CVPRW), 2018, pp. 1082–1088, doi: 10.1109/CVPRW.2018.00143.

100. J. Tobin et.al. Domain randomization for transferring deep neural networks from simulation to the real world. *IEEE/RSJ International Conference on Intelligent Robots and Systems (IROS)*, 2017, pp. 23–30, doi: 10.1109/IROS.2017.8202133.
101. A. Radford, L. Metz, and S. Chintala. Unsupervised representation learning with deep convolutional generative adversarial networks. *arXiv preprint arXiv:1511.06434*, 2015.
102. Z.G. Xiao, and C. Menon. Performance of forearm FMG and sEMG for estimating elbow, forearm and wrist positions. *Journal of Bionic Eng.*, 14, pp. 284–295, 2017.
103. Y. Li et. al. Discrete hand motion intention decoding based on transient myoelectric signals. *IEEE Access*, 7, pp. 81360–81369, 2019.
104. L. Zhang et.al. sEMG based human motion intention recognition. *Journal of Robotics*, 2019, doi:10.1155/2019/3679174.
105. U. Côté-Allard et.al. Virtual Reality to Study the Gap Between Offline and Real-Time EMG-based Gesture Recognition. *arXiv 2009*, arXiv:1912.09380. (Submitted on December 2019).
106. M. Sakr, and C. Menon. Exploratory evaluation of the force myography (FMG) signals usage for force control of a linear actuator. *IEEE International Conference on Biomedical Robotics and Biomechatronics (Biorob)*, Enschede, The Netherlands, Aug. 2018; pp.903–908.
107. D.P. Ferris, G.S. Sawicki, and M.A. Daley. A physiologist’s perspective on robotic exoskeletons for human locomotion. *Int. Journal on Humanoid Robot*, 4, pp.507–528, 2007, doi:10.1142/S0219843607001138.
108. L. Zhou, S. Bai, and Y. Li. Energy Optimal Trajectories in Human Arm Motion Aiming for Assistive Robots. *Journal on Model. Identif. Control*, 38, pp.11–19, 2017, doi:10.4173/mic.2017.1.2.
109. M. Malosio, N. Pedrocchi, F. Vicentini, and L. M. Tosatti. Analysis of Elbow-Joints Misalignment in Upper-Limb Exoskeleton. *IEEE International Conference on Rehabilitation Robotics*, Zurich, Switzerland, July 2011, pp. 456–461.

## Appendix. Additional Observations

The material presented in this appendix is excerpted, reproduced, and modified with permission from the following papers:

[56] U. Zakia and C. Menon, "Estimating Exerted Hand Force via Force Myography to Interact with a Biaxial Stage in Real-Time by Learning Human Intentions: A Preliminary Investigation", *Sensors*, vol. 20, no. 7, (22pp), Apr. 2020.

[57] © [2021] IEEE with permission. U. Zakia and C. Menon, "Toward Long-Term FMG Model-Based Estimation of Applied Hand Force in Dynamic Motion During Human–Robot Interactions," in *IEEE Transactions on Human-Machine Systems*, vol. 51, no. 4, pp. 310-323, Aug. 2021, doi: 10.1109/THMS.2021.3087902.

[58] U. Zakia and C. Menon, "Force Myography-Based Human Robot Interactions via Deep Domain Adaptation and Generalization," *Sensors*. 2022; 22(1):211. <https://doi.org/10.3390/s22010211>.

[59] © [2022] IEEE with permission. U. Zakia and C. Menon, "Human Robot Collaboration in 3D via Force Myography based Interactive Force Estimations using Cross-Domain Generalization," accepted in *IEEE Access* (Mar. 2022).

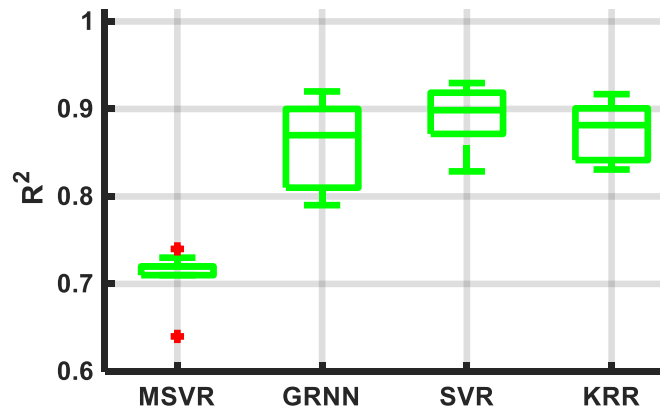
[60] © [2022] IEEE with permission. U. Zakia, A. Barua, X. Jiang, and C. Menon, "Unsupervised, Semi-Supervised Interactive Force Estimations During pHRI via Generated Synthetic Force Myography Signals," *IEEE Access*, June 2022, doi: 10.1109/ACCESS.2022.3187115.

Sections of this appendix are reprinted or adapted from the above articles for clarification and to fit the formatting and scope of the appendix.

### 1. Selection of ML algorithms

In objective 1, the SVR and the KRR algorithms were chosen among several machine learning algorithms and the hyperparameters and features were carefully selected. These algorithms, other than the MSVR (capable of estimating force in one direction while considering forces acting in other dimensions) and the GRNN (a neural

network algorithm for regression), were selected for force estimation. The MSVR was appropriate for 2D motions only and did not provide good estimation and therefore was not implemented in real time. Although the GRNN worked well for 1D motions and could achieve comparable cross-validation accuracies to those of the SVR and the KRR, it suffered in real-time 2D interactions (specially in DM motions) because of longer computation time when more complex arm motions are present. Five-fold LOOCVs were carried out for 2D DM motion patterns to justify the selection. Figure A.1 shows the force estimation accuracies of these algorithms (for MSVR:  $R^2 = 73\%$ , and GRNN:  $R^2 = 87\%$ ). Among these, the other two algorithms, i.e., SVR and KRR, were implemented in real-time interactions and were proven efficient.



**Figure Appendix.1.** Five-fold cross-validation results for 2-DoF interactions in diamond arm motion. Reproduced from [56] with permission.

The FMG technique can be a viable alternative to the traditional sEMG. In this study, raw FMG signals were used for learning and estimating, which did not require complex signal preprocessing like sEMG signals [44,45]. A similar study implemented several machine learning classification algorithms to decode discrete hand motion intention using high-density transient EMG signals with a short window (only 150ms) [103]. A survey on the sEMG technique reported it was adopted in discrete arm motions using classification (approximately 73–98%) and in continuous arm motions and forces using regression (approximately 84–93%) involving offline machine learning and deep learning techniques [104]. Although there is a gap between offline and online performances using sEMG signals, interestingly, the FMG technique was found to perform better in online classification and regression than the sEMG technique [105].

## **2. Real-time interactive force estimations**

The proposed control scheme in objective 1 evaluated machine learning techniques in real time, and comparable estimation accuracies (approximately 88–89% averaged across all motions) were obtained with FMG signals, which were in affiliation with the literature. The accuracies of these estimators were higher in 1-DoF in the x-direction, which were 94% and 92% for the SVR and the KRR, respectively; these results were comparable with the reported accuracies of 90% and 92% for the SVR and the KRR, respectively, when one participant interacted with a linear actuator in the x-axis using the FMG technique [106]. The performances of the estimators gradually descended with the increased complexity of 2-DoF arm motion patterns, although being reasonably efficient in real-time interactions.

As a preliminary study of objective 1, our focus was to investigate the feasibility of FMG-based force estimation in dynamic motions in collaboration with a simple linear robot. The experimental setup was constrained in 2D only, capturing FMG signals were maximized with multidimensional channels, and human interactions were conducted with the biaxial stage with exerted hand forces in dynamic motions. Due to the transient and nonstationary nature of FMG signals and individual-specific muscle contraction during interactive tasks, the changed positions of the FSRs (if the FMG band was removed and put back again) led to retraining the models. The regressors performed well, as the models were trained for estimating forces in a certain motion only; therefore, evaluating all interactions were time-consuming and was not practical. In addition, to capture the unique features when grasping a force in each motion, both bands were required. This might not reflect a practical scenario of HRI, but the outcome proved the viability of the FMG-based control mechanism.

## **3. Redundant degree-of-freedom of human arm**

In general, people tend to move their arms similarly for certain tasks to minimize energy expenditure tendency [107-108]. Although participants were instructed to interact in certain motions (the general shape of a path to follow with no restriction), the movements were individual-specific. In objective 1, each participant manipulated the stage in the same way during a certain task to avoid muscle fatigue and energy expenditure during interactions. Considering a torso as a ground (origin) and a hand being fixed as a



rigid body by grasping the gripper, the unilateral arm motion was guided by the intended path the participant would choose from redundant degrees of freedom. The full elbow extension (full arm length:  $74 \pm 4$  cm) was avoided (to prevent elbow singularity) [109] and reached the boundary point in the workspace area (to avoid boundary singularity for the biaxial stage). Otherwise, misalignment might happen, and the biaxial stage would fail to follow a compliant trajectory. It is worthwhile mentioning that the range of arm motions and trajectories performed by the participants were affected by hand forces, motions, and ranges of MVCs to maintain muscle fatigue and sitting positions

#### **4. Instantaneous force recognition without fine-tuning (no calibration)**

In objective 2A, although LCFMG-0 failed in estimating user-applied forces, surprisingly it worked exceptionally well in one or two instances. In recognizing unseen X motion, the Inter-Participant-LCFMG-0 model obtained higher estimation accuracies ( $R^2=70\%$ ) for a learned participant ( $P_L: P_8$ ), while the Intra-Motion-LCFMG-0 model estimated well ( $R^2=77\%$ ) for recognizing an unseen participant ( $P_U: P_{13}$ ) applying force in a learned motion  $M_1$ . These two incidents indicated that a long-term FMG model might estimate user-applied forces during a simple straightforward motion even without 'calibration data'. This would be achievable only when the population dataset includes all possible force ranges in dynamic motions from more participants and requires further investigation.